

Verisk Earthquake Model for Hawaii

Publication Date: June 2018

Copyright

Verisk Analytics. All rights reserved.

Trademarks

Touchstone is a registered trademark of Verisk Analytics (Verisk). Touchstone Re, ALERT, and Analyze Re are trademarks of Verisk. Please refer to the following link for an up-to-date list of trademarks: www.air-worldwide.com/Legal/Trademarks/.

In accordance with international patent conventions and treaties, if you use these trademarked items in any document you must also include the trademark symbol and prominently acknowledge Verisk as the owner of the trademarks.

Verisk (Nasdaq:VRSK)



Internet Explorer and Windows Server are registered trademarks of Microsoft Corporation. SQL Server, Windows, and Excel are trademarks of Microsoft Corporation.

Contact Information

Verisk Analytics
Lafayette City Center, 2nd Floor
Two Avenue de Lafayette
Boston, MA 02111
USA

Tel: (617) 267-6645
Fax: (617) 267-8284

Verisk welcomes feedback on its documentation. If you need assistance in using the software or understanding the information in this document, please email us at DocumentationFeedback@verisk.com.

Revision history

Revision Date	Description
July 2014	Updated modeled industry losses in Section 1 to reflect the updates to the US industry exposure database (IED), which reflect risk counts and replacement values as of the end of 2013, and the updated take-up rates. This includes the occurrence and aggregate loss estimates.
June 2016	Updated modeled industry losses in Section 1 to reflect the updates to the US industry exposure database (IED), which reflect risk counts and replacement values as of the end of 2015. This includes the occurrence and aggregate loss estimates and modeled losses for historical events (Tables 3 and 4). In addition, modeled losses for Extreme Disaster Scenarios in Sections 7.1 and 8.1 were updated to reflect the updates to the IED

Table of Contents

REVISION HISTORY.....	iii
1 FACTS AT A GLANCE.....	1
1.1 Model facts.....	1
1.2 Hawaii – state facts.....	2
1.3 Data sources.....	4
1.4 Historical catalog.....	4
1.5 Stochastic catalog.....	4
1.6 Model resolution.....	6
1.7 Modeled lines of business.....	6
1.11 Navigating the model description.....	6
2 EARTHQUAKES IN HAWAII.....	8
2.1 Earthquakes: an overview.....	8
2.2 Earthquake risk in Hawaii.....	14
2.3 Significant historical earthquakes in Hawaii.....	17
3 EVENT GENERATION.....	23
3.1 Data sources.....	23
3.2 Modeling regional seismicity.....	24
3.3 Modeled earthquake variables.....	29
3.4 Stochastic catalog summary statistics.....	31
3.5 Extreme Disaster Scenario (EDS) events.....	31
3.6 Validating stochastic event generation.....	32
4 LOCAL INTENSITY CALCULATION.....	35
4.1 Ground shaking intensity.....	35
4.2 Ground motion prediction equations.....	35
4.3 Site classification.....	37
4.4 NGA local site amplification.....	39
4.5 Ground motion intensity and spatial correlation.....	41
4.6 Validating local intensity.....	45
5 DAMAGE ESTIMATION.....	48
5.1 Building classification.....	48

5.2 Evolution of seismic building codes in Hawaii.....	52
5.3 Shake damage.....	54
5.4 Development of building damage functions.....	55
5.5 Building damage functions.....	64
5.6 Assessment of business interruption losses for small-scale industrial facilities.....	69
5.7 Large-scale industrial facility damage functions.....	71
5.8 The distribution of damage: uncertainty in damage estimation.....	82
5.9 Builders risk.....	83
5.10 Contents damage.....	89
5.11 Automobile damage.....	89
5.12 Workers compensation losses due to earthquakes.....	90
5.13 Validating the model’s damage estimation module.....	94
6 INSURED LOSS CALCULATION.....	104
6.1 Aggregating losses probabilistically.....	104
6.2 Demand surge.....	105
6.3 Validating modeled losses.....	106
SELECTED REFERENCES.....	108

List of Figures

- Figure 1. Population density map of Hawaii.....2
- Figure 2. islands of Hawaii and their ZIP Code boundaries..... 3
- Figure 3. Counties in Hawaii..... 3
- Figure 4. Annual frequency distribution of all simulated earthquakes in Hawaii..... 5
- Figure 5. Annual frequency distribution of loss-causing simulated earthquakes in Hawaii..... 6
- Figure 6. Components of the model.....7
- Figure 7. Earth’s layers at a subduction zone.....9
- Figure 8. Data completeness as functions of earthquake source dimension..... 12
- Figure 9. Sample Gutenberg-Richter distribution..... 13
- Figure 10. Historical seismicity by magnitude since 1868..... 14
- Figure 11. Ages of the Hawaiian islands, in millions of years.....15
- Figure 12. The seaward flanks and rift zones of the Mauna Loa and Kilauea volcanoes..... 16
- Figure 13. Epicentral locations of significant earthquakes in Hawaii..... 18
- Figure 14. Model domain for Hawaii earthquake model..... 23
- Figure 15. Seismic source zones in the model..... 25
- Figure 16. Focal depth..... 30
- Figure 17. Epicenters of EDS events in the World Scenarios event set..... 32
- Figure 18. Frequency-magnitude distributions for the simulated and historical catalogs, Hawaii Island.....33
- Figure 19. Cumulative historical vs. simulated depth distributions..... 34
- Figure 20. Current and previous soil classification maps for Hawaii Island..... 39
- Figure 21. Soil classification map for Niihau, Kauai, Oahu, Molokai, Lani, Kahoolawe, and Maui Islands.....39
- Figure 22. Comparison of NGA and NEHRP site amplification factors with respect to a reference engineering rock site for long period waves..... 41
- Figure 23. Recreations of the 1994 Northridge earthquake’s ground motion footprint..... 43
- Figure 24. Multiple ground motion maps with spatial correlation and the corresponding distribution of modeled losses for the 1994 Northridge earthquake..... 44
- Figure 25. Loss exceedance curves with (green) and without (blue) spatial correlation..... 45



Figure 26. Modeled vs. observed spectral acceleration, 2006 Kiholo Bay earthquake.....	46
Figure 27. Spectral acceleration (0.3s) for the 2006 Kiholo Bay earthquake using median ground motion without stochastic ground motion simulatio.....	47
Figure 28. Open-end (left) and thatched-end (right) hale structures (Source: "Adoption of Chapter 15-110 Rules Pertaining to Indigenous Hawaiian Architecture Structures," County of Maui).....	49
Figure 29. Example of a small-scale industrial facility.....	50
Figure 30. Examples of large-scale industrial facilities.....	51
Figure 31. Examples of some industrial facility components.....	52
Figure 32. History of building codes in effect in all four Hawaiian counties, 1956-2006 (After: Uniform Statewide Building Code Task Force, 2005).....	54
Figure 33. Conceptual flow of analyses adopted for building damage functions (adapted from FEMA 440).....	56
Figure 34. Schematic depiction of static pushover analysis used in the capacity spectrum method (excerpted from FEMA 440).....	57
Figure 35. Maximum acceleration and displacement of a series of oscillators.....	58
Figure 36. Peak response of a structure determined by its capacity curve.....	59
Figure 37. Maximum displacement and building damage depends on ground motion and building characteristics.....	60
Figure 38. Using NDA to determine building response (courtesy of FEMA 440).....	61
Figure 39. Maximum peak inter-story drift ratios (MIDR) and maximum peak floor accelerations (MPFA).....	62
Figure 40. Relationship between spectral accelerations at the fundamental period of a building and the induced MIDR and IDR.....	63
Figure 41. Six failure modes captured by NDA for a four-story concrete moment-resisting frame building (courtesy of Dr. Curt B. Haselton, California State University).....	64
Figure 42. Damage functions for various construction types of unknown height and current age in Hawaii County.....	66
Figure 43. Damage functions for low-rise unreinforced masonry commercial buildings of the current age band for different Hawaiian counties.....	67
Figure 44. Damage functions for low-rise wood frame residential buildings for different age bands in Hawaii County.....	68
Figure 45. Damage functions for light wood frame, or single wall wood frame (AIR code 102), residential buildings for different age bands in Hawaii County.....	69
Figure 46. Hypothetical event tree of BI estimation for an office and a hotel.....	70
Figure 47. Business interruption damage functions for different occupancy classes.....	71

Figure 48. Damage functions for industrial facility components in Hawaii county.....	73
Figure 49. Building damage functions in Hawaii county.....	74
Figure 50. Building damage functions for various industrial facilities in Hawaii county.....	75
Figure 51. Damage functions for tanks based on technical literature and reviews, average damage from each source.....	76
Figure 52. Damage functions for on-grade tanks based on observed damage data.....	76
Figure 53. Pushover analysis results for an open-frame structure showing PGA values at several limit states.....	78
Figure 54. Damage functions for an open-frame steel plant structure.....	79
Figure 55. Damage functions for an open-frame steel dock structure.....	79
Figure 56. Damage functions for industrial facilities in Hawaii county.....	80
Figure 57. Damage functions for industrial facilities in Maui/Kalawao and Honolulu counties.....	80
Figure 58. Damage functions for industrial facilities for Kauai county.....	80
Figure 59. Time element functions for industrial facility components.....	81
Figure 60. Time element functions for industrial facilities in Hawaii county.....	82
Figure 61. Sample damage function and distribution with non-zero probabilities of 0% and 100% loss.....	83
Figure 62. Duration of phases for a mid-rise commercial building.....	84
Figure 63. Duration of some sub-phases for a mid-rise commercial building.....	85
Figure 64. Changes in replacement value during construction of a commercial building, for different heights.....	86
Figure 65. Changes in replacement value during construction of low-rise buildings with different occupancy classes.....	87
Figure 66. Changes in replacement value during construction of mid-rise commercial buildings with different occupancy types.....	87
Figure 67. Changes in seismic vulnerability at each construction phase.....	88
Figure 68. Variations of replacement cost and vulnerability of buildings under construction.....	89
Figure 69. Injury severity level by building damage state for a reinforced masonry building.....	93
Figure 70. Calculation of Workers Compensation Loss for an Individual Building.....	94
Figure 71. Damage distribution in Hawaii County, according to data obtain from Hawaii County (Takahashi et al. 2011).....	96
Figure 72. Modeled damage ratio footprint for the 2006 Kiholo Bay earthquake.....	97

Figure 73. Damage functions and observed damage data for chemical processing plants in a high seismicity area..... 100

Figure 74. Damage functions and observed damage data for a thermo-power plant in a high seismicity area..... 101

Figure 75. Damage functions and observed damage data for potable water systems in a high seismicity area..... 101

Figure 76. Modeled vs. observed fatalities from 29 historical earthquakes in the U.S..... 103

Figure 77. Comparison of modeled (Green) and Munich Re reported (Blue) losses for the October 15, 2006 Hawaii earthquake (2006 USD millions)..... 107

List of Tables

- Table 1. Distribution of all simulated events by magnitude..... 4
- Table 2. Distribution of loss-causing simulated events by magnitude..... 5
- Table 3. Seismic source zones in the Verisk Earthquake Model for Hawaii..... 24
- Table 4. Depth ranges by seismic source zone..... 26
- Table 5. Ground motion prediction equations and weighting factors used for shallow source-zone events.....36
- Table 6. Ground motion prediction equations and weighting factors used for deep source-zone events.....37
- Table 7. Soil classifications and average shear-wave velocities..... 37
- Table 8. Soil maps implemented in the Verisk Earthquake Model for Hawaii..... 38
- Table 9. Industrial facility components used in the Verisk Earthquake Model for Hawaii.....72
- Table 10. Historical earthquakes used for tank damage data..... 77
- Table 11. Building phases during construction..... 84
- Table 12. Percentage of the total cost at each construction phase for apartment buildings of different heights.....86
- Table 13. Collapse probabilities used in the Verisk Earthquake Model for Hawaii..... 91
- Table 14. Distribution of nonfatal injuries for five California earthquakes..... 92
- Table 15. Injury severity levels used for workers compensation (FEMA 2009)..... 92
- Table 16. Historical earthquakes used for facility and component damage function validation..... 98
- Table 17. Some facilities and components validated with damage data from historical earthquakes.....99
- Table 18. Comparison of observed and modeled casualties for selected historical earthquakes in California..... 102
- Table 19. Source parameters for the October 15, 2006 Hawaii earthquake..... 106



1 Facts at a Glance

1.1 Model facts

Item	Value	Description
Model name	Verisk Earthquake Model for Hawaii	Verisk Model 13
Release date	June 2013	
Version	2.0	This model was first released in version 1.5 of Touchstone and version 15.0 of CATRADER
Modeled perils	Ground shaking from earthquakes	<ul style="list-style-type: none">• Fire-following and tsunamis are not included in the current version of the model.• The effects of ground failure (liquefaction and landslides) are not explicitly modeled; however, to the extent that modeled losses have been calibrated to and validated against actual reported losses, the impact of ground failure on modeled losses is captured implicitly.• The presented modeled losses do not include loss adjustment expenses.
Supported construction and occupancy classes	The model supports 78 construction classes and 104 occupancy classes.	

Model abstract:

The Verisk Earthquake Model for Hawaii is an event-based model that captures the effects of earthquake-induced ground shaking on properties in Hawaii. The model captures complex seismicity of the modeled region by generating events along volcano flanks, rift zones, and within a number of seismic source zones through smoothed background seismicity. The earthquake generation process determines the magnitude, location, rupture length and

width, depth, and fault orientation and mechanism. Empirical attenuation relationships, faulting mechanisms, and local site conditions that affect the site-amplification factors are considered in the local ground-shaking intensity calculations. The engineering component of the model has been extensively validated against published research and observed damage data from historical earthquakes. Overall model performance has been validated against historical loss data from various events. The Verisk Earthquake Model for Hawaii has been developed to meet the wide spectrum of earthquake risk management needs of all stakeholders, including the insurance and reinsurance industry and accounts for policy conditions specific to Hawaii.

1.2 Hawaii – state facts

In 2011, the population of Hawaii was estimated to be 1,374,810.

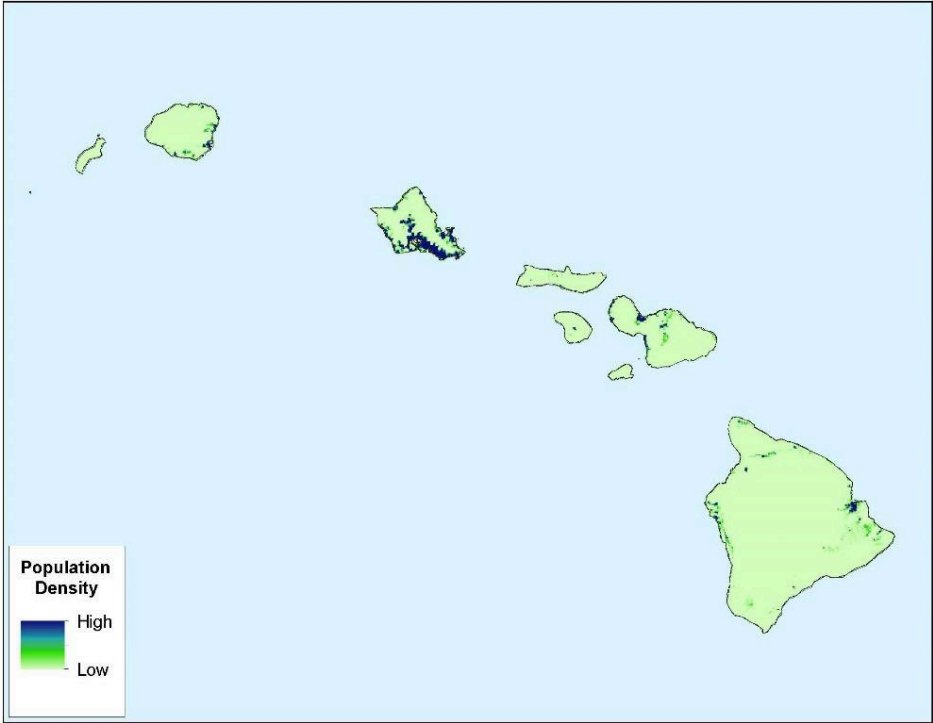


Figure 1. Population density map of Hawaii



Figure 2. islands of Hawaii and their ZIP Code boundaries.

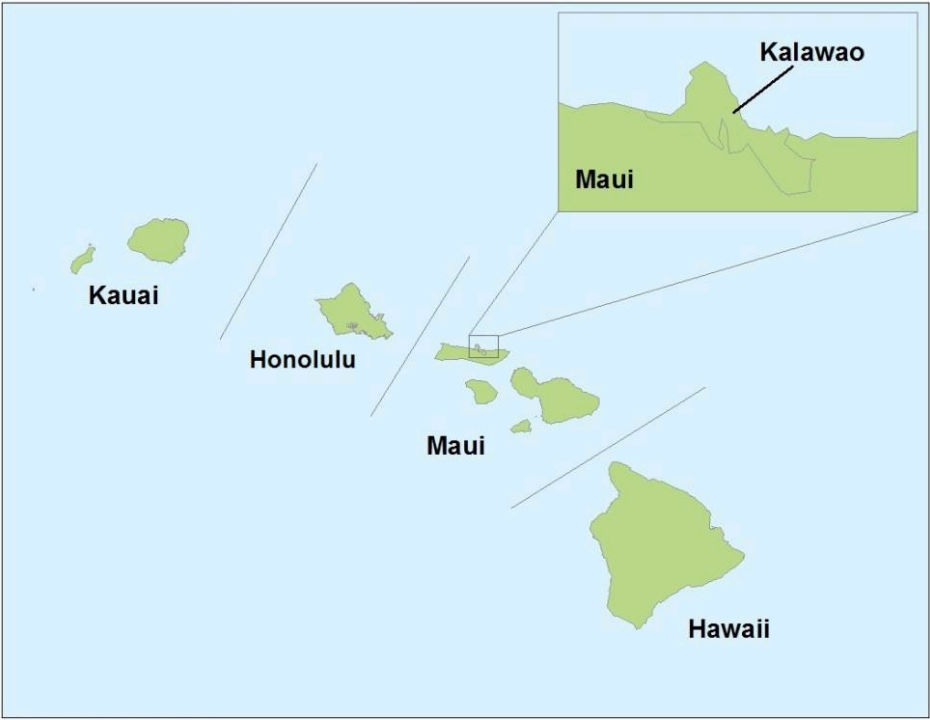


Figure 3. Counties in Hawaii

1.3 Data sources

Key data sources used in the development of the Verisk Earthquake Model for Hawaii are as follows:

Event Generation: Historical earthquake data is primarily sourced from the United States Geological Survey (USGS). The seismic source zones in the model are based on the 1998 USGS seismic hazard model (Klein et al., 2001).

Local Intensity: The model incorporates a weighted combination of GMPEs for shallow source-zone (depth < 20 km) and deep source-zone (depth ≥ 20 km) events. For shallow source-zone events, the model utilizes a weighted combination of Atkinson (2010), and the Next Generation of Ground Motion Attenuation Models (NGA) of Abrahamson and Silva (2008), Campbell and Bozorgnia (2008), and Chiou and Youngs (2008). For deep source-zone events, the model utilizes a weighted combination of Atkinson (2010), Atkinson and Boore (2003), and Youngs et al. (1997). The soil maps in the model are sourced from the USGS and the Hawaii Commission on Water Resource Management.

1.4 Historical catalog

The model includes information on earthquakes in Hawaii that took place during the years 1868 to 2010. The earthquakes in the historical record are of magnitude 3.0 and greater. The catalog information was obtained from the USGS, including data gathered by the Hawaiian Volcano Observatory from a network of stations from 1959 to 1997. Prior to 1959, the catalog is based on Wyss and Koyanagi (1992), which covers events from 1858-1989 that are of magnitude 6.0 and greater, and Cox (1986), which covers events in the Oahu-Maui area.

1.5 Stochastic catalog

The Verisk Earthquake Model for Hawaii incorporates a 10,000-year stochastic catalog¹ of 14,823 simulated events, of which 11,717 cause loss to the industry exposure. Stochastic events included in the model are of magnitude 5.0 and greater.

Note that stochastic catalogs of 50,000 and 100,000 years are also available.

Table 1. Distribution of all simulated events by magnitude

Magnitude	> 8	7.5 to 8.0	7.0 to 7.5	6.5 to 7.0	6.0 to 6.5	5.5 to 6.0	5.0 to 5.5	Total
Event Count	10	76	127	670	1,433	3,549	8,958	14,823

¹ Note that stochastic catalogs of 50,000 and 100,000 years are also available

Magnitude	> 8	7.5 to 8.0	7.0 to 7.5	6.5 to 7.0	6.0 to 6.5	5.5 to 6.0	5.0 to 5.5	Total
Percentage	0.07%	0.51%	0.86%	4.52%	9.67%	23.94%	60.43%	100.00%

Table 2. Distribution of loss-causing simulated events by magnitude

Magnitude	> 8	7.5 to 8.0	7.0 to 7.5	6.5 to 7.0	6.0 to 6.5	5.5 to 6.0	5.0 to 5.5	Total
Event Count	10	76	127	662	1,343	3,046	6,453	11,717
Percentage	0.09%	0.65%	1.08%	5.65%	11.46%	26.00%	55.07%	100.00%

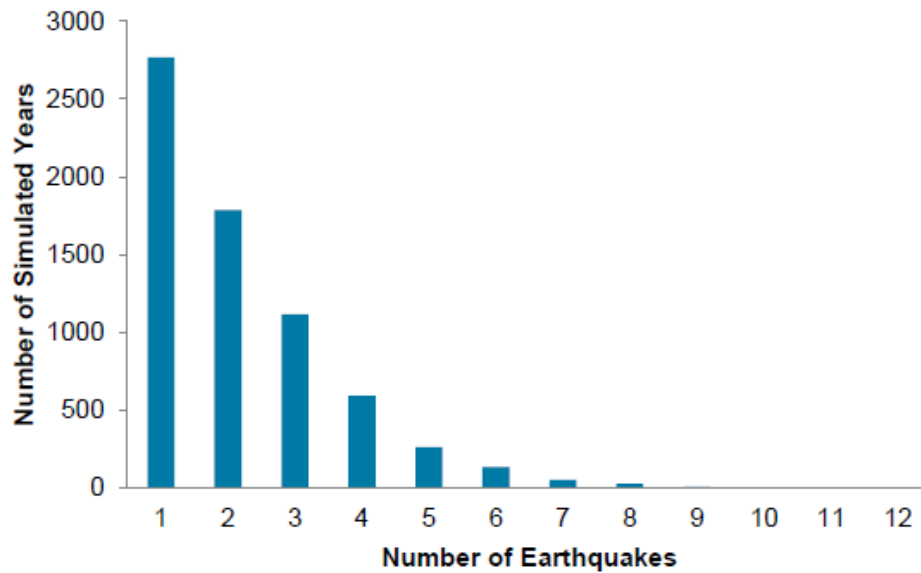


Figure 4. Annual frequency distribution of all simulated earthquakes in Hawaii

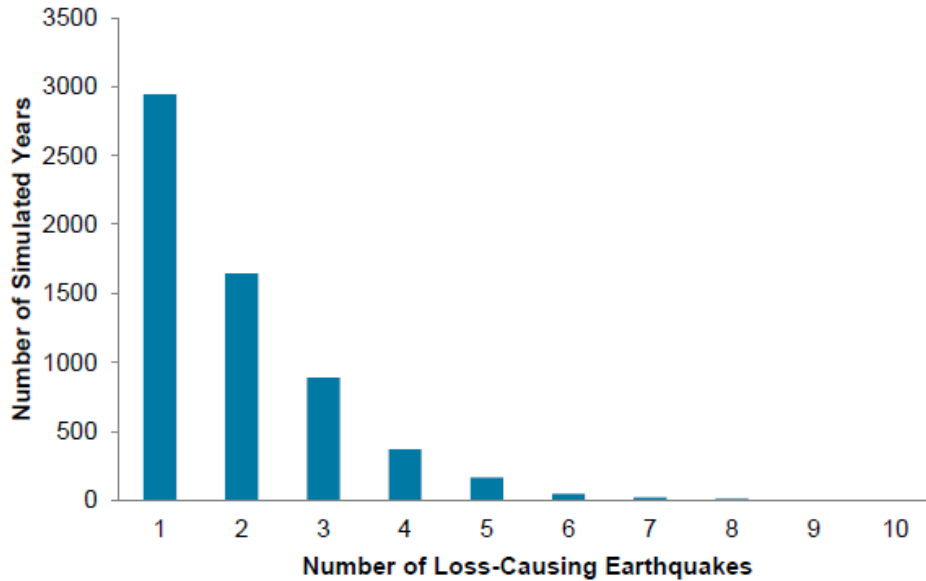


Figure 5. Annual frequency distribution of loss-causing simulated earthquakes in Hawaii

1.6 Model resolution

Two sets of surface geology maps were used to create the soil maps in the Verisk Earthquake Model for Hawaii. The first set of maps covers Hawaii County at a scale of 1:100,000. The soil maps developed from this set are created at a spatial resolution of approximately 100 m. The second set of geological maps covers the islands of Kauai, Lanai, Maui, Niihau, Molokai, Kahoolawe, and Oahu at a scale of 1:62,500. The soil maps developed from this second set of maps are at a spatial resolution of 75 m.

1.7 Modeled lines of business

The lines of business included in the Verisk Earthquake Model for Hawaii are residential, commercial, industrial, mobile homes, builders' risk, and automobile.

1.11 Navigating the model description

The components of the Verisk Earthquake Model for Hawaii are described in this model description and illustrated in the following figure. The description includes summaries of:

- earthquakes and earthquake risk in Hawaii
- the generation of simulated events that populate the stochastic catalog

- how ground shaking is modeled at each affected site
- the model's damage functions for residential, commercial, and automobile
- the financial module and insured loss calculation
- the implementation of the Verisk Earthquake Model for Hawaii in Verisk software



Figure 6. Components of the model

2 Earthquakes in Hawaii

2.1 Earthquakes: an overview

An earthquake results from a sudden displacement of rock along a fault. It accompanies a rapid release of energy in the form of seismic waves, which propagate outward from a focus. The process begins when rocks that experience stress along faults begin to deform as the strain builds within them. When the stress exceeds the strength of the rock and overcomes the friction that resists the relative movement of opposite sides of the fault, the fault ruptures and releases energy. Some of the energy released dissipates as friction along the fault; the rest is transferred as seismic waves that radiate from the initial point of rupture and cause ground motion at the earth's surface.

Faults are rarely found in isolation; instead, they tend to form zones of related fault traces. Long faults may be segmented, with each segment having an individual rupture history and mechanism. Ruptures during a weak to moderate earthquake are believed to be contained within one segment of a fault, but more powerful earthquakes may manifest themselves along multiple segments. Fault zones vary in depth, width, and orientation.

A fault plane can be vertical or sloping in relation to the earth's surface. In sloping faults, the rock volume above the fault plane is known as the hanging wall, and the rock volume below the fault plane is the footwall. One type of earthquake faulting mechanism is dip-slip, which can be subclassified as either normal or reverse faulting. Normal faulting occurs when the hanging wall slips down relative to the footwall, resulting in an extension of crustal matter. Reverse faulting occurs when the hanging wall lifts relative to the footwall, which causes a shortening of the crustal material. Strike-slip faults have a nearly vertical surface; their movement is horizontal, parallel to the strike of the fault surface. Oblique-slip faulting is a combination of strike-slip and normal or reverse faulting.

While faults may form a visible trace on the earth's surface, some remain buried within the earth. These blind faults represent a significant seismic hazard, as they are often difficult to detect prior to rupture. Hazard assessment of blind faults is challenging and often plagued with uncertainty.

Generally, active faults are those which have demonstrated activity during the last 10,000 years, or during the Holocene period. Potentially active faults are those that have demonstrated activity during the last 1.65 million years, or during the Quaternary period.

Plate tectonics

The theory of plate tectonics was developed to explain the evidence for large-scale motion of the earth's continents. The crust and upper mantle form the rigid, strong lithosphere, which is divided into large plates that move relative to one another. The largest plates are the Pacific, North American, South American, Eurasian, African, and Australian plates.

These lithospheric plates move over the asthenosphere, a hot, viscous layer of weak rock that is continuously moving and transferring heat from the interior to the surface of the earth. The boundaries between plates are where most earthquake and volcanic activity occurs.

There are several types of boundaries between neighboring plates. Convergent boundaries occur where two plates move towards one another; if one of these plates sinks, or subducts, beneath the edge of the other plate, a subduction zone is formed (see Figure below). Seismic activity may be particularly rampant in subduction zones.

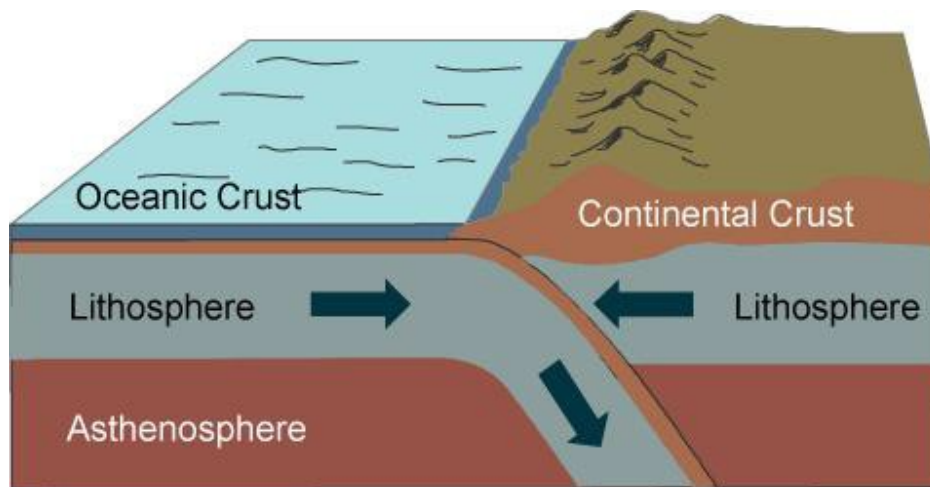


Figure 7. Earth's layers at a subduction zone

Continental-collision boundaries occur where two low-density plate edges move towards one another; this process may result in crustal rock being thrust upward, which is how linear mountain systems are formed. Divergent boundaries occur where plates move away from one another, which allows for the formation of new crustal material.

Transform boundaries occur where one plate moves past another. Due to massive amounts of friction, however, the plates do not simply glide past each other. Rather, stress builds up in the rocks along the fault until the strain is too great. At that point, the potential energy is released in the form of an earthquake.

While the majority of earthquakes do occur at plate boundaries, intraplate earthquakes can occur along fault zones in the interior of a plate. A large intraplate earthquake usually has a long recurrence time, which makes it difficult to estimate the associated risk.

Seismic waves

Seismic waves transmit tectonic energy through the earth at speeds of up to several miles per second. Seismic waves produce ground motion on the earth's surface that may damage buildings, trees, cars, roads, and other structures. Soil properties, local geological features, and other factors play a role in attenuating or amplifying seismic waves at a given location.

There are several types of seismic waves. Body waves travel through the earth, while surface waves travel along its surface. The two types of body waves that are generated by an earthquake are primary and secondary waves, also known as P and S waves, respectively. P waves are faster and capable of traveling through both solids and liquids. These waves

exhibit an alternating compression-dilatation motion in the direction of wave propagation. S waves are slower and travel only through solid material. These waves produce a sideways-shearing motion perpendicular to the direction of wave propagation.

Surface waves, which are responsible for the majority of earthquake damage, include Love waves and Rayleigh waves. Love waves move horizontally, perpendicular to the direction of wave propagation. Rayleigh waves are slow waves that move in an elliptical, or rolling, motion. Note that seismic-wave amplitude, which is the height of an individual wave cycle, or the maximum displacement, decreases with increasing depth in the earth for these surface waves. The amplitude of a seismic wave is one measure of its destructive potential.

In addition to amplitude, there are several ways to mathematically describe wave activity. The wave frequency is the number of wave cycles per second that pass a reference point. A wave's period is the elapsed time, in seconds, between peaks, or the time it takes one complete cycle of the wave to pass a reference point. The wavelength is the distance between repeating units of a propagating wave of a given frequency, at some instant in time.

Measuring earthquake magnitude and intensity

The severity of an earthquake can be measured by the damage it inflicts on structures at the earth's surface or by the energy released at its focus, which is where the rupture originates. Earthquake magnitude characterizes the total energy released by an earthquake, while earthquake intensity refers to the resulting level of ground shaking at a particular location and the observed effects of an earthquake on people, buildings, and other features. While the magnitude of an earthquake is a characteristic of the earthquake as a whole, intensity varies from place to place within an affected region.

An earthquake's intensity at different locations can be described semiquantitatively using the Modified Mercalli Intensity (MMI) scale,² which was developed in its original form in 1902 and is based on observations of shaking severity and its effects at different locations. The MMI at a particular location is based on human judgment and the observed post-event damage. Today, ground-motion intensity can be directly measured using strong-motion seismographs. The characteristics of ground-motion intensity can be quantified by physical parameters such as peak ground acceleration (PGA) and spectral acceleration (Sa). Shaking intensity at a particular location depends not only on earthquake magnitude, but also on the local surface geology and the proximity of the location to the earthquake source.

Magnitude is a measure of an earthquake's size. There are several types of earthquake magnitude, including moment magnitude (MW), Richter magnitude (ML), body-wave magnitude (Mb), and surface-wave magnitude (Ms). Magnitude scales are generally logarithmic in nature; that is, an increase of one point on a magnitude scale represents approximately a tenfold increase in wave amplitude and a thirtyfold increase in the amount of energy released during the earthquake. Verisk models utilize the moment-magnitude scale, which is based on seismic moment. The seismic moment is defined as: $M_0 = \mu AD$ where μ is the shear modulus of elasticity of the rupturing material, A is the rupture area, and D is the average slip over the rupture area

² Please see <https://www.usgs.gov/media/images/modified-mercalli-intensity-mmi-scale-assigns-intensities> for a more detailed description of this intensity scale

The moment magnitude is considered superior to other magnitude scales because it is based on earthquake source parameters, rather than on a particular type of seismic wave, like the surface-wave or body-wave magnitude scales, or a particular type of instrument, such as the Richter magnitude scale. The type and amplitude of the seismic waves that reach an instrument and are recorded depend on earthquake magnitude, the radiation pattern of seismic waves, which depends on the rupture mechanism, and the complex structures along the wave propagation path between the source and the seismic stations. Different earthquakes can generate different types of seismic waves. Small earthquakes generate seismic waves with short periods, while larger earthquakes can generate seismic waves with long to very long periods.

Most seismic waves will saturate beyond a certain magnitude; that is, wave amplitude will not increase beyond that magnitude. Therefore magnitude scales based on the amplitude of a particular type of seismic wave will also experience saturation. Moment magnitude does not have such a limitation.

Paleoseismic and geodetic data

The modeling of earthquakes requires historical data. For large earthquakes, the catalog is complete further back in time because such events are more likely to have been observed and documented than smaller events. However, improvements in instrument sensitivity and coverage have led to increased recordings of smaller events. The completeness of a historical catalog is therefore a function of time and magnitude.

Paleoseismic and geodetic data are often used to augment instrumentally recorded earthquake catalogs in order to estimate current seismic hazard. Paleoseismology is the study of the location, timing, and size of prehistoric earthquakes. Prehistoric earthquakes are evidenced by offsets in geological formations found in exhumed fault zones, signs of rapid uplift or subsidence near coastal areas, laterally offset stream valleys, and liquefaction artifacts, such as sand boils.

The geodetic measurement of fault slip rate is another source of information that is used to supplement historical data. The Global Positioning System (GPS) is now the most widely used technology for measuring crustal deformations in a region. The observed crustal deformation represents elastic strain accumulation in the crust. By calculating the rate at which elastic strain accumulates along a fault or seismic zone, estimates can be made as to how often large earthquakes may occur. Paleoseismic and geodetic data assist in estimating the frequency of large-magnitude earthquakes; for smaller events, the historical earthquake data tends to be more complete. For earthquakes above some magnitude, which is region-dependent, geodetic and paleoseismic data become more reliable compared to historical earthquake data, as the Figure below illustrates.

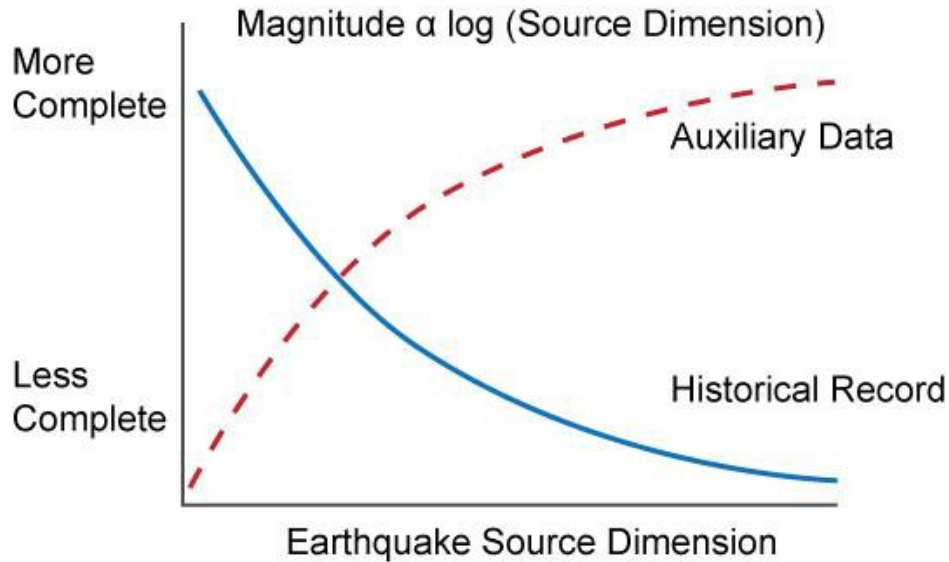


Figure 8. Data completeness as functions of earthquake source dimension

The Gutenberg-Richter relationship

The Gutenberg-Richter relationship expresses the association between magnitude and the earthquake occurrence rate on a fault or in a given area, at or above each magnitude. The relationship can be used to provide a more complete picture of seismicity in regions where historical data is lacking, as it holds over a wide variety of magnitudes and locations.

The Gutenberg-Richter relationship is parameterized by the a-value, which is the logarithm of the earthquake occurrence rate above some reference magnitude, and the b-value, which is the rate at which the logarithm of the cumulative annual frequency decreases as the magnitude increases. Scientists usually truncate this relationship at a limiting magnitude above which the probability of an earthquake's occurrence is zero (see Figure below).

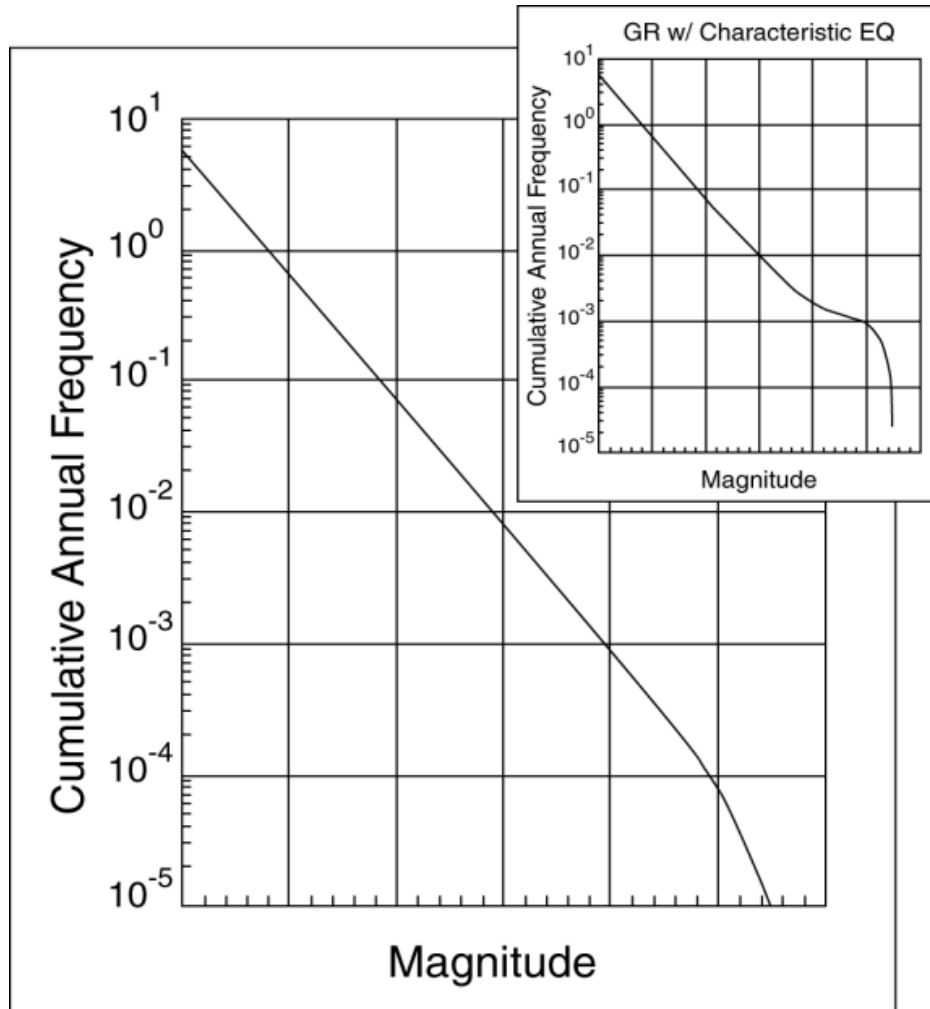


Figure 9. Sample Gutenberg-Richter distribution

Note that the a -value is the logarithm of the y -intercept of the distribution, and the b -value represents the slope of the graph away from the characteristic earthquake or limiting magnitudes. The presence of large-magnitude characteristic earthquakes increases the frequency at these magnitudes.

Historical seismicity data, paleoseismic data, and geodetic slip-rate data are used to estimate the upper-bound magnitude of the Gutenberg-Richter distribution.

Characteristic earthquakes

The characteristic-earthquake theory states that active faults tend to generate earthquakes of about the same magnitude at regular time intervals. This concept is used to simulate seismic activity along active faults. In order to model characteristic earthquakes, the earthquake magnitude and return period must be specified. Magnitude can be estimated from historical data, paleoseismological data, and fault length. The return period is estimated

from paleoseismological data, fault slip rates, or seismic-moment rates as estimated from fault slip rates.

2.2 Earthquake risk in Hawaii

The hazard

Thousands of earthquakes occur every year on Hawaii. Earthquakes are particularly common on the south side of Hawaii County, where the largest events have taken place and where the historical earthquake rate is relatively high as shown in the Figure below. Approximately 20 earthquakes of magnitude 6.0 or greater have occurred on Hawaii County since 1868, and 6 events of magnitude 6.0 or greater have taken place northwest of Hawaii County, from Maui to Molokai. Most of Hawaii's earthquakes are linked to volcanic activity while other earthquakes occur at the base of volcanoes or deep within the crust beneath the islands. Thus, the earthquake risk in Hawaii can be analyzed both in terms of the geologic history of the region and the relationship between seismicity and volcanic activity.

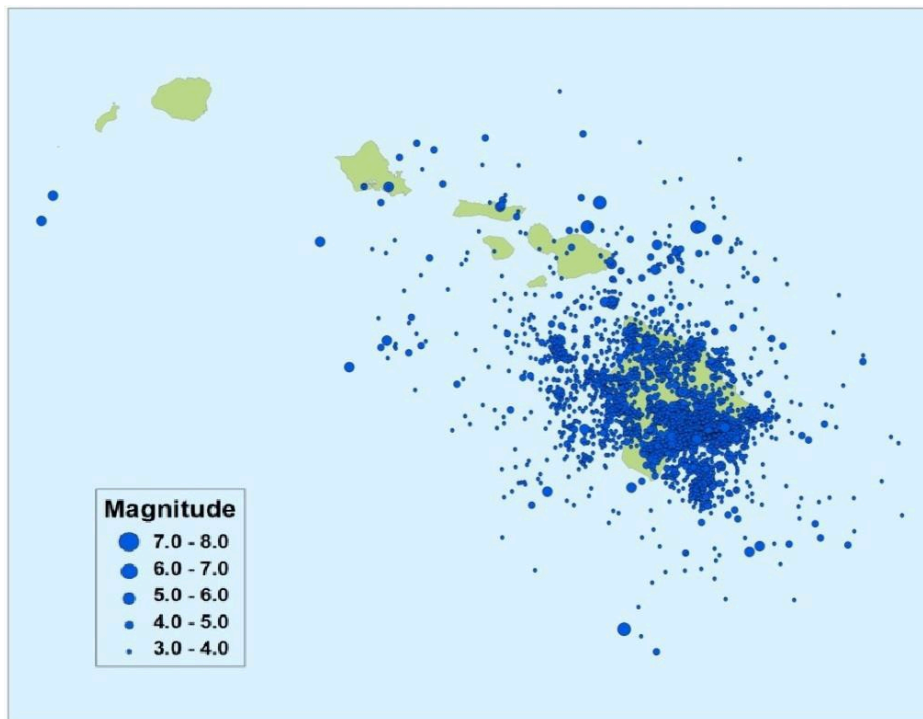


Figure 10. Historical seismicity by magnitude since 1868

Geologic history of Hawaii

Hawaii is located at the southeastern end of an extensive volcanic chain consisting of hundreds of islands and islets spread across approximately 1,500 miles in the central Pacific Ocean. These islands formed as a result of both plate movement and hotspot volcanic activity nearly 70 million years ago.

A volcano is an opening in the earth's surface through which hot magma, volcanic ash, and gases erupt. Volcanoes are typically located along the boundaries of converging and diverging tectonic plates. However, a small percentage of volcanoes, such as those in Hawaii, are located in plate interiors. These volcanoes usually form as a result of hotspot activity. Hot spot volcanoes form when mantle plumes, or hot rock, rise through the earth's mantle and tectonic plate, erupting at the surface. An active seamount, or a mountain that rises from the ocean floor, forms as a result of an eruption. Over time, countless eruptions cause the seamount to grow until it finally emerges above sea level to form an island volcano.

As the Pacific tectonic plate, which is over the source of the Hawaiian hotspot, moved in a northwesterly direction, the seamount also moved. Since the hotspot remained fixed in place, the seamount was cut off from the source of the hotspot. However, a new seamount formed in its place. Over time, these successive seamounts caused an undersea mountain range, known as the Hawaiian-Emperor seamount chain to form. The Hawaiian Islands are the exposed peaks of this chain.

As a result of being further from the hotspot, the northwest Hawaiian islands are older than those in the southeast and have lower rates of volcanic and seismic activity. The eight main islands of Hawaii and their ages are shown in the Figure below.

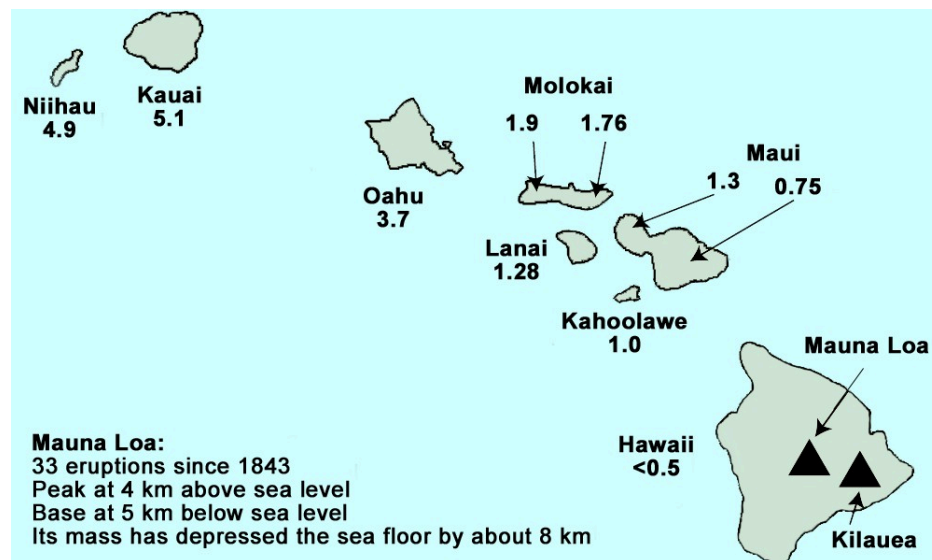


Figure 11. Ages of the Hawaiian islands, in millions of years.

Volcanic activity and Hawaii's seismicity

Each Hawaiian island is made up of at least one primary volcano, although many islands are made up of more than one volcano. Hawaii County has five major volcanoes: Kilauea, Mauna Loa, Mauna Kea, Hualalai, and Kohala. Mauna Loa is one of the largest and most active volcanoes on the earth, measuring approximately 30,000 feet in height from the sea floor.

Most of the earthquakes that occur beneath the Hawaiian Islands are a direct result of volcanic activity. Earthquakes may occur before or during a volcanic eruption, or they may result from the movement of magma beneath the earth's surface. Earthquakes which are not

a direct result of volcanic activity, are often caused by the stress that the heavy volcanoes place on the Pacific lithosphere. This stress is released when an earthquake occurs.

Numerous small, shallow earthquakes usually accompany the eruptions and the movement of magma within active Hawaiian volcanoes. These earthquakes originate in regions of magma storage or along the pathways magma creates as it moves prior to an eruption. Hundreds of shallow earthquakes may also occur over the several hours or days before an eruption, as magma forces its way into a new area. These earthquakes seldom cause widespread damage, but they may produce extensive ground fracturing close to the eruption site. Once an eruption begins, the earthquakes typically diminish.

Magma that never reaches the earth's surface may also create enough pressure to cause earthquakes. For example, Kilauea's east rift zone³ is continually wedged apart by the injection of new magma. Since Mauna Loa immobilizes the northern flank of Kilauea as shown in the Figure below, pressure builds in the zone. The southern flank of Kilauea periodically shifts seaward to release the built-up pressure, causing earthquakes to occur. The southwest and southeast flanks of Mauna Loa behave similarly. The strongest earthquake in the recorded history of Hawaii, an estimated M7.9 event, took place on the southeast flank of Mauna Loa in 1868. Large earthquakes can also occur in the area between the Kilauea and Mauna Loa volcanoes. Other earthquakes in Hawaii County are likely associated with Hualalai, the island's third most active and third youngest volcano.

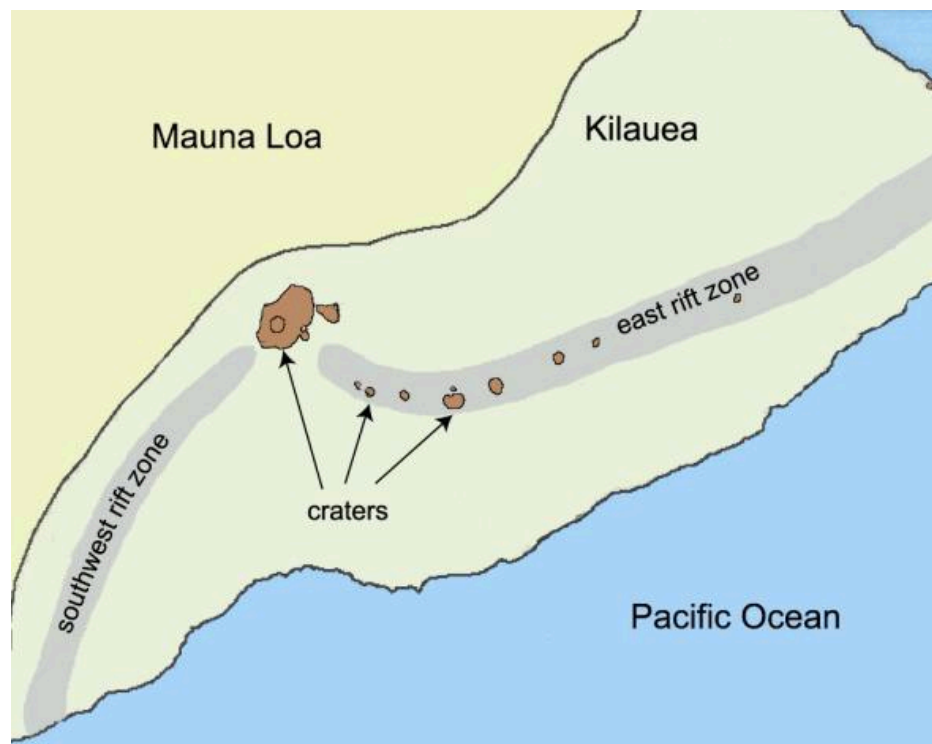


Figure 12. The seaward flanks and rift zones of the Mauna Loa and Kilauea volcanoes

³ A rift zone is a linear series of fissures along a volcano where lava or gas can erupt from the flank, or side, of the volcano, rather than the summit.

The exposure

The majority of insured risk in Hawaii is located in the capital and most populated city of Honolulu, with a population in excess of 300,000 residents, and the census-designated places of Hilo and Kailua, which have populations of over 40,000 and 35,000 residents, respectively.

Honolulu, located on the island of Oahu, is considered the business and trade center of Hawaii and is home to many government offices, shopping districts, tourist attractions, museums, theaters, schools, and wealthy residential areas such as Nuuanu, Pauoa, Waialae, and Kahala. The census designated place of Kailua is also located on the island of Oahu. With a central urban core and surrounding residential areas, Kailua is also place of considerable exposure.

Hilo, on the island of Hawaii, is located near two volcanoes – Mauna Loa, which is active, and Mauna Kea, which is dormant. Hilo is home to the world’s leading producer of macadamia nuts, and has a vibrant cultural center filled with many galleries, theaters, and museums. Many shopping centers, cafes, hotels, restaurants, and a zoo can all be found in Hilo.

For more details on Verisk’s Industry Exposure Database (INDUSTRY EXPOSURE), please see the Hawaii sections of the document Verisk Industry Exposure Databases for the United States, which is available from the client access portion of the Verisk website.

2.3 Significant historical earthquakes in Hawaii

The Figure below shows the locations of some significant earthquakes that have occurred in Hawaii. These events are described in detail in the following sections. One of these earthquakes, the 2006 Kiholo Bay earthquake, is included in the model’s historical catalog.



Figure 13. Epicentral locations of significant earthquakes in Hawaii

South flank of Kilauea (1823)

On June 2, 1823, an estimated magnitude (ML) 7.0 earthquake took place along the southern flank of the Kilauea volcano. It was the first seismic event of magnitude 5.0 or greater to be recorded in Hawaii. The event is theorized to have been a result of magma flow. It spawned ground fissures and sand blows, or sand volcanoes, due to ground liquefaction. Reports indicate that the temblor caused structural and nonstructural damage to homes, churches, and stone walls throughout the area.

Kau District (1868)

On April 2, 1868, the largest recorded earthquake in the history of the Hawaiian Islands, an estimated magnitude (ML) 7.9 event, struck the Kau District of Hawaii County. The event struck at a depth of six miles, and its epicenter was located approximately 5 miles northeast of Pahala. The temblor was caused by the seaward slip of the southern flanks of both the Mauna Loa and Kilauea volcanoes. There were at least 77 deaths as a result of the temblor, which caused damage throughout Hawaii County and was felt as far away as Kauai.

The damage from this temblor was extensive. In Kau, all of the houses and stone walls were destroyed and in Waiohinu, a large stone church collapsed. Nearly all of the wooden homes in the Keiawa and Punaluu areas of Oahu, as well as in the Ninole area of Hawaii were knocked off their foundations, while all of the straw homes set on posts were destroyed.

Landslides occurred in the areas of Waipio and Hamakua, burying ten houses and sweeping away trees, animals, and people, resulting in 31 deaths. Ground fissures stretched from Pahala to the town of Kilauea. A 5-km long fissure in Kohuku caused a volcanic eruption to

occur on April 7—a few days after the quake. The earthquake caused land to subside by as much as 2 meters along the Puna coast of Hawaii County.

A destructive tsunami wave struck the Kau-Puna coast, causing extensive damage in the areas of Honuapo, Keauhou, and Punaluu. At Keauhou, the water rose 12 to 15 m, destroying nearly all of the buildings in the area and killing 46 people.

Molokai (1871)

On February 20, 1871, a magnitude (ML) 6.8 earthquake occurred along the Molokai fracture zone, which is an extension of a transform fault from the East Pacific Rise that stretches from Molokai to the Gulf of California. This event was felt throughout Hawaii and caused severe damage in Lanai, Molokai, and Maui, and minor damage in Hawaii and Oahu.

The southern coast of Lanai was severely impacted by the groundshaking as a large portion of the Pali Kaholo Bluff and enormous pieces of ocean wall between Manele Bay and Kamaiki Point fell into the sea. Also in Lanai, earth fissures opened, boulders fell from mountainsides, and ravines filled with rock.

In Molokai and Maui, there were ground fissures and land slippage, and cracks formed in stone and adobe homes as well as in roadways. In addition, many stone walls toppled to the ground, and several old churches were completely destroyed.

In Oahu, many walls cracked and two houses split apart. The chimneys of a school and the belfry tower of a church also collapsed. While Honolulu experienced primarily minor damage, some experts theorize that if such an event were to occur today, there would be extensive damage in parts of Honolulu due to pockets of intense ground motion on hilltops or in areas of infill.

Holualoa (1929)

On October 6, 1929, a magnitude (ML) 6.5 earthquake struck Holualoa, Hawaii. Ground motion from the event was felt as far away as Lanai, Maui, and Oahu. Holualoa sustained moderate damage that included the collapse of walls and foundation displacement. In North Kona, numerous roads were cracked, and trees and telephone poles tipped over. In the Kealakekua area, several water tanks burst or were thrown off their foundations, and several poorly constructed buildings collapsed. In Puu Waawaa Ranch, many masonry structures experienced mild to moderate damage.

Maui (1938)

On January 23, 1938, a magnitude (MS) 6.8 earthquake struck below the ocean floor approximately 20 kilometers northeast of Keanae Point in east Maui. The event was felt throughout Hawaii but caused the most damage and destruction in Maui. The cause of the temblor was built-up stress in the earth's crust due to the island's large mass rather than the most common cause of Hawaiian temblors, volcanic activity.

The earthquake sent many Maui residents into a panic; however, no lives were lost and injuries were few. Landslides occurred along the northern coast of Maui, blocking roads and severing communication to Hana for several days. Building damage included fallen chimneys and cracked walls. Two large oil tanks near Hana were shattered, resulting in

30,000 gallons of oil flowing into the sea. Several ranches in southern Maui sustained heavy damage to water tanks and stone walls. The Olinda Reservoir was cracked severely, and the steel storage dam on the Wailuku-Kahului line was also damaged.

While the worst damage occurred in east Maui, west Maui and the other Hawaiian islands were not left unscathed. Concrete buildings cracked from Kahului to Lahaina. The fire station tower in Kahului shifted 13 millimeters on its foundation. In Oahu, rocks rolled onto roadways, and some plaster cracked and fell in buildings; however, most damage was limited to broken crockery and glassware. In Molokai and Lanai, small cracks opened in the ground, and water pipes broke in a few places. On the Big Island, dishes were broken, pictures fell from the walls, and plaster cracked.

Kona (1951)

On August 21, 1951, a magnitude (MS) 6.9 earthquake took place epicentered off the coast of Honaunau-Napoopoo, Hawaii. The quake, which struck at an approximate depth of 5 miles, was the third strongest temblor to affect Hawaii. The earthquake was caused by the seaward sliding of a large part of the western flank of Mauna Loa Volcano along a near-horizontal fault plane. Interestingly, the two strongest earthquakes to affect Hawaii were caused by a similar shift in the southern flank of the Kilauea Volcano. Observers reported that the ground shook continuously for an hour after the main event with many weaker aftershocks occurring in the region through September 1951.

While residents in Hawaii, Maui, and Oahu all felt the ground shaking, the worst damage occurred in Kona district from Kealahou to Hookena. Damage was most severe in central Kona, where several structures, including homes, churches, and a school, were damaged severely, and about 200 water tanks were destroyed. In addition, many stone walls were knocked down, and many roadways were either cracked or blocked due to landslides. Telephone and power services were disrupted throughout the affected area.

Residents along the coast fled the area, fearing a tsunami. While one did occur, its height of 2 feet, was not large enough to endanger people or property.

Honomu (1973)

On April 26, 1973, a magnitude (MW) 6.2 earthquake struck 48 kilometers beneath the town of Honomu along the northeast coast of Hawaii County. Ground motion from the event was felt all along the east coast of Hawaii as well as in Kahoolawe, Kauai, Lanai, Molokai, and Oahu. There were no fatalities, but approximately 11 people were injured during the event.

Damage to buildings, roads, and utilities was extensive in the affected area prompting officials to declare a state of emergency. All told, approximately 355 homes and 72 commercial establishments were significantly impacted. In addition, water pipes and tanks were damaged, utility services were disrupted for days, and tombstones and chimneys were overturned. In Hilo, 17 houses were shaken from their foundations, and five houses collapsed. Also in Hilo, many storefront windows were cracked, and all unsupported roof overhangs fell to the ground. Seven major landslides occurred in the Hamakua district following the earthquake, which blocked State Highway 19 for at least seven hours.

Kalapana (1975)

On November 29, 1975, a magnitude (MS) 7.2 earthquake struck just west of Kalapana, Hawaii, near the south flank of the Kilauea volcano. The event took place at a depth of 8 km. Data and observations in the aftermath of the temblor suggest that the injection of magma into rift zones caused a buildup of pressure against the south flank of Kilauea. This pressure was released during the earthquake as much of Hawaii County slid horizontally towards the ocean and subsided. This earthquake was the largest magnitude event to occur in the state in more than a century, and the most powerful ever to be recorded by the Hawaiian Volcano Observatory.

The earthquake spawned a tsunami wave that was over 7.9 m high in Halape, which resulted in two deaths, 19 injuries, and widespread subsidence along the southeast coast of Hawaii. Less than an hour after the main quake, a small volcanic eruption took place, which was likely triggered by the vigorous ground motion.

Ground motion was felt throughout the Big Island, Lanai, Molokai, and Oahu. Most of the buildings near the epicenter sustained little or no damage, while structures in Hilo, located 45 km away, experienced slight-to-moderate damage including minor cracking, floor-wall separation, and wall bowing. Many roads throughout the area were damaged, and numerous landslides were reported. Gaping fissures opened in the ground in Puna and Kau, and car-sized boulders tumbled down the steep crater walls of Hawaii Volcanoes National Park.

Kaoiki Fault Zone (1983)

The most destructive earthquake to affect Hawaii since the 1975 Kalapana event took place on November 16, 1983. This M6.7 event occurred along the Kaoiki fault zone, between the summits of the Mauna Loa and Kilauea volcanoes. The 1983 event was one of five earthquakes that occurred in the Kaoiki fault zone between 1941 and 1983, making it a zone of recurring earthquakes. Ground motion from the 1983 event was felt throughout Kauai, Lanai, Maui, Molokai, and Oahu. But the worst damage occurred on the Big Island between Volcano and Hilo.

Over 400 structures were impacted on the Big Island with typical damage consisting of homes shifted off their foundations, cracked walls, and collapsed chimneys. Additionally, several highways were severely cracked, numerous elevated water tanks were damaged, and telephone and power service was disrupted throughout the impact area. There was also structural damage at Hilo Hospital.

The earthquake also caused ground cracking and numerous landslides in southern Hawaii. In Hawaii Volcanoes National Park, for example, parts of Crater Rim Drive collapsed into the adjacent caldera.

Kiholo Bay (2006)

On October 15, 2006, a magnitude (MW) 6.7 event took place nearly 10 miles north-northwest of Kailua-Kona, at a depth of approximately 29 km. The quake was followed by several strong aftershocks, including one measuring M6.0. Ground motion from this earthquake was felt on the islands of Hawaii, Maui, Lanai, Molokai, and Oahu. The most severe damage reports came

from the northern and western sides of Hawaii Island, while minor damage was reported throughout Oahu.

Nearly 1,800 buildings were damaged during this event, including many luxurious hotels and historical churches located near the event's epicenter. A hospital near the epicenter suffered ceiling damage resulting in the evacuation of about 10 patients to nearby Hilo. Numerous roads were cracked or blocked by landslides. Kailua-Kona's main highway was blocked by a landslide. Power outages occurred throughout the area, and in some cases electricity was not restored for nearly 14 hours. There were airport delays, as well as travel and communication disruptions following the event.

While earthquakes in Hawaii are predominantly due to volcanic activity, this earthquake was likely due to the crustal flexure in response to the heavy weight of the island. Deep earthquakes—deeper than 16 to 19 kilometers—are considered to be of this type as there is a positive correlation between the number of deep earthquakes and the level of reported crustal subsidence.

3 Event Generation

The Verisk Earthquake Model for Hawaii captures the effect of earthquake ground shaking on properties in Hawaii. The model domain is shown below:

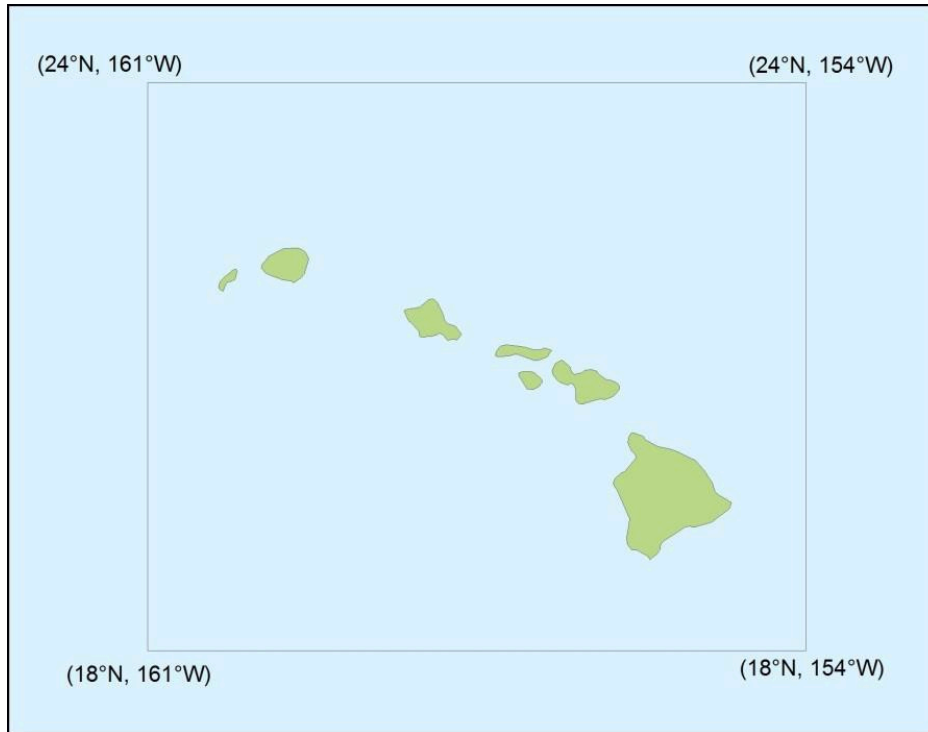


Figure 14. Model domain for Hawaii earthquake model

The Verisk model integrates historical seismicity records and regional seismicity models developed by the USGS. The model includes information on earthquakes that took place during the years 1868 to 2010. The earthquakes in the historical record are of magnitude 3.0 and greater. The catalog information was obtained from the USGS, including data gathered by the Hawaiian Volcano Observatory from a network of stations from 1959 to 2010 and another older catalog (1868-1959). In areas where the earthquake rate is significantly lower than in the modern catalog, the pre-1959 catalog is used for completeness. The pre-1959 catalog is also used when more information is needed to determine the rate of earthquakes of magnitude 5.0 and greater.

3.1 Data sources

The stochastic catalog is based on historical data from a variety of sources, including the United States Geological Survey (USGS), Cox (1986), and Wyss and Koyanagi (1992).

3.2 Modeling regional seismicity

In the Verisk Earthquake Model for Hawaii, regional seismicity is modeled using all available earthquake hazard data, including historical earthquake catalogs, geological fault information, and volcanic activity. The model domain is divided into 5 types of 22 seismic zones based on the 1998 USGS seismic hazard model (Klein et al., 2001).⁴ The following Table provides the names of these zones and the magnitudes of events simulated in each of the zones,⁵ and the Figure below shows their locations.

Table 3. Seismic source zones in the Verisk Earthquake Model for Hawaii

Type of Seismic Zone	Seismic Zone Name	Seismic Zone Abbreviation	Magnitudes of Simulated Events
Volcano Flank ⁶ Zones	Kilauea South Flank Zone	SFL	5.0 to 8.2
	Kaoiki Flank Zone	KAO	
	Hilea Flank Zone	HLE	
	Kona Zone / Mauna Loa West Flank Zone	KON	
	Hualalai / Mauna Loa South Flank Zone	HUA	
Kilauea (Rift) Zones	Kilauea Caldera Rift ⁷ Zone	CAL	5.0 to 6.5
	Southwest Rift Zone	SWR	
	East Rift Zone	ERZ	
Shallow Smoothed Seismicity Zones	Shallow Zone 1	S1	5.0 to 7.0
	Shallow Zone 2	S2	
	Shallow Zone 3	S3	
	Shallow Zone 4	S4	
	Shallow Zone 5	S5	
	Shallow Zone 6	S6	
	Shallow Zone 7	S7	

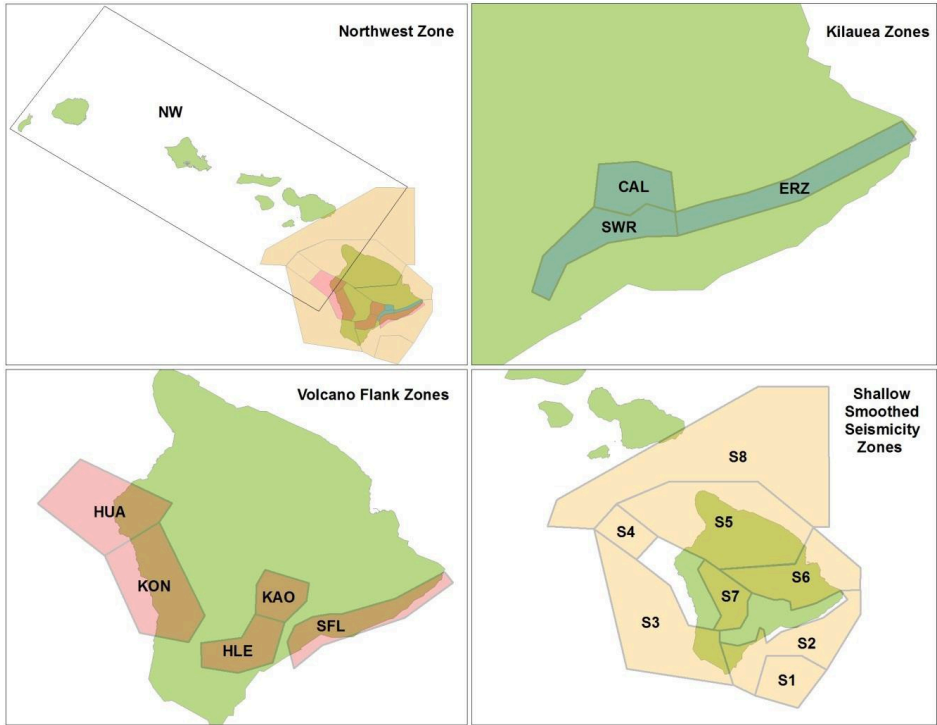
⁴ These are the latest USGS seismic hazard maps available for Hawaii. There are no plans to update them in the near future. The USGS updates seismic hazard maps for the continental U.S. roughly every six years.

⁵ These are the latest USGS seismic hazard maps available for Hawaii. There are no plans to update them in the near future. The USGS updates seismic hazard maps for the continental U.S. roughly every six years.

⁶ A flank is the side of a volcano

⁷ Rift zones radiate away from the summits of Hawaiian volcanoes and mark the preferred directions of sub-horizontal magma flow.

Type of Seismic Zone	Seismic Zone Name	Seismic Zone Abbreviation	Magnitudes of Simulated Events
Deep Smoothed Seismicity Zones	Deep Zone 1	D1	5.0 to 7.0
	Deep Zone 2	D2	
	Deep Zone 3	D3	
	Deep Zone 4	D4	
	Deep Zone 5	D5	
	Deep Zone 6	D6	
Northwest Zone	Northwest Zone	NW	5.0 to 7.0



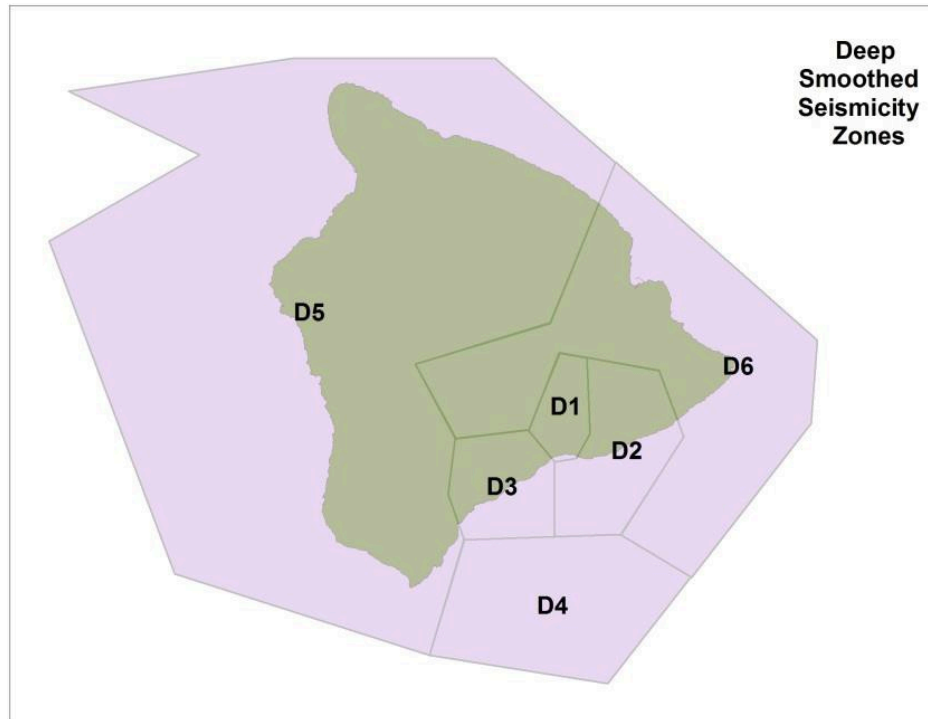


Figure 15. Seismic source zones in the model

Depth layers of the seismic source zones

The entire domain of the Verisk Earthquake Model for Hawaii is divided into two depth layers, 0 to 20 km and 20 to 60 km, based on the distribution of historical events. The depths of simulated events are distributed uniformly in the model. The simulated depth ranges for each seismic source zone are listed in the Table below.

Table 4. Depth ranges by seismic source zone

Seismic Source Zone	Depth Range
Volcano Flank Zones	0 - 20 km
Kilauea Zones	0 - 20 km
Shallow Smoothed Seismicity Zones	< 20 km
Deep Smoothed Seismicity Zones	20 - 60 km
Northwest Zone	5 - 20 km

Modeling seismicity in the seismic source zones

Seismic activity in each of the source zones is modeled using a gridded seismicity approach and a combination of spatially uniform source zones near active volcanoes and smoothed seismicity in other zones. In the gridded seismicity approach, each zone is divided into small cells in which the seismicity depends on both the historical seismicity rate and how far each

cell is from historical earthquakes. Unlike a spatially uniform source zone, the distribution of earthquakes in a smoothed seismicity zone is not uniform.

To generate the stochastic catalog, the Verisk Earthquake Model for Hawaii simulates earthquakes of magnitude 5.0 and greater, as significant damage is unlikely to result from smaller events. However, events of magnitude 3.0 and greater are used to develop the model, as they provide a more complete picture from which to estimate earthquake parameters. Regional seismotectonics and the magnitudes of the largest historical earthquakes in each zone are used to estimate the upper-bound magnitude for each seismic zone.

The Gutenberg-Richter magnitude frequency relationship is used to estimate the earthquake frequencies of various magnitudes. To determine the Gutenberg-Richter a- and b-values, frequency-magnitude distributions are plotted for each source zone in the model, and fits to these distributions are completed by picking a minimum magnitude and using the maximum likelihood method of Aki (1965). Least-square fitting, where each point on the frequency magnitude plot is weighted equally, is used in some cases where there are just a few large historical earthquakes. The following equation defines the frequency-magnitude distribution.

$$\text{Log}(R)=a - bM$$

R is the annual rate of earthquakes greater than or equal to a magnitude M, a is the logarithm of the earthquake occurrence rate above some reference magnitude, and b is the rate at which the logarithm of the cumulative annual frequency decreases as the magnitude increases. The a-values from the distribution are used in the hazard calculation in the five flank zones and the three rift zones.

The following sections provide an overview of the modeled seismicity in each of the source zones.

Volcano flank and Kilauea source zones

Active volcanoes, such as Kilauea, Mauna Loa, and Hualalai, cause most of the earthquakes in the volcano flank and Kilauea source zones with the largest events typically occurring under the flanks of these volcanoes. The risk is greatest from events that rupture through all or most of a zone. The seaward flank zones located in the south and west of Hawaii also pose a risk, as these zones are among the most seismically active in the state having historically hosted some powerful earthquakes. These flank zones store compressional stress as they sit adjacent to active rift zones. In a seaward slip, the flank zone releases this compressional stress causing an earthquake to occur. The landward flank zones are typically less active, as the presence of volcanoes prevents them from moving. Earthquakes rarely rupture across the Kilauea rift zones as these zones form confining, structural boundaries.

The modeled seismic activity in the flank zones is spatially uniform. The a-values in the Gutenberg-Richter magnitude frequency relationship are influenced by the rate of historical events of magnitude 5.0 and greater. A relatively long catalog is essential for modeling seismicity in flank source zones in order to accurately estimate the rate of large earthquakes. Flank earthquake seismicity is captured well by a semi-characteristic model comprised of two Gutenberg-Richter distributions.

Each of the five flank zones are modeled individually for events of magnitude 5.0 to 7.0. For events of magnitude 7.0 to 8.2, the three southern flank zones—Kilauea South, Kaoiki, and

Hilea—are combined into one source zone, because the focal mechanisms of most large earthquakes here have a south- to-southeast slip vector. Large earthquakes in the Kona/ Mauna Loa West and Hualalai / Mauna Loa South flank zones are not modeled because large earthquakes have not historically occurred in those locations. Thus, any estimation of their rates would be very uncertain.

The modeled seismic activity in the Kilauea zones is also spatially uniform. These zones are small and enclose areas where the movement of magma causes earthquakes. The hazard in these areas is low because earthquakes seldom exceed magnitude 4.0, and events occur here relatively infrequently.

Shallow and deep smoothed seismicity source zones

The maximum magnitude for all events in the shallow and deep smoothed seismicity zones on Hawaii is 7.0. The modeled focal depths range from less than 20 km for shallow events to 20 to 60 km for deep events. The Gutenberg-Richter b-values are determined separately for each zone and are assumed to be constant. The a-values vary spatially for each zone and are calculated using the maximum likelihood method of Weichert (1980) in which the number of events with a magnitude greater than 3.0 is counted on a grid. These rates are then smoothed using a Gaussian distribution with a correlation distance of 10 km. The hazard is calculated by summing the rates associated with each grid cell over a range of magnitudes

Northwest seismicity source zone

Seismicity decreases gradually northwest of Hawaii Island. However, the modeled seismicity in the area must capture pockets of relatively high seismicity, such as a cluster of activity located 50 km east of Maui. The model therefore utilizes a linearly ramped a-value in combination with smoothed a-values to capture the hazard. The ramping a-value was calculated by counting the number of events of magnitude 4.0 to 7.0, which occurred at any depth, in 30 km bins along the 220 km long box representing the area. The counts are smoothed by averaging before fitting using the least-squares method. To determine the smoothed a-values for events greater than magnitude 4.0, seismicity is gridded at points 0.02 degrees apart, and the a-values were smoothed with a Gaussian function with a correlation distance of 50 km. The a-values from the ramped and smoothed seismicity are weighted equally in the hazard analysis.

Characteristic earthquakes on crustal faults

The characteristic magnitudes of crustal faults are based on information about local seismotectonics, historical data, and fault characteristics. Verisk seismologists apply a Gaussian distribution around the characteristic magnitude to capture the stochastic nature of earthquake magnitude.

Gridded background seismicity

Background seismicity captures earthquake activity that is not explicitly modeled on known faults or in known subduction zones. Background seismicity is based on the seismicity pattern evident in the historical data, with a degree of randomness imposed. This approach

allows simulated earthquakes to occur anywhere within a source zone, with an annual probability appropriate for each location. Thus, simulated earthquakes are not limited to the locations of previous earthquakes. The frequency-magnitude distribution of the background seismicity in the Verisk Earthquake Model for Hawaii is based on the Gutenberg-Richter distribution.

Verisk scientists analyzed the historical data for Hawaii on a 0.1° X 0.1° degree latitude/longitude grid for each of two focal depth ranges, ≥20 km and <20 km. For each focal depth range, the data were spatially smoothed using two-dimensional Gaussian probability distributions, the parameters of which partially depend on the distribution of the historical events in space and time. The two-dimensional Gaussian distribution is given by the following equation.

$$N_i = \frac{\sum_j N_j \exp\left(-\frac{D_{ij}^2}{L^2}\right)}{\sum_j \exp\left(-\frac{D_{ij}^2}{L^2}\right)}$$

Here, N_i is the number of earthquakes in the i^{th} cell after smoothing, N_j is the number of earthquakes in the j^{th} cell before smoothing, D_{ij} is the center-to-center distance between the i^{th} and j^{th} cells, and L is the correlation distance, which controls the degree of smoothing. The results are smoothed, nonuniform distributions of historical seismicity. Parameters of the Gutenberg-Richter relationship are estimated for each cell and depth range based on these smoothed distributions.

3.3 Modeled earthquake variables

Each event in the model's stochastic catalog is associated with an epicenter, magnitude, rupture length and width, azimuth, dip, dip azimuth, depth, and rupture mechanism. This section provides an overview of these parameters.

Epicenter

The epicenter of an earthquake is the location on the earth's surface directly above the point of initial rupture. Understanding the spatial distribution of earthquake epicenters is greatly facilitated when the faults are visible on the surface. In the case of blind faults, epicenter locations must be inferred from the seismic activity of the area or by subsurface-sounding techniques; many faults remain undiscovered, however.

Magnitude

Magnitude, a measure of the energy released during an earthquake, provides a useful way to compare seismic events. A variety of magnitude scales have been used to describe earthquakes. The Verisk Earthquake Model for Hawaii utilizes the moment magnitude (M_w) scale, which is considered to be superior to other magnitude scales because it is estimated based on the physical properties of the earthquake source and is more accurate for large

earthquakes. Moment magnitude is a more quantitative measure than the Richter magnitude scale, and is applicable over a wider range of rupture sizes.

Focal depth

The focal depth is the vertical distance between the point where the fault rupture originates and the earth's surface (see Figure below). Most earthquakes that take place outside of subduction zones occur within the top 20 km of the crust. Earthquakes that occur deeper than 30 km are usually associated with subduction zones. The focal depth of earthquakes in subduction zones can range from a few kilometers to 700 km from the surface of the earth. Focal depth is an important parameter because seismic waves are attenuated as they travel through the earth away from their source, and deeper earthquakes of a given magnitude typically cause less damage than those at shallower depths. Therefore crustal events, in general, may cause more damage than deeper events not only because they often occur within land areas but also because they are shallower and thus closer to the earth's surface.

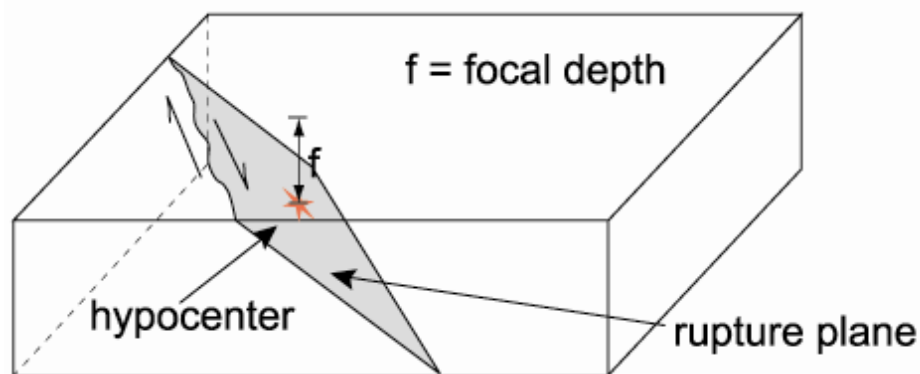


Figure 16. Focal depth

Focal depth is modeled both by a statistical approach based on historical earthquakes and by a physical approach using tectonic characteristics, as discussed earlier in the section on gridded seismicity.

Rupture length

Rupture length is the span of the fault that ruptures during an earthquake. In the Verisk Earthquake Model for Hawaii, rupture length is modeled as a function of the magnitude of the event, with the relationships between rupture length and magnitude determined through empirical regression analysis. The rupture lengths of different types of earthquakes are determined using different magnitude-rupture length relationships appropriate for a particular type of earthquake.

Rupture azimuth and dip angle

The rupture azimuth and dip angle are parameters that define the orientation of a fault. The rupture azimuth is the angle between true north and the line of intersection between the rupture plane and the surface of the earth, measured clockwise from north as viewed

from above. By convention, the dip azimuth is 90 degrees clockwise of the rupture azimuth. Because energy is distributed along the rupture, a fault's spatial orientation is important for damage estimation.

Subduction dip angles are estimated based on seismic-survey data, historical-earthquake rupture parameters, and published research.

Fault rupture mechanism

See [Earthquakes: an overview](#) for a description of the rupture mechanisms of faults. In the Verisk Earthquake Model for Hawaii, the fault rupture mechanisms for earthquakes are based on historical and seismic-survey data.

3.4 Stochastic catalog summary statistics

The Verisk Earthquake Model for Hawaii incorporates a 10,000-year stochastic catalog of 14,823 simulated events, of which 11,717 cause loss to the industry exposure.⁸ Stochastic events included in the model are of magnitude 5.0 and greater.

3.5 Extreme Disaster Scenario (EDS) events

With this model release, Verisk is introducing two Extreme Disaster Scenarios (EDS) for the Hawaii earthquake model. EDS events are meant to provide clients with additional touch points to assist in assessing large loss potential. While they represent unlikely—and in some cases extremely unlikely—scenarios, they are nevertheless scientifically plausible.

Note that these events are not included in the model's 10,000-year stochastic catalogs and no attempt has been made to assign an associated probability of occurrence or return period. They should be seen as deterministic scenarios—or even, if we relax the definition, black swans. The losses from some EDS events may lie beyond the 0.01% exceedance probability (10,000-year return period). Others may be much further down the EP curve, but may be events that impact concentrations of exposure characterized by high take-up rates. They are events that standard stochastic modeling techniques are unlikely to capture, either because of the relative scarcity of historical data or because a full scientific consensus on their likelihood has not yet been reached.

Brief descriptions of the EDS events, the locations of which appear below in [Figure 17](#), are provided below.

Hawaii County M8.2 event

The first EDS earthquake is an M8.2 event that strikes the southeastern side of Hawaii County at a depth of 15.1 kilometers. This event has a higher magnitude than any event in

⁸ Note that stochastic catalogs of 50,000 and 100,000 years are also available

the historical catalog and would generate at least USD 1.2 billion in insured losses (estimate includes demand surge but not worker's compensation), with the greatest losses likely occurring in highly populated cities such as Hilo and Kailua.

Oahu M6.9 event

The second event is an M6.9 earthquake, which strikes Oahu at a depth of 12.5 kilometers. This earthquake has a higher magnitude than any event in the historical catalog for the Oahu area. Given that this temblor's epicenter is located approximately 12.5 kilometers northwest of Honolulu; it would generate at least USD 9.1 billion in insured losses (estimate includes demand surge but not worker's compensation).



Figure 17. Epicenters of EDS events in the World Scenarios event set

3.6 Validating stochastic event generation

Each component of the Verisk Earthquake Model for Hawaii has been validated against data obtained on historical events. This section provides a few exhibits that validate the stochastic event generation procedure.

Validating event frequency

Figure 18 shows a comparison of the historical and simulated frequency magnitude distributions for events that take place on Hawaii. Note that the vertical axis displays the total annual event rate at or above each magnitude. As discussed earlier in the section, events in the simulated catalog are for M5.0 to M8.2 only, but the historical catalog contains events of M3.0 and higher. The Figure below indicates that the simulated catalog is consistent with the historical data. Also, note that the Verisk model follows the USGS model for Hawaii and that the magnitude-frequency distribution in the Verisk model is fully compatible with those from the USGS model.

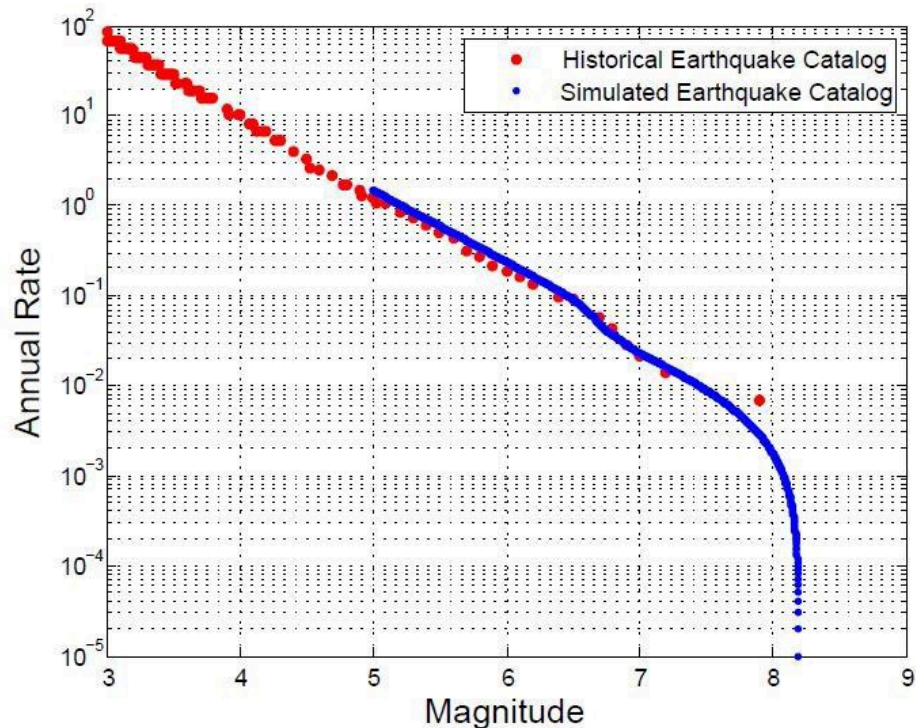


Figure 18. Frequency-magnitude distributions for the simulated and historical catalogs, Hawaii Island

Validating focal depth

Figure 19 compares the densities of historical and simulated events as functions of depth in Hawaii. Note that the graphs were created by separating out the total number of events in each distribution into bins corresponding to 2.5 kilometer increments of depth. The density for each bin is calculated by dividing the number of events per bin by the total number of events in each distribution.

Note that for the simulated distribution, there are no events corresponding to depths greater than 60 kilometers and for the historical distribution there are only five events corresponding to depths greater than 60 kilometers.

The Verisk model used the depths of all events in the USGS historical catalog to produce the historical depth distribution graph. The depths of simulated events have been assigned

uniformly, depending on the seismicity component, with the requirement that the earthquake ruptures do not extend above the surface. Note that the distributions compare well.

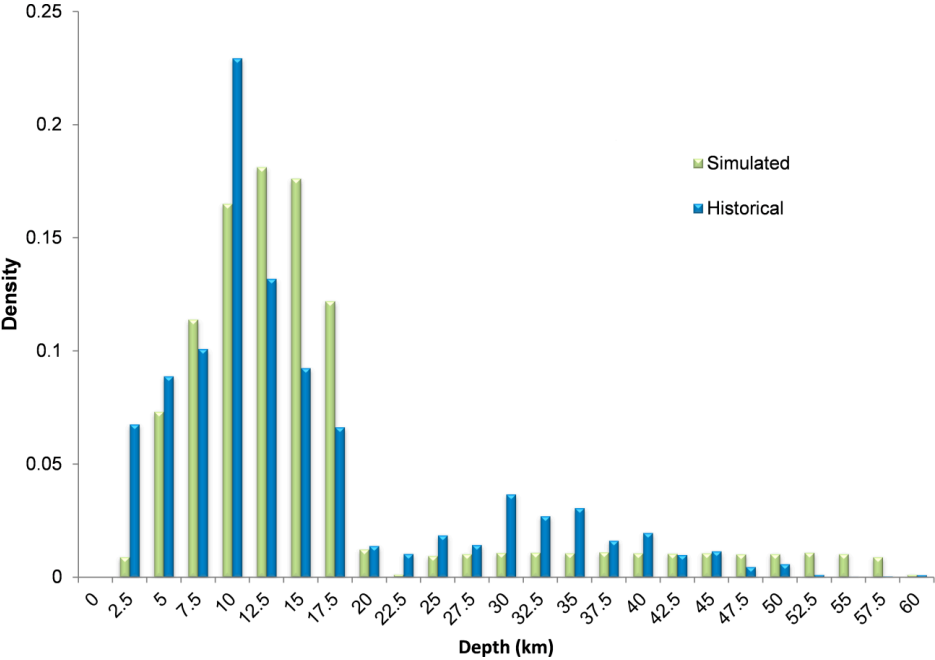


Figure 19. Cumulative historical vs. simulated depth distributions

4 Local Intensity Calculation

The intensity of ground motion during an earthquake can range from barely perceptible trembling to violent shaking, depending on the magnitude of the event, distance from the rupture to the affected site, geological characteristics of the region, and local site conditions. For accurate loss analysis, it is necessary to calculate the intensity of ground shaking at all exposure locations affected by each event in the stochastic catalog. Ground motion prediction equations (GMPEs) are commonly used for this purpose. The effects of the local site conditions, in terms of site amplification factors, are added to the GMPE ground motion estimates for the reference site conditions.

4.1 Ground shaking intensity

Ground shaking intensity is commonly measured in terms of peak ground acceleration (PGA) and spectral acceleration (Sa). The peak ground acceleration is the maximum value of the ground acceleration and is measurable in the horizontal and vertical directions. Spectral acceleration approximates what a building experiences as modeled by a particle mass on a massless vertical rod having the same natural period of vibration as the building.

Different buildings respond differently to the ground motions of a particular earthquake. A building will be most sensitive to ground motion whose dominant frequency is close to the natural period (or natural frequency of oscillation) of the building. Thus, while PGA is the maximum acceleration experienced at a free ground surface, spectral acceleration is more relevant for the estimation of building damage.

4.2 Ground motion prediction equations

Engineering seismologists create empirical ground motion prediction equations, or GMPEs, to estimate earthquake ground motion intensity primarily as a function of magnitude, distance, and rupture mechanism and geometry. These equations, which have also been called attenuation relationships, describe how the intensity of certain ground motion parameters decay as the seismic waves propagate outward from the rupture source.

Typically, ground motion decreases with distance due to geometric spreading and the absorption and scattering of energy as the waves travel through the earth. However, particularly complex phenomena can sometime significantly amplify ground motions even at great distances from the rupture; for instance, deep alluvium basins, such as those under Los Angeles and Mexico City, can amplify long period ground motions, and soft, shallow soils over bedrock or stiff soil formations can amplify ground motions at a variety of seismic-wave frequencies.

It is important to note that in many regions of high seismicity, GMPEs are based on physical models of the rupture and wave propagation but are corroborated by an abundance of ground

motion recordings of past earthquakes, especially for small and moderate magnitude events (5.5 to 7.0) and moderate to large distances (greater than 10-20 km). The ground motion prediction for such events and distance range is extremely robust, while for larger magnitude events and short distances it is more uncertain.

On the other hand, in low seismicity regions away from the tectonic plate boundaries, GMPEs rely much more on physical models because the very scarce existing empirical recordings are only available for small local earthquakes of minor engineering importance or are borrowed from other areas of the world where rare large magnitude of similar tectonics have been observed and recorded in historical times. In general, therefore, GMPEs for these low-seismicity regions are associated with a higher degree of uncertainty than the GMPEs for more seismically active regions.

The general form of the GMPEs used in the Verisk Earthquake Model for Hawaii is as follows:

$$S_a = f(M, D, d, C, F, T)$$

where

S_a = spectral acceleration or peak ground acceleration

M = earthquake magnitude

D = distance from rupture plane

d = focal depth

C = site condition

F = faulting mechanism

T = period (inverse of frequency)

The parameters of the GMPEs vary from one region to another, reflecting the underlying geology of the region and the nature of tectonic stress. The Verisk Earthquake Model for Hawaii incorporates a weighted combination of GMPEs for shallow source-zone (depth < 20 km) events, and deep source-zone (depth \geq 20 km) events. For shallow source-zone events, the model utilizes a weighted combination of Atkinson (2010), and the Next Generation of Ground Motion Attenuation equations (NGA) of Abrahamson and Silva (2008), Campbell and Bozorgnia (2008), and Chiou and Youngs (2008). For deep source-zone events, the model utilizes a weighted combination of Atkinson (2010), Atkinson and Boore (2003), and Youngs et al. (1997). References for all GMPEs and the weighting factors used for Hawaii are given in the following Tables.

Table 5. Ground motion prediction equations and weighting factors used for shallow source-zone events

Ground Motion Prediction Equation	Weighting Factor
Atkinson (2010)	.25
Abrahamson and Silva (2008)	.25
Campbell and Bozorgnia (2008)	.25
Chiou and Youngs (2008)	.25

Table 6. Ground motion prediction equations and weighting factors used for deep source-zone events

Ground Motion Prediction Equation	Weighting Factor
Atkinson (2010)	.50
Atkinson and Boore (2003)	.25
Youngs et al. (1997)	.25

4.3 Site classification

As seismic waves travel through the earth from the rupture source to the earth's surface, earthquake ground motion intensity may be amplified or de-amplified due to local site conditions. The degree of amplification depends on the level of ground motion, the material properties of the site, and the frequency composition of the incoming waves.

If the incoming seismic waves are of low-to-moderate intensity, a site with a soft surface geology may experience significantly higher levels of ground motion than a rock site, especially from low-frequency seismic waves, which are most damaging to mid- and high-rise buildings. However, if the incoming ground motion is of a high intensity, the process is more complex due to the nonlinear behavior of soil materials.

Soil behaves in a linear fashion when seismic waves are weak. That is, the wave amplitudes increase as seismic stress increases. However, as the intensity of ground shaking increases, the reduced strain in the soil layers also increases, which results in a higher seismic energy absorption within the soil layers. This phenomenon will reduce the level of ground motion amplification capability of the shallow soil layers.

The expanded National Earthquake Hazard Reduction Program (NEHRP) soil classifications account for variations in ground motion amplification, since the amplification factors are calculated directly from the mean shear-wave velocities. These soil classes are defined in the Table below, which also lists the average shear-wave velocities for each soil class. Note that intermediate soil types are expressed as a combination of two classes. The average shear-wave velocity for a given soil type is determined from the shear-wave velocities observed at locations identified with that soil type.

Table 7. Soil classifications and average shear-wave velocities

Soil Class	Description	Average Shear Wave Velocity (m/s)
A	Very hard rock (crystalline rock with few fractures)	1620
AB	Hard rock	1150
B	Firm to hard rock	1050
BC	Firm rock	760

Soil Class	Description	Average Shear Wave Velocity (m/s)
C	Soft to firm rock (gravelly soil and soft rock)	540
CD	Soft rock (gravelly and stiff soil)	370
D	Stiff clay and sandy soil	330
DE	Soft soil to firm soil (silty clay and sand)	280
E	Soft soil (includes mud)	160

The Verisk Earthquake Model for Hawaii uses surficial geological maps and available shear wave velocity measurements to develop soil classification maps at various scales. The following Table provides the map scale, model resolution and references of the soil maps.

Table 8. Soil maps implemented in the Verisk Earthquake Model for Hawaii

Map Scale	Model Resolution	Region	References
1:100,000	100 m	Hawaii Island	USGS
1:62,500	75 m	Kauai, Lanai, Maui, Niihau, Oahu	Hawaii Commission on Water Resource Management

[Figure 20](#) shows the soil classification maps for Hawaii County. The soil map is consistent with the findings from the SASW (spectral-analysis-of-surface-waves) surveys performed by the University of Texas, Austin (UT); the University of Arkansas; and URS Corporation (Wong et al., 2011) and other borehole data. Previous to the SASW surveys, areas of basalt around much of the island were thought to be of hard consistency. The measurements indicated that the basalt is actually soft rock. The SASW surveys obtained shear wave velocity data in the ground beneath the 22 USGS free-field strong-motion sites by generating surface waves at one strong-motion site and recording them as they pass by pairs of receivers at other sites. The shear wave velocity measurements were then correlated to a geologic map which covers Hawaii Island at a scale of 1:100,000.

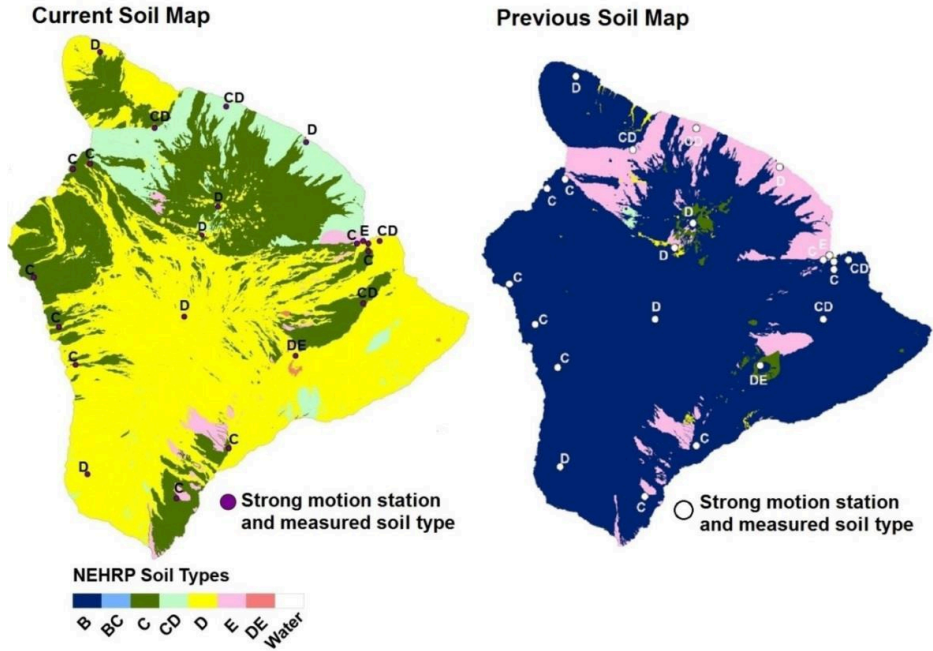


Figure 20. Current and previous soil classification maps for Hawaii Island

Figure 21 shows the soil classification map for Niihau, Kauai, Oahu, Molokai, Lanai, Kahoolawe, and Maui Islands.

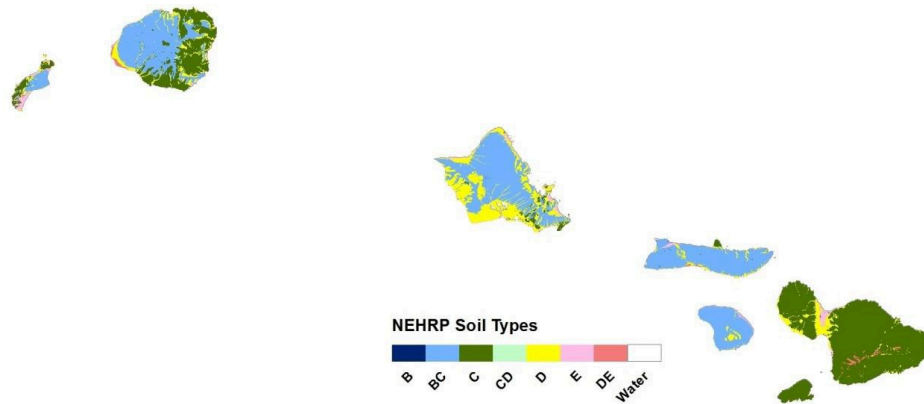


Figure 21. Soil classification map for Niihau, Kauai, Oahu, Molokai, Lani, Kahoolawe, and Maui Islands

4.4 NGA local site amplification

In the Verisk Earthquake Model for Hawaii, local site amplification is calculated using an empirical algorithm that relates the V_{s30} ⁹ of a site (which is inferred from local site condition maps) to its amplification factor. The algorithm used in the Verisk model was developed as a part of the 2008 Next Generation Attenuations (NGA) project (Power et al. 2008). In this project, researchers developed analytical and parametric site response relationships to explore the non-linear and linear responses of shallow soil layers to ground shaking (Walling et al. 2008).

Prior to the development of the NGA site amplification algorithm, the National Earthquake Hazard Reduction Program (NEHRP) site conditions were used to calculate earthquake wave amplification or de-amplification at different locations. Although both methods (NGA and NEHRP) use V_{s30} values to quantify local site amplification, there are two primary advantages to using the NGA algorithm:

- In the NGA database, V_{s30} values are assigned to each strong motion recording station based on borehole and site observations, age, and other geological and technical information. Thus, the NGA database contains a comprehensive set of V_{s30} measurements for quantifying ground motion amplification. In contrast, the NEHRP database contains relatively few observations of amplified ground shaking at soft soil sites, and the majority of these observations come from just two earthquakes (the 1989 Loma Prieta and the 1994 Northridge earthquakes).
- Use of the rich NGA project database has allowed several studies to better quantify the non-linear behavior of upper soft ground layers during different levels of ground shaking (Power et al. 2008).

Thus, use of the NGA equations has significantly improved our understanding of site responses to different levels of ground shaking. These equations are used to calculate local site amplification in the Verisk model. For comparison, amplification factors yielded by the NGA and the NEHRP methods (for a reference engineering site condition with V_{s30} of 760 m/s) are provided in the Figure below.

Note that for soil classes B (firm to hard rock) and C (soft to firm rock), there is good agreement between the amplification of ground shaking predicted by these two methods for all levels of ground motion. For soft soil classes D and E, however, the NGA and NEHRP methods predict quite different amplification factors. As highlighted above, this difference is due to the improved understanding and modeling of shallow site responses to ground shaking that is facilitated by the NGA database.

⁹ V_{s30} = the average shear wave velocities for the top 30 meters of the earth's surface.

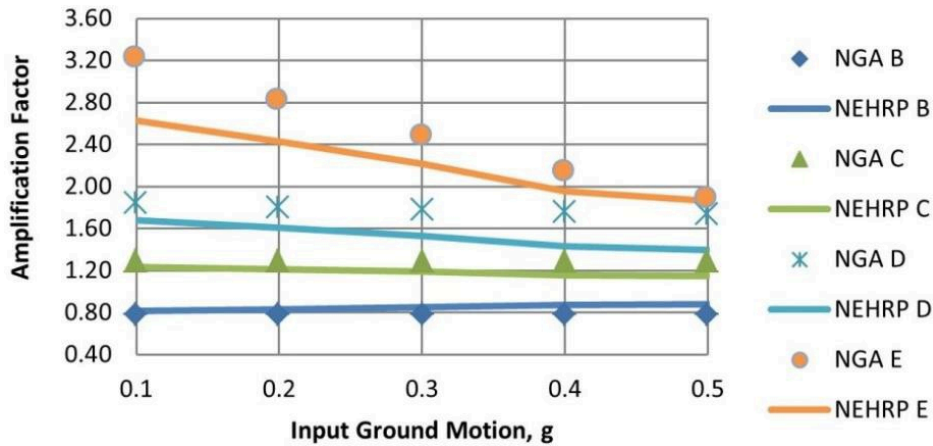


Figure 22. Comparison of NGA and NEHRP site amplification factors with respect to a reference engineering rock site for long period waves.

4.5 Ground motion intensity and spatial correlation

The assessment of ground motion intensity has traditionally been based on an approach that used event magnitude, the source-to-site distance, and the local soil conditions. These calculations also accounted for variability in the ground motion, based on observed deviations during historical earthquakes. The variable ground motion intensities were included in the equations by means of a lognormally-distributed error term, also known as a "residual."

Recent studies of these ground motion residuals show that, rather than being randomly distributed through an area during an earthquake, there is a distinct correlation between residuals at one site and residuals at nearby sites. Observations have shown that if the ground motion is higher than expected at a particular site, it is more likely that a nearby site will also experience higher-than-expected ground motion.

Because the USGS national seismic hazard maps are designed to capture the hazard at any given single site, the focus of the USGS and developers of the NGA equations has not been on correlated ground motion. However, such correlation has important implications for portfolios of properties held by insurance providers. For example, these pockets of high or low ground motion may be very large and encompass an entire metropolitan area. When a higher-than-expected ground motion pocket occurs in a densely populated area, the losses will be much larger than expected everywhere in that area. The converse is true when a lower-than-expected ground motion pocket occurs in a densely populated area. The Verisk Earthquake Model for Hawaii explicitly takes into account the effects of site-to-site correlation of ground motion intensity measurements when estimating the loss due

to seismic activity for spatially extended portfolios.^{10, 11} The modeling of ground motion correlation by Verisk is therefore a departure from the USGS national seismic hazard maps. [Figure 23](#) provides a visual illustration of ground motion correlation for the 1994 Northridge, California earthquake. Even though this event did not take place in Hawaii, it provides an excellent example of how spatial correlation is implemented in the Verisk Earthquake Model for Hawaii. [Figure 23a](#) shows a recreation of the 1994 Northridge earthquake's ground motion footprint using the latest NGA equations without modification. [Figure 23b](#) is considerably more complex because it takes output from the NGA equations and modifies it using information on soils and basin effects. [Figure 23b](#) represents median ground motion as calculated by the Verisk model. [Figure 23c](#), however, is the best estimate of "actual", or observed, ground motion taken from the USGS ShakeMap.

While the overall comparison between [Figure 23b](#) and [Figure 23c](#) is reasonably good, the actual ground motion footprint reveals pockets of very high concentrations of ground motion. In this case, the pockets are located in heavily populated areas, which led to losses that were much higher than would otherwise be expected from an earthquake of Northridge's magnitude (M6.7) and epicentral location.

¹⁰ For further technical details, see P. Bazzurro et al., "Effects of Spatial Correlation of Ground Motion Parameters for Multi-Site Seismic Risk Assessment: Collaborative Research with Stanford University and Verisk" available on the USGS website.

¹¹ For further details on the methodology used by Verisk to simulated ground motion with spatial correlation, see Park, J., Bazzurro, P. and J.W. Baker "Modeling Spatial Correlation of Ground Motion Intensity Measures for Regional Seismic Hazard and Portfolio Loss Estimation," Proceedings of ICASP10 (Tokyo, Japan, July 31-August 4, 2007)

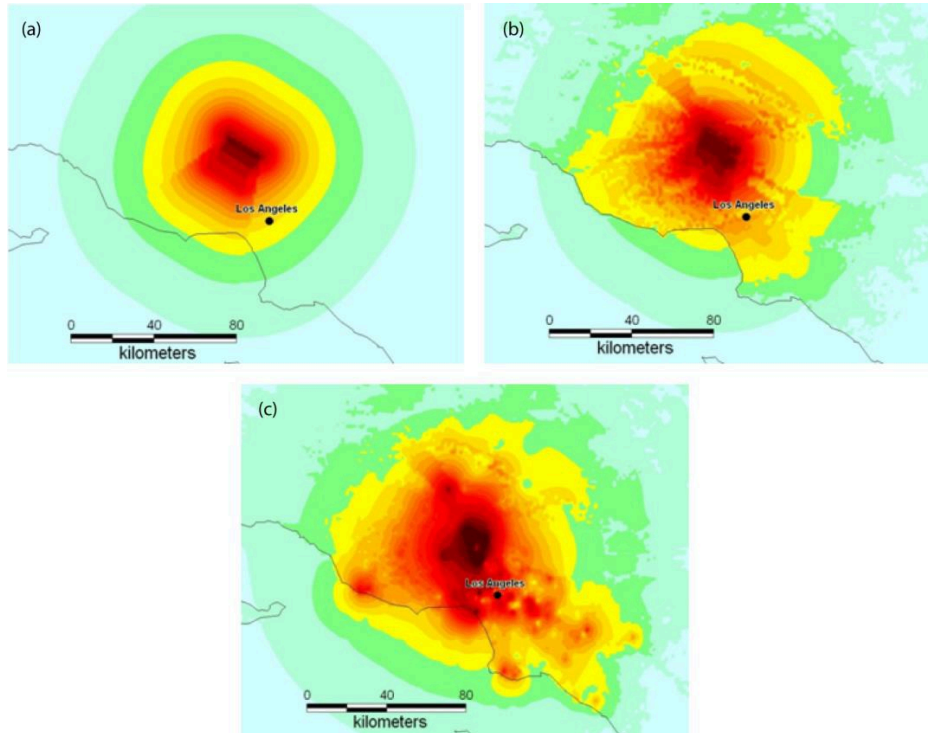


Figure 23. Recreations of the 1994 Northridge earthquake’s ground motion footprint. (a) using the latest NGA equations without modification, (b) using the latest NGA equations including information on soils and basin effects, and (c) using data from the USGS shakemap

The impact of these spatial patterns and the interaction with the distribution of risks or assets in a portfolio can generate very different loss estimates. Indeed the next earthquake that occurs, even if it occurs on the Northridge fault, is not going to look like the map in [Figure 23c](#). Using actual ground motion recordings as well as the spatial correlation model, the Verisk model can generate ground motion footprints of any historical events that are consistent with recorded peak ground motion parameters. By generating these accurate and consistent simulated maps dozens or even hundreds of times, the model produces a realistic distribution of losses and one that is consistent with observed losses.

[Figure 24](#) shows an example of this concept, again applied to the 1994 Northridge earthquake. The figure shows four of 50 simulated ground motion maps of the Northridge earthquake that are consistent with recorded ground motions and allow for spatial correlation. The chart on the right shows the resulting loss distribution from all 50 simulations. The observed (reported) losses for Northridge fall very close to the middle of the distribution.

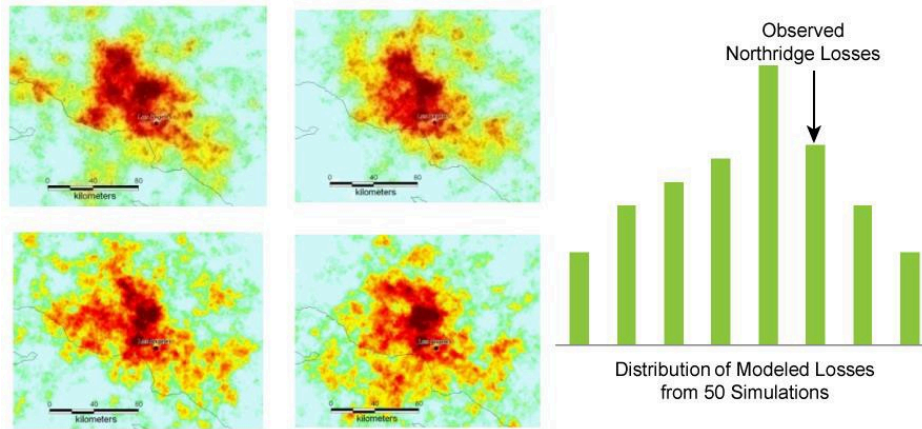


Figure 24. Multiple ground motion maps with spatial correlation and the corresponding distribution of modeled losses for the 1994 Northridge earthquake

Effects of Spatial Correlation on Portfolio Losses

As mentioned earlier, site-to-site correlation increases as the distance between the sites decreases, producing pockets of unexpectedly high or low ground motion. This of course means that the correlated residuals have a greater effect on clustered exposures, which has important implications for portfolios of properties. For example, the pockets of high or low ground motion may be very large and encompass an entire metropolitan area. When a high ground-motion pocket occurs in a densely populated area, the losses will be much larger than expected everywhere in that area. The converse is true when a lower-than-expected ground motion pocket occurs in a densely populated area.

While large portfolios that are distributed over a large area will, in general, be less affected by spatial correlation than smaller, more concentrated portfolios, in both cases failure to account for ground motion correlation will underestimate the probability of both very high and very low losses, the former being the more serious matter.

The Figure below shows the impact on the loss exceedance curve. When ground motion uncertainty is considered with spatial correlation, the annual exceedance probability tends to drop more steeply for frequently exceeded losses, thereby lowering the overall losses in this part of the curve. However, the annual exceedance probability then levels and extends farther to include the larger and less frequent losses. Because the exceedance probability curves generated using spatial correlation are based on many more simulations and hence more information, they are more robust—particularly in the tails of the distribution.

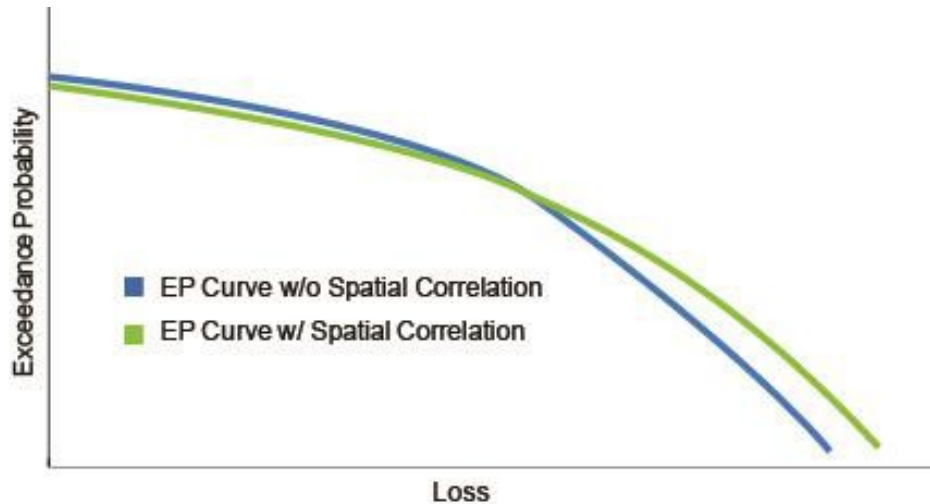


Figure 25. Loss exceedance curves with (green) and without (blue) spatial correlation

4.6 Validating local intensity

To accurately estimate losses from earthquakes, a comprehensive risk analysis model must be calibrated against losses from historical events. An important component of the calibration process is the simulation of ground motion at exposure locations. The Figure below compares the simulated (indicated by the background coloration) vs. observed (indicated by the colored circles) ground motion intensities for the 2006 Kiholo Bay earthquake. This M6.7 event occurred just off the northwest coast of Hawaii Island causing damage to nearly 1800 buildings with the worst damage occurring along the northern and western portions of Hawaii Island.

The USGS shake maps, which incorporate ground motion recordings, geological conditions, and earthquake location and magnitude, were used to obtain data for the simulated ground motion. As discussed in the prior section, these maps represent the best estimate of actual ground motion. The below figure indicates that the observed ground motion intensities compare well to the simulated intensities.

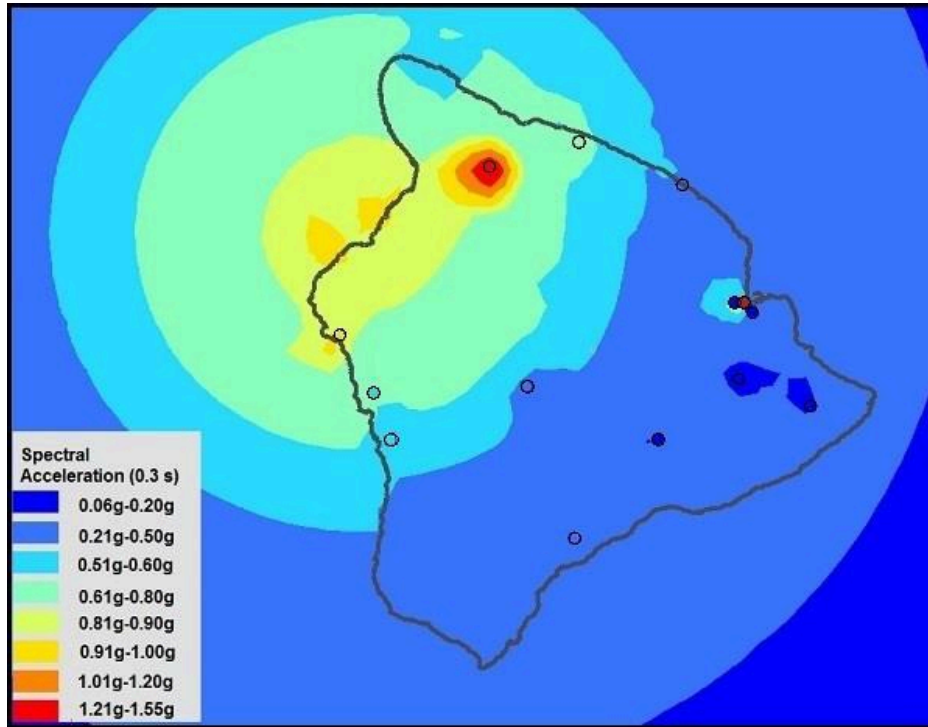


Figure 26. Modeled vs. observed spectral acceleration, 2006 Kiholo Bay earthquake

It is important to note that [Figure 26](#) also shows how the actual ground motion varies through the use of site-to-site correlation. As discussed in the previous section, site-to-site correlation provides a more realistic stochastic ground motion simulation field by taking into account the effects of ground motion uncertainty. Conversely, the ground motion footprint in the Figure below ([Figure 27](#)) does not include information on observed ground motion and thereby assumes that all locations follow the median GMPEs. [Figure 27](#) does not compare as well as [Figure 26](#) does to the observed ground motion intensities thereby validating the use of site-to-site correlation in the Verisk model. Note that the color scale in [Figure 27](#) is the same as that in [Figure 26](#), and the brown trace shows the position of the rupture projection for this event.

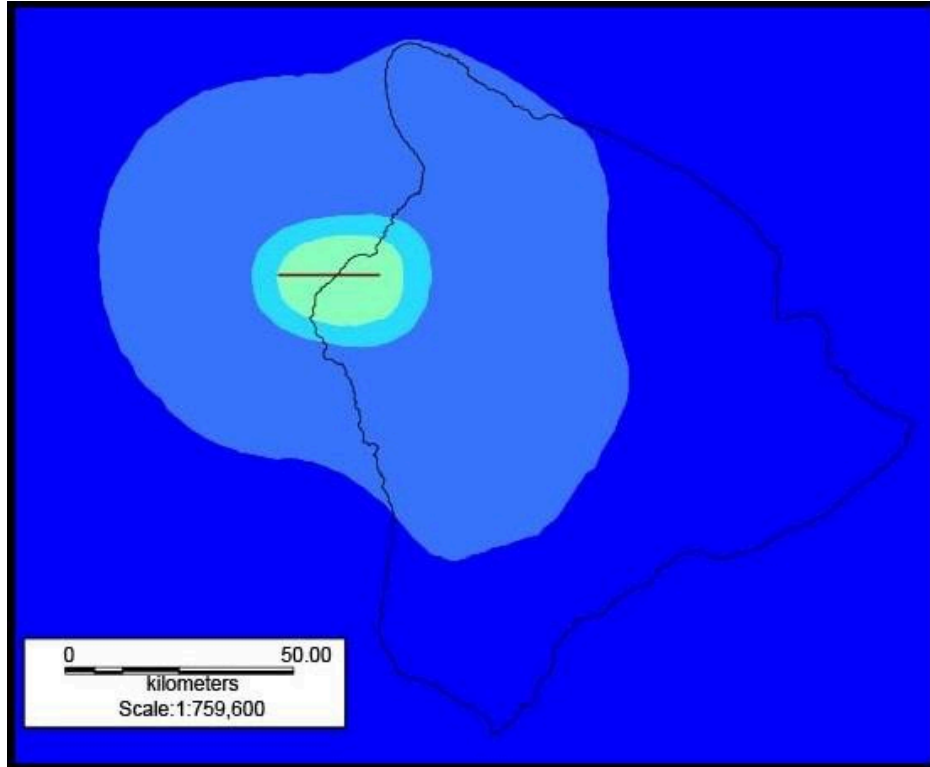


Figure 27. Spectral acceleration (0.3s) for the 2006 Kiholo Bay earthquake using median ground motion without stochastic ground motion simulation

5 Damage Estimation

After the ground-motion intensity is estimated at each location, damage estimates are generated for the exposures. To calculate losses, the appropriate damage function is applied to the replacement value of the insured property. The damage functions for the Verisk Earthquake Model for Hawaii were developed using the latest published information regarding various construction types and their ability to withstand earthquake ground motion. The damage functions incorporate the seismic codes of each region and their enforcement, local construction practices, construction material, building height, and the year built of each property.

This chapter is one of the most extensive in the document. It begins with a brief overview of local construction classes and the history of the seismic code. From there, the various methods that Verisk researchers use to develop damage functions are discussed. Then, various damage functions are introduced. The next sections discuss uncertainty in the damage functions along with the builders' risk line of business, contents and automobile damage, and workers compensation. The final section provides validation for the damage functions.

5.1 Building classification

The major construction classes that are supported for residential buildings, commercial and industrial buildings, and industrial facilities are listed in the Chapter Verisk Earthquake Model for Hawaii in Touchstone Chapter.. This section discusses some of the most prominent of these classes, and how each is affected by ground shaking due to earthquakes. For more information about construction classes in both Hawaii and the continental United States, refer to the document Verisk Industry Exposure Database for the United States.

Residential buildings

Most of the single family and duplex homes in Hawaii consist of wood frame construction. Approximately 60% of these homes, primarily the newer ones, are of conventional, or double wall, construction. Double wall construction uses sheathed wood studs to bear the gravity load. About 40% of these wood frame residences use a light wood frame, or single wall, construction method, which consists of continuous one inch thick plywood boards that act as load-bearing walls. The roof systems for both types of wood frame construction consist of composite shingles on wood decking or corrugated metal decking attached to wooden rafters. Double wall construction typically performs better than single wall construction during earthquakes.

Many of the wood frame residences in Hawaii utilize a post and pier system which consists of floor joists and girders supported by timber posts bearing on precast concrete footing blocks—commonly referred to as “tofu blocks.” This structure raises homes off the ground on unanchored wooden piers. Post and pier foundations were popular until the mid-1970s because of their simplicity, reduced cost, and thermal and pest advantages. However, these

buildings are susceptible to foundation damage during ground motion from an earthquake. Many of these homes were damaged during the 2006 Kiholo Bay earthquake.

Aside from light wood frame and conventional wood frame single family homes, Hawaiian architecture also includes indigenous homes, such as hale structures and mission homes, and “plantation style” homes. Hale structures are open-walled buildings constructed of native grasses and wooden posts. These structures are explicitly included in the model. The thatched roofs of hale structures may lack gables (termed “open-ended hale”), or may have gables composed of additional thatching. Both types of hale are shown in [Figure 28](#).

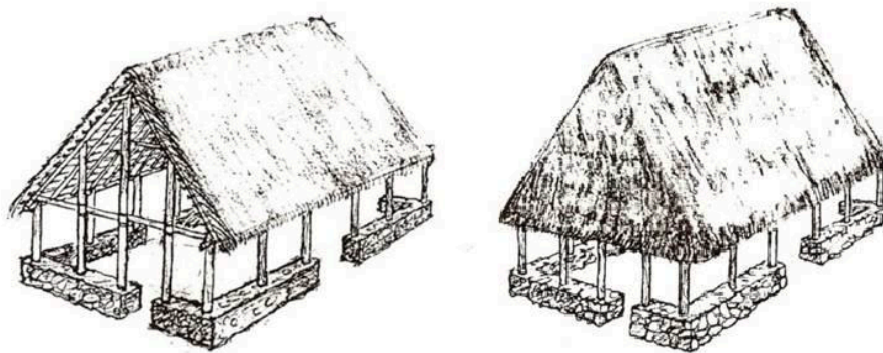


Figure 28. Open-end (left) and thatched-end (right) hale structures (Source: “Adoption of Chapter 15-110 Rules Pertaining to Indigenous Hawaiian Architecture Structures,” County of Maui)

The mission style of homes feature high thatched roofs and walls made from wooden siding or coral blocks. During the 20th century, sugar and pineapple plantations flourished on Hawaii, inspiring a plantation style home that typically features a large porch with a long overhang. These overhangs may help to keep the home cool, but also make the structure more susceptible to earthquake damage if they are not properly braced.

Some Hawaiian homes contain unreinforced masonry in the form of concrete masonry units (CMU) or cemented rubble masonry (CRM). Shear walls, infill walls, and covers for concrete columns are often made from CMUs, which are subject to cracking and in- and out-of-plane displacement during earthquakes. The walls, columns, chimneys, and other architectural features of some older homes are made of a combination of local stone and mortar, or CRM. Possible CRM damage during earthquakes includes the shifting of stones and the collapse of walls. The partial collapse of walls made from CRM was observed during the October 15, 2006 Kiholo Bay earthquake (Gupta and McDonald, 2008).

Most apartments and condominiums in Hawaii are characterized by wood frame, concrete shear wall, reinforced masonry, or light steel construction, and are thus similar to commercial buildings with respect to their engineering requirements. In Hawaii, apartments and condominium buildings may be low, mid, or high-rise structures. Steel or reinforced concrete elements include beams, columns, or shear walls, which make up the building’s primary lateral load-resisting system. The configuration and the construction methods used for these systems vary considerably between different building types. As a result, different building types may show significantly different behavior during ground shaking.

Commercial buildings and small-scale industrial facilities

The majority of commercial buildings and small-scale industrial buildings in Hawaii are of wood frame, concrete shear wall, reinforced masonry, reinforced concrete, or light steel frame construction. Some examples of small industrial facilities include small-scale mining operations, small fabrication plants, and some food and drug processing plants. The Figure below shows one example of a small industrial plant. Note that these commercial and industrial structures are included in the 300-series of occupancy classes in Touchstone.



Figure 29. Example of a small-scale industrial facility

The majority of engineered buildings in Hawaii have infill walls between concrete-frame columns that stop short of the upper beam, in order to leave space for windows. During an earthquake, this irregularity alters the building's strength and stiffness, causing deformation and cracking of the short columns (Gupta and McDonald, 2008). Also, due to the corrosive nature of the salt-rich environment, the condition of the building stock in Hawaii, particularly

of commercial and industrial buildings, such as reinforced concrete structures, is often poor, and as a result, could be more vulnerable to shake damage in an earthquake.

Large-scale industrial facilities

Large-scale industrial facilities have diverse classes of structures or components, including stacks, cooling towers, pipes, and tanks located in a widespread open area. All of these different components, have different vulnerabilities when subjected to ground shaking. Examples of large industrial plants and their components are shown in the Figures below. Refer to [Large-scale industrial facility damage functions](#) for details on how large-scale industrial facilities are modeled. Note that large-scale industrial facilities are included in the 400-series of occupancy classes in Touchstone.



Figure 30. Examples of large-scale industrial facilities.

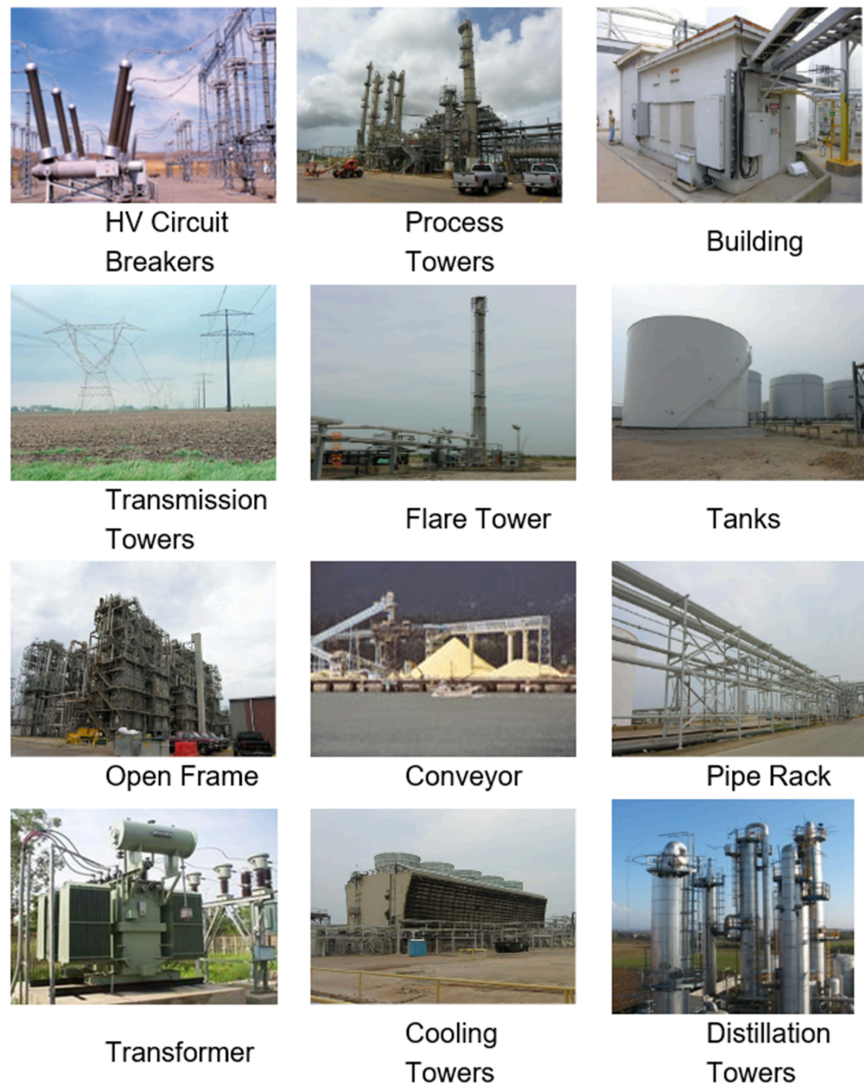


Figure 31. Examples of some industrial facility components

5.2 Evolution of seismic building codes in Hawaii

Today, there are similar building standards across Hawaii. Yet, each Hawaiian county has a unique history of seismic building code implementation and varying degrees of construction enforcement. Furthermore, while the general history of Hawaiian building codes parallel those in the continental United States, the timing of building code adoption may differ greatly between the mainland and Hawaii. Seismic codes were typically first implemented in the continental United States, and then adopted in Hawaii a few months to years later.

In 1950, the Hawaiian counties adopted their first seismic building code which was based on the 1949 Uniform Building Code (UBC 1949). This code contained seismic hazard maps for only the continental United States and provisions for unreinforced masonry. The UBC was updated again in 1973, 1976, and 1979, and all of the Hawaiian counties adopted at least one of these editions. Both the 1973 and 1976 updates were based on research from the damaging 1971 San Fernando Valley earthquake, which resulted in the collapse of multiple freeway overpasses and numerous older, unreinforced masonry buildings, as well as the destruction of the then newly built Olive View Hospital in Sylmar, California. Accompanying the enforcement of this code, there was a shift to utilize ductile concrete frames in contrast to non-ductile frames. The 1979 edition of the UBC introduced the R factor to reduce the elastic demand on structures.

In 1976, the United States passed the Manufactured Home Construction and Safety Standard so as to regulate the construction of mobile, or manufactured, homes. All of the Hawaiian counties implemented this standard simultaneously.

In 1985, the UBC was updated again, and when Honolulu adopted this code in 1987 and Maui in 1989, they added the additional requirement that single-family homes employ roof-to-wall uplift ties. While this additional requirement was a result of lessons learned from the damaging Hurricane Iwa, which tracked through Hawaii in 1982, the requirement concurrently improved seismic design by providing better lateral load path connections. Hawaii County did not add this requirement until it adopted the 1991 version of the UBC—the first building code to include seismic hazard maps for Hawaii. These maps separated Hawaii into multiple seismic zones based on the 1976 USGS seismic hazard maps, although the seismic hazard was underestimated in Honolulu and Hawaii Counties. The UBC was updated again in 1994, during which a limit was placed on the period of vibration, leading to larger seismic loads.

The 1997 release of the UBC featured a major update to the seismic provisions. In addition, the seismic zones were also updated to be consistent with the 1996 USGS seismic hazard maps. Both Honolulu and Maui adopted this code in 2000, while Kauai adopted it in 2001. Hawaii County did not adopt this code as it continued to abide by UBC 1991. Providing further evidence of the variation in the timing and type of code adoption amongst the counties, Honolulu was the only county to adopt the 2003 International Building Code (IBC 2003) in 2006. The timing and adoption of building codes from 1956-2006 is shown graphically in the Figure below for each county of Hawaii.

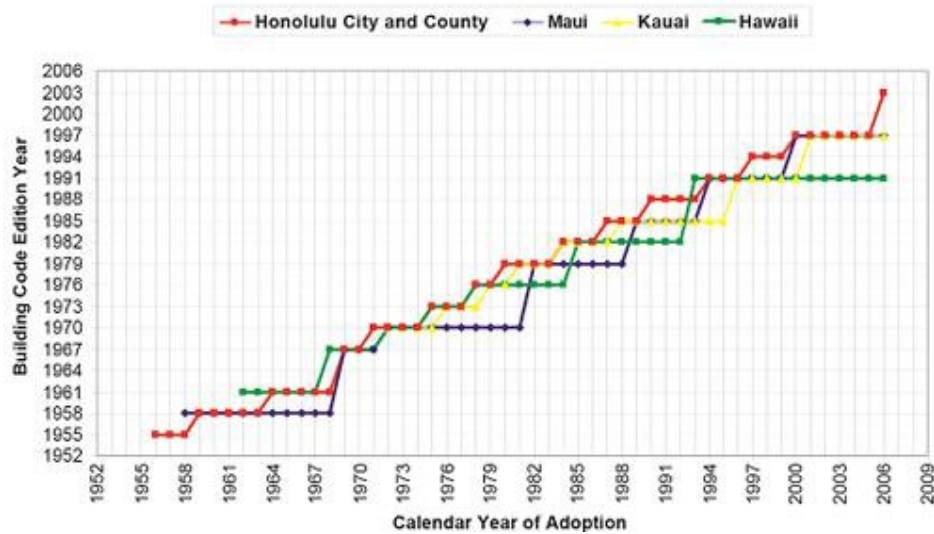


Figure 32. History of building codes in effect in all four Hawaiian counties, 1956-2006 (After: Uniform Statewide Building Code Task Force, 2005)

Between 2004 and 2007, the legislature proposed building code provisions for indigenous Hawaii architecture, particularly for traditional grass hut structures with thatched roofs (Hale). The legislature was first adopted in Maui around 2004 and 2005, and then statewide in 2007 (State of Hawaii Senate Resolution, 2007).

In 2010, the state of Hawaii adopted IBC 2006 as a statewide building code that would be uniform across all counties (State of Hawaii Annual Report, 2010). The IBC provides simplified engineering requirements for small wooden structures, and includes seismic hazard maps for Hawaii rather than seismic zones.

Despite recent advances, the building codes in Hawaii still do not require the removal, replacement, or retrofitting of older structures. The state's imposed shipping and labor costs already make construction in Hawaii expensive, and earthquake-proofing a building can add 10-20% to the cost. Furthermore, the various counties still do not use the same code regulations exactly, nor is the enforcement uniformly stringent across counties. As a result, the modeled age bands in the Verisk Earthquake Model for Hawaii were developed to reflect the utilization and enforcement of specific construction types in the five Hawaiian counties. Note that there are no modeled age bands for the indigenous building construction type.

5.3 Shake damage

Earthquake-induced building damage is brought on by a building's dynamic response to ground motion, which depends on characteristics of both the ground motion and the structure itself. The ground motion characteristics with the greatest impact on damage are the amplitude and frequency composition of the incoming seismic waves. These

wave characteristics vary by location and depend on the local geological and geotechnical conditions along the path from the earthquake focus to the building site. A building's dynamic response to these wave characteristics depends on whether or not the ground motion contains a component that is close to the natural period of the building and if so, whether the building stretches beyond its elastic limit.

A building's natural period of vibration, or the reciprocal of natural frequency, is one of the most important characteristics for determining a building's response to ground motion. A building's natural period is the time required for the building to make one complete cycle of free vibration. Natural period is a function of a building's mass and stiffness distribution, which in turn is determined by construction type, dimension and layout, load bearing and lateral-force resisting systems, and structural details. In general, buildings that are heavier and more flexible have a longer period than buildings that are lighter and stiffer. For this reason, a tall building has a longer natural period than a shorter building of similar construction. Also, a wide building has a smaller natural period than a narrow one of similar construction.

A building responds to ground motion in a complex manner. As the earth shakes, a building's foundation is displaced and deformed. Building mass concentrations at floor level generate inertial resistance, and as a result, the building begins to vibrate as though subject to lateral forces proportional to the product of the mass and the floor acceleration. Simultaneous movements of both the ground and the building impose coupled inertial forces on the building. When the ground vibration contains a component that is close to the natural frequency of the building, the ground motion will amplify the vibrations of the building through a phenomenon known as resonance. Amplification causes increased structural damage.

A building may not respond completely elastically to seismic waves. Depending on the severity of the shaking, a structure can deform beyond its elastic limits and develop large cracks, fractures, and permanent displacements. The resulting damage leads to reduced stiffness and strength in a building. Ductility, which is a building's ability to undergo large deformations without complete failure, is the most important factor affecting performance during an earthquake. A structure with high ductility will absorb more seismic energy and thus have a lower probability of collapse than one with low ductility. One of the main objectives of modern earthquake-resistant design is to ensure that a building possesses sufficient ductility to withstand any earthquakes likely to occur during its lifetime.

Building height can also significantly impact shake damage, particularly for masonry structures. As mass is concentrated at greater heights, a building becomes less stable during ground shaking and more vulnerable to damage. Without a proper system to increase the lateral stiffness of the building, an increase in mass increases the period, and potentially the amplitude, of the vibration of the structure. This may cause severe deformation, cracking of construction materials, and ultimately building collapse.

5.4 Development of building damage functions

The damage functions implemented in the Verisk Earthquake Model for Hawaii correlate an appropriate ground-motion intensity measure with the building damage ratio, or the ratio of the building's repair cost to its replacement value.

If an enormous amount of damage and loss data, including records of ground motion at each building location, were available for buildings of all construction classes and age bands, then the derivation of damage functions would only entail a statistical exercise involving regression techniques. However, such large databases are not available, for several reasons, the primary one being that damaging earthquakes do not occur frequently enough to provide extensive data. The result is that data is generally scarce and the data that do exist is often poorly recorded. Therefore, the most accurate damage functions for all construction classes, all age bands, and all regions, can only be derived using a combination of engineering and statistical tools.

Hence, the Verisk damage functions are based on engineering analyses, damage data collected after historical earthquakes, claims data at both property and aggregated levels, loss estimates for past earthquakes, and a careful evaluation of the prescription in the building codes. The balance in the adoption of these tools varies with different construction classes.

All engineering analyses performed for the purpose of evaluating the response of a building to different levels of ground shaking follow the conceptual flow-chart depicted in the Figure below.

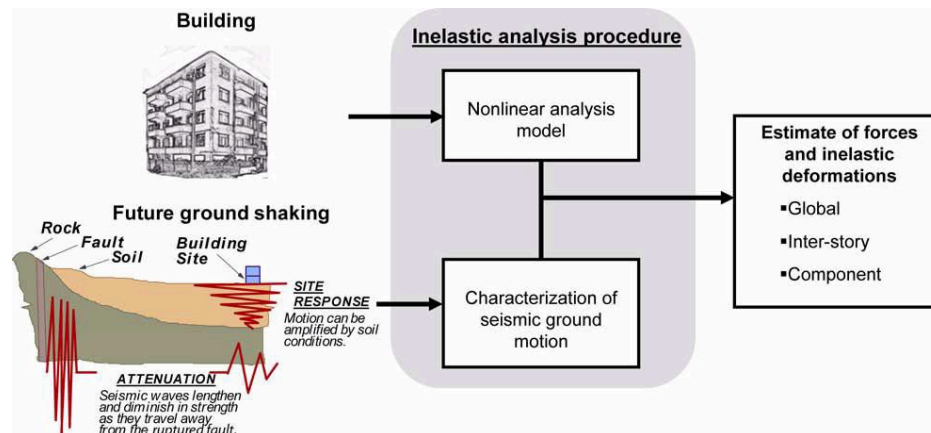


Figure 33. Conceptual flow of analyses adopted for building damage functions (adapted from FEMA 440)

The engineering analyses require the use of a computer representation of a building, and of the characterization of ground motions that such a building may be subjected to during an earthquake. The following two sections discuss in some detail the nonlinear analyses that can be performed to estimate a building's response to different ground motion intensities.

The capacity spectrum method and the use of nonlinear static analysis

A static, nonlinear procedure, often called pushover analysis, is one method of estimating a building's response to ground shaking. To begin the analysis, a computerized model of the building is subjected to a lateral load pattern representing the force generated by ground motion. This lateral load pattern, or load vector, has the same shape as the fundamental mode of the structure's vibration. The total load is then increased in successive steps to create a relationship between the intensity of the applied load (measured in terms of base shear) and the deformation of the building (measured in terms of roof drift). The analysis ends when the virtual building collapses, and the force/deformation curve that results is called a pushover curve.

The Capacity Spectrum Method (CSM) is an expedient way of predicting a building's response to ground motion. In CSM, the building is modeled by an equivalent oscillator, such as the inverted pendulum shown in the Figure below. The equivalent oscillator has the same natural frequency and degraded stiffness, after yielding, as the building. The equivalent oscillator is disturbed so that the full building pushover curve is transformed into a curve with the oscillator's response measurements. More precisely, the applied load is translated into spectral acceleration, and the building deformation is translated into spectral displacement.¹² The pushover curve that results from plotting the spectral displacement and spectral acceleration is called a capacity curve. This curve correlates the lateral deformation of a building (expressed in terms of spectral displacement) to a specific level of dynamic demand (expressed in terms of spectral acceleration). A building's capacity curve reflects various seismic characteristics of the building, including stiffness, material brittleness or ductility, and strength.

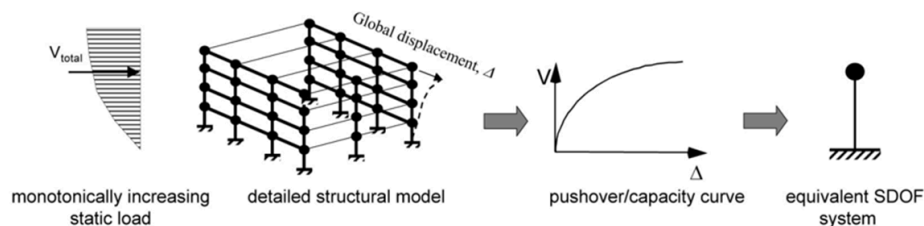


Figure 34. Schematic depiction of static pushover analysis used in the capacity spectrum method (excerpted from FEMA 440)

Another method that engineers use to model how ground motion could affect a building is called the response spectrum method. This method, which works well within the framework of the Capacity Spectrum Method, uses the maximum acceleration and displacement of a series of oscillators to model the demand imposed on a building by ground motion. The response of these oscillators is plotted as a curve of acceleration/displacement pairs known as the demand curve.

¹² Spectral acceleration and spectral displacement are two response measures of oscillators with given vibration period and damping.

The Figure below provides an example of the response spectrum method in which a series of inverted pendulums are subjected to ground shaking. The peak responses of the pendulums are plotted on the graph to the right, showing the spectral acceleration against the spectral displacement. The radial lines on the graph represent the periods of the pendulums.

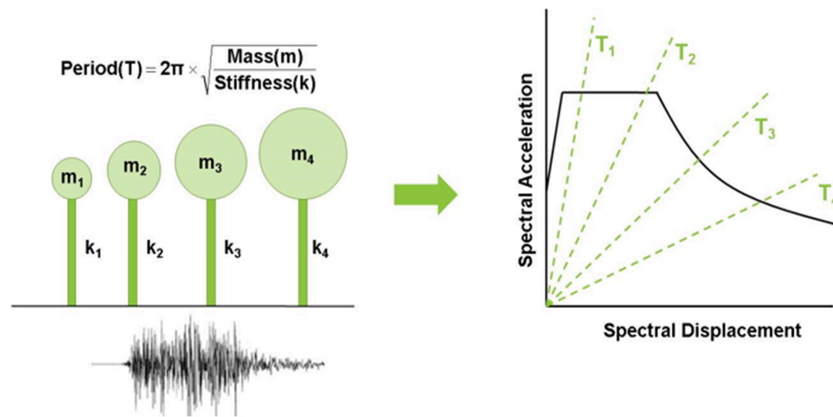


Figure 35. Maximum acceleration and displacement of a series of oscillators

Engineers can plot both the demand and capacity curves in the same spectral acceleration vs. spectral displacement plane since both curves contain the same parameters. The intersection of the curves on this plane corresponds, within a constant, to the maximum roof displacement of the building relative to the ground in response to that ground motion. Thus, as the following Figure shows, engineers can obtain the peak response of the structure from the intersection of these curves.

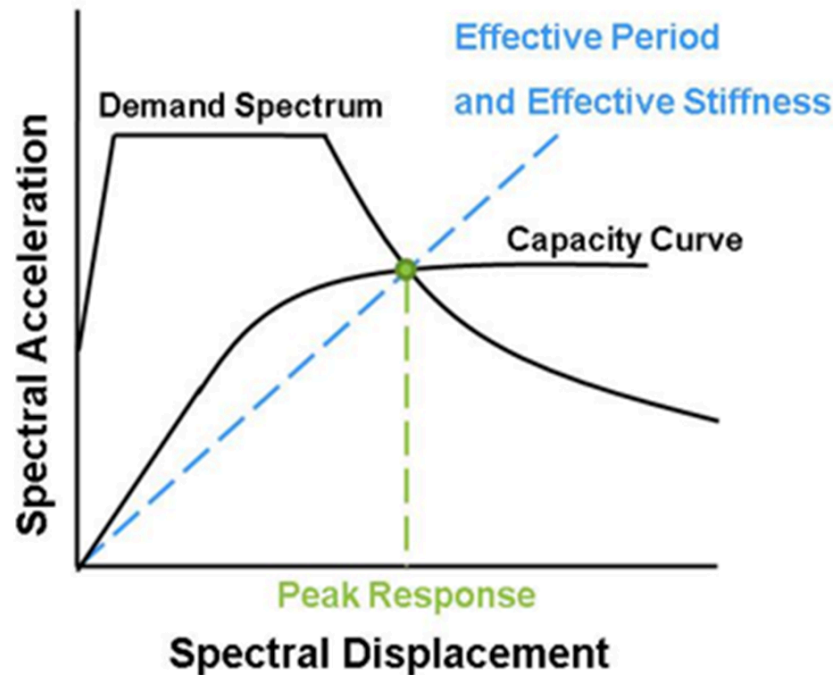


Figure 36. Peak response of a structure determined by its capacity curve

The deformation at roof level can also be used, given certain assumptions, to derive the damage at the story level. All component types, including both structural (e.g. columns and beams) and non-structural (e.g., cladding, partitions, ceiling tiles, etc.), contribute to the damage that each story of a building incurs during ground shaking. Derivations of damage allow repair strategies for each component to be priced in advance as a fraction of the replacement cost of the entire building.

To create a damage curve representing a building of a certain construction class, the building's capacity curve is plotted on the same plane as the demand spectra curves for different ground motion intensities. The capacity curve will have a unique intersection with each of the demand spectra curves as shown in the left panel of Figure 8. Each intersection represents one point of the damage function for that building. The entire damage function is then generated from multiple intersections. The right panel of the Figure below features the conceptual damage functions for three buildings, A, B, and C, all of which belong to the same construction class. This method of generating a damage function is the essence of the Advanced Component Method (ACM), which Verisk introduced in 2000. The Verisk Earthquake Model for Hawaii uses a similar approach as ACM to develop damage functions for a few construction classes in which damage data, claims data, and detailed nonlinear time-history analysis results are not available.

The left panel of the below Figure also shows that the capacity curves for different buildings of the same class will have unique intersections with a single response spectrum curve. These curves and their intersections allow one to distinguish between the responses of various building classes to different ground motion intensities.

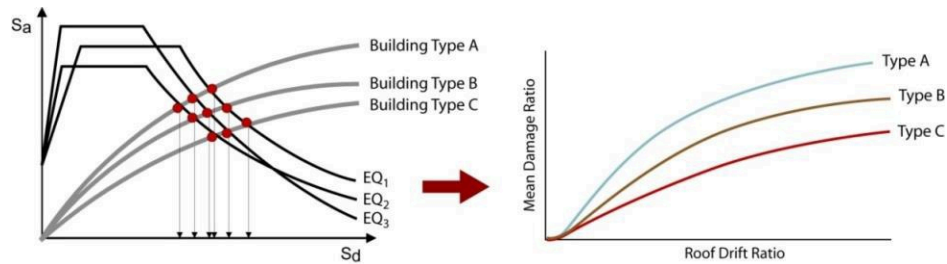


Figure 37. Maximum displacement and building damage depends on ground motion and building characteristics

Nonlinear dynamic analysis

The capacity spectrum method is a perfectly viable analysis technique for addressing the inelastic response of buildings that respond predominantly in the fundamental mode of vibration. However, because of its inherent assumptions, CSM analysis may lose accuracy in predicting the seismic response of long-period buildings, whose higher modes of vibration need to be considered, and of other buildings with complex post-elastic behavior. In particular, pushover analysis has been shown to overestimate the displacement of brittle structures, especially stiff ones (e.g., old, low- and mid-rise concrete buildings) and of stiff, ductile structures (e.g., wood frames), and to underestimate the displacement of flexible, ductile structures (e.g., high-rise steel buildings).

With the release of the current model, Verisk engineers have taken yet another step in the advancement of objective, engineering-based earthquake vulnerability assessment by replacing static pushover analysis with nonlinear dynamic analysis (NDA) for addressing the response of many buildings to earthquake ground motion. Computationally very expensive and practicable only as a result of major advances in computing power, NDA is the current state-of-the-art methodology for predicting building response to earthquake ground motion.

NDA is incorporated into the same framework as in ACM. The primary difference is in how the relationship between ground motion intensity and building response is established.

As with CSM (and ACM), the first step in NDA analysis is to create a computer representation of a building that captures the nonlinear post-elastic behavior of a building's structural elements that undergo damage (see Figure below). Then, a large number of historical ground motion records of varying intensities are loaded into the software to perform time-history (dynamic) analysis. The virtual building is then shaken (rather than pushed) using the recorded ground motion. Note that the use of multiple earthquakes allows the model to obtain an estimate of a building's mean response to a certain level of ground motion and to account for the variability in the building's nonlinear response to different records of the same intensity.

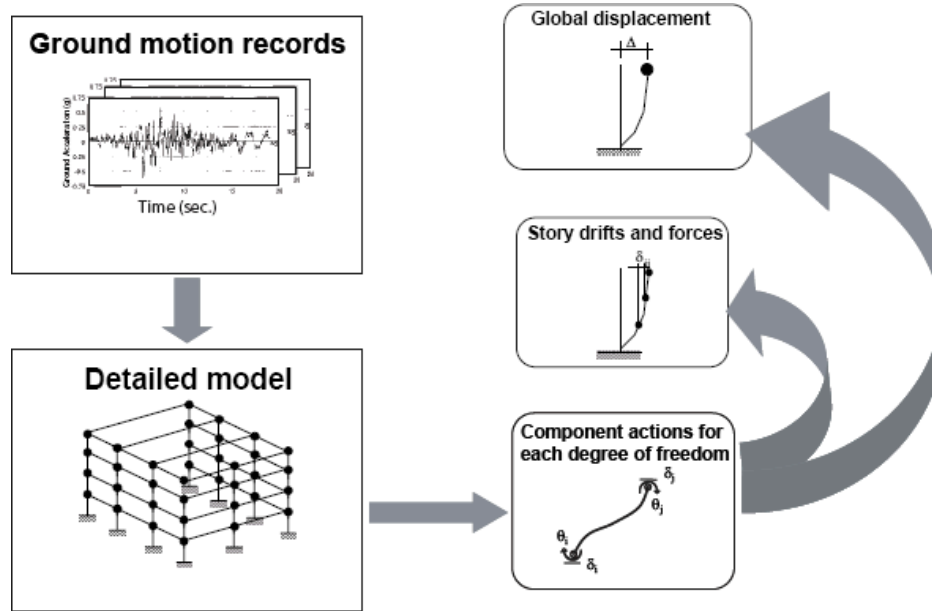


Figure 38. Using NDA to determine building response (courtesy of FEMA 440)

The use of time-history analysis allows an explicit consideration of the effects of the duration of earthquake shaking on the cumulative damage of building components. In each analysis, the forces and deformations occurring in all structural members of the model are computed. These computations are then used to evaluate global response measurements such as maximum peak inter-story drifts and forces, roof displacement, and peak floor accelerations.

At this point, a few definitions are in order. The peak inter-story drift is the highest lateral displacement between two consecutive floors, normalized by the inter-story height while the maximum peak inter-story drift is the largest observed drift among all stories over the entire duration of the earthquake. The maximum peak inter-story drift is well correlated with the damage of structural elements (e.g., beams and columns) and of deformation-sensitive non-structural elements (e.g., wall partitions). The peak floor acceleration (PFA) is the highest acceleration of a particular floor in response to ground shaking while the maximum peak floor acceleration is the highest PFA found along the entire height of the building. The maximum peak floor acceleration is well correlated with damage to acceleration-sensitive, nonstructural components (e.g., suspended ceilings), and to contents.

The Figure below provides an example of the estimates of maximum peak inter-story drift and maximum peak floor acceleration obtained via NDA. In this example, ground motions from 100 earthquakes were applied to a 10-story steel moment-resisting frame.

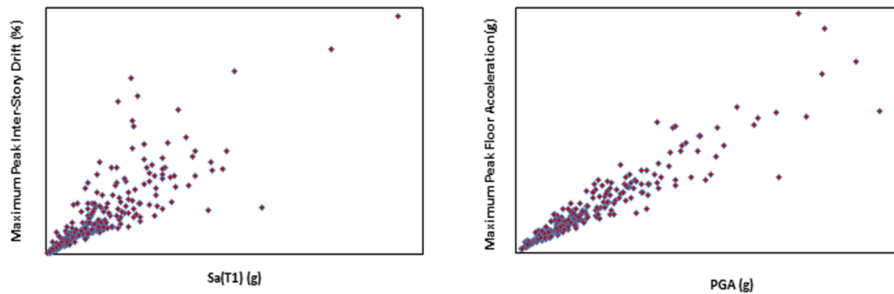


Figure 39. Maximum peak inter-story drift ratios (MIDR) and maximum peak floor accelerations (MPFA)

To establish the best relationships between the ground motion intensity parameters (e.g. the spectral acceleration at the fundamental period of the building ($S_a(T)$) and PGA) and the building's global response measurements, a regression analysis is performed on the results in [Figure 39](#). From there, a special statistical treatment is applied to account for ground motions that cause the complete collapse of the building. This response is not shown in [Figure 39](#).

[Figure 40](#) shows the expected maximum peak interstory drift and interstory drift at different stories for the same 10-story steel moment-resisting frame whose responses to non-collapsing ground motions were shown in [Figure 39](#). The drift values were found using regression analysis. The figure also shows the relationship between the global response measurements and the intensity of the ground motion when the collapse cases are considered (solid lines) or disregarded (dotted lines). Collapse cases must be considered since the building will not withstand indefinitely large deformation without failing.

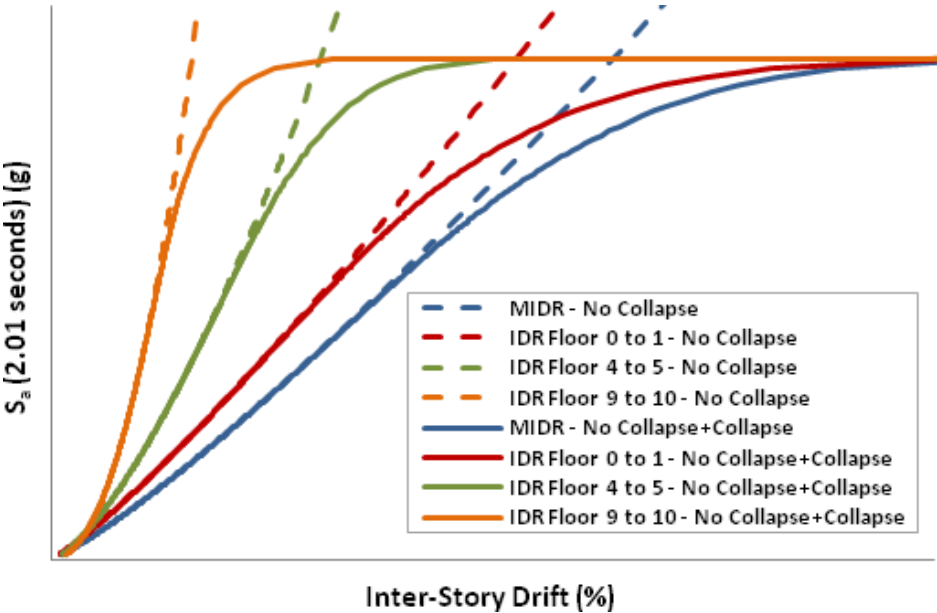


Figure 40. Relationship between spectral accelerations at the fundamental period of a building and the induced MIDR and IDR.

NDA directly provides, without any limiting assumptions, the force imposed on a building by ground motion. Deformation levels (or story acceleration levels, when necessary) are then used to determine component damage and the associated repair strategy. The monetary loss for the entire building is estimated by combining component repair costs.

Note that with NDA, building deformation at each story is computed from a fully detailed model of the building. Because building response is calculated along the height of the building, NDA allows higher modes of vibration to be captured as well as different failure modes, as shown in the following Figure:

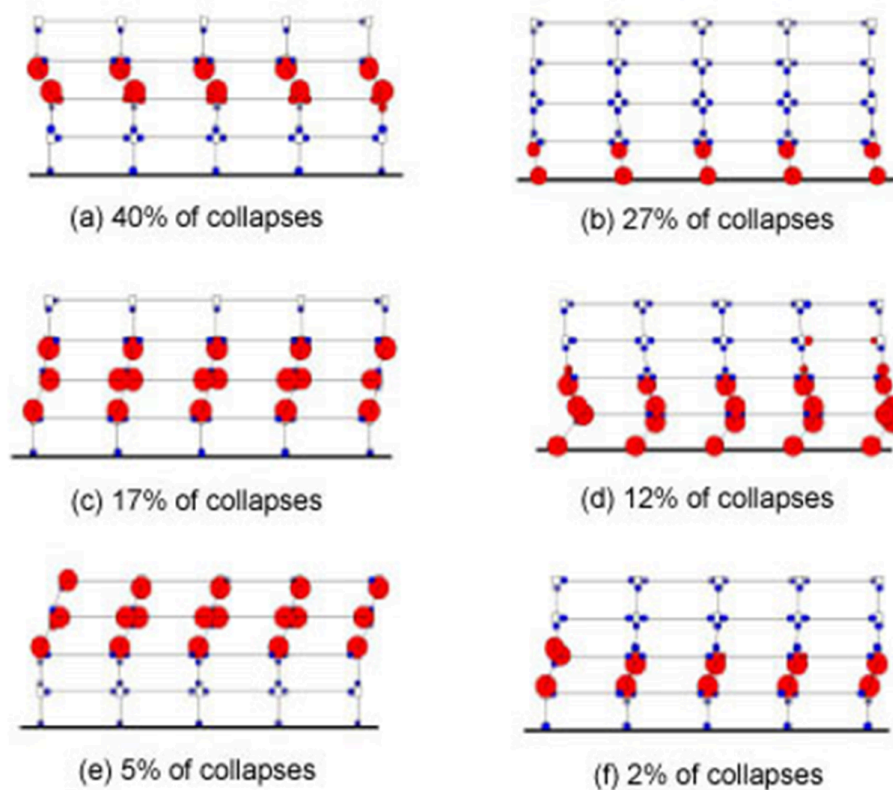


Figure 41. Six failure modes captured by NDA for a four-story concrete moment-resisting frame building (courtesy of Dr. Curt B. Haselton, California State University)

5.5 Building damage functions

As discussed previously, damage functions for different building construction classes are developed using a combination of tools that include engineering analyses, evaluation of building codes prescriptions, and damage and loss data. Since Hawaii does not have nearly as much damage and loss data as does the continental United States, many of the damage functions employed in the Verisk Earthquake Model for Hawaii leverage data and analysis used in the Verisk Earthquake model for the United States. These damage functions are a sound choice due to similarities in design load, construction practices, and code requirements between Hawaii and the continental United States.

When empirical data is scarce, engineering analyses are critical and, therefore, are heavily used. NDA was heavily used for the following types of buildings:

- Low-rise, mid-rise, and high-rise brittle and ductile reinforced concrete (RC) frame buildings
- Low-rise, mid-rise, and high-rise modern moment-resisting steel frame buildings

For each of these construction classes, NDA is performed by both Verisk engineers and other researchers, for multiple buildings within each class, to acquire an understanding of building-to-building response to similar ground shaking. The details of such engineering analyses were discussed in the previous section using an illustrative example of a 10-story steel moment-resisting frame building. NDA analyses performed for other buildings may differ in some details, but they are conceptually equivalent to those discussed earlier in the section. NDA was also considered, but to a lesser degree, for developing damage functions for wood frame buildings.

The damage functions for single-family wood frame (WF) residences are based on those damage functions that were developed for California for corresponding age bands. These damage functions are based on claims data from the 1994 Northridge earthquake, and on damage and loss data from a number of historical events, including the 1989 Loma Prieta earthquake, the 2003 San Simeon earthquake, and the 2008 Chino Hills earthquake. Engineering analysis was also employed in developing these damage functions as the quality of the data is not accurate enough to differentiate houses with different characteristics (e.g., foundation type or number of stories). Engineering analysis can easily model the effects that these differences have on damage ratios. For more information on how single-family wood frame damage functions were developed, please refer to the complete documentation provided in the Verisk Earthquake Model for the United States, which is available by signing into the Client Portal at www.air-worldwide.com.

Even in the continental United States, extensive databases of claims data, such as those for single-family wood frame structures, are not available for other construction classes. There are, however, detailed databases of historical damage data, rather than claims data, for several construction classes other than wood frame. In place of the loss from a claim, the damage data provides detailed descriptions of the damage caused to an asset at a given location. Of course, the damage data can be used to estimate the repair cost and, after normalization by the replacement cost of the building, the damage ratio. Datasets of damage data are available for a variety of construction types, including concrete tilt-up buildings, unreinforced masonry buildings, steel moment-resisting frame buildings, and concrete moment-resisting frame buildings.

To summarize, the damage functions in the Verisk Earthquake Model for Hawaii are credible and realistic and are a culmination of empirical claims data and engineering analysis. The Figures below provide examples of these damage functions. Please note that the Verisk Earthquake Model for Hawaii offers separate building damage functions for all modeled counties, as well as different construction types, occupancies, height ranges, and age bands. [Figure 42](#) shows the damage functions for Hawaii County for selected construction classes of unknown height and the most recent age band. These damage functions were modified for buildings in Maui, Honolulu, and Kauai Counties to account for the different design loads and construction practices. Note that damage functions for Maui and Kalawao counties, which together comprise Maui Island, are the same.

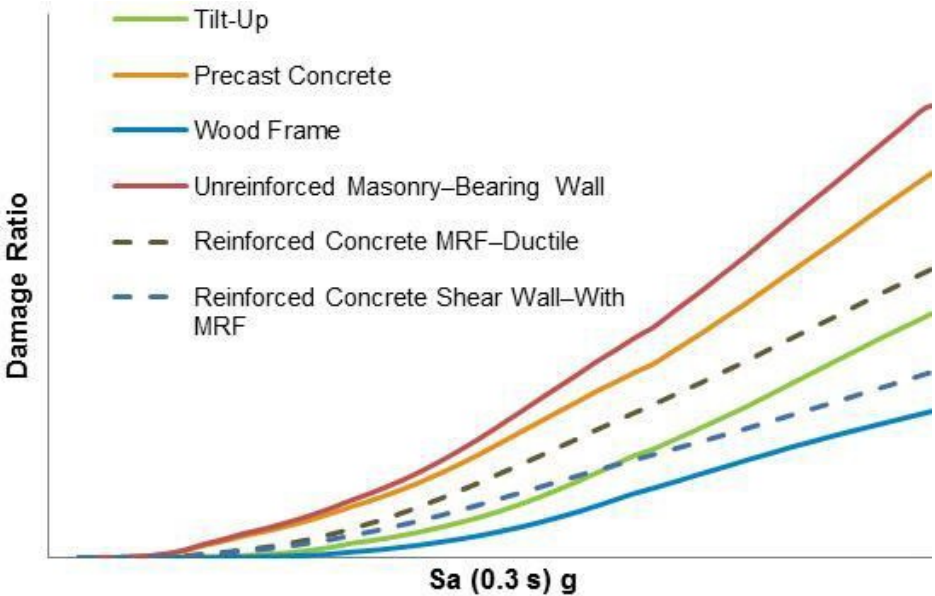


Figure 42. Damage functions for various construction types of unknown height and current age in Hawaii County

Due to differences in building code adaptation and enforcement, the vulnerability of a given construction type may vary by county. [Figure 43](#) provides the damage functions for low-rise unreinforced masonry commercial buildings for the different counties. The most recent age band is assumed for the unreinforced masonry construction type. Note that specifically for low-rise unreinforced masonry commercial buildings, Maui, Kalawao and Honolulu counties share the same age band (2001 to present) and the same damage function.

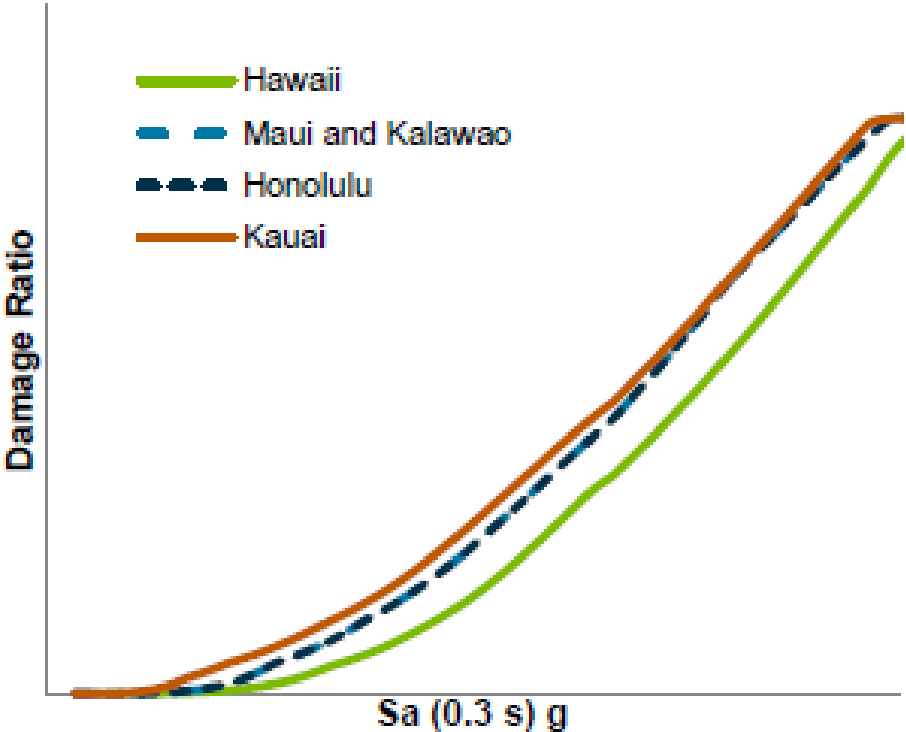


Figure 43. Damage functions for low-rise unreinforced masonry commercial buildings of the current age band for different Hawaiian counties

As previously discussed, the age bands in the Verisk Earthquake Model for Hawaii, reflect seismic-code provisions and the evolution of construction techniques. Typically older buildings in all the modeled counties are quite vulnerable to shake damage, as many were built without fully accounting for the region’s seismicity and modern seismic construction practices. [Figure 44](#) displays the Hawaii county damage functions for low-rise wood frame residential buildings for three modeled age bands.

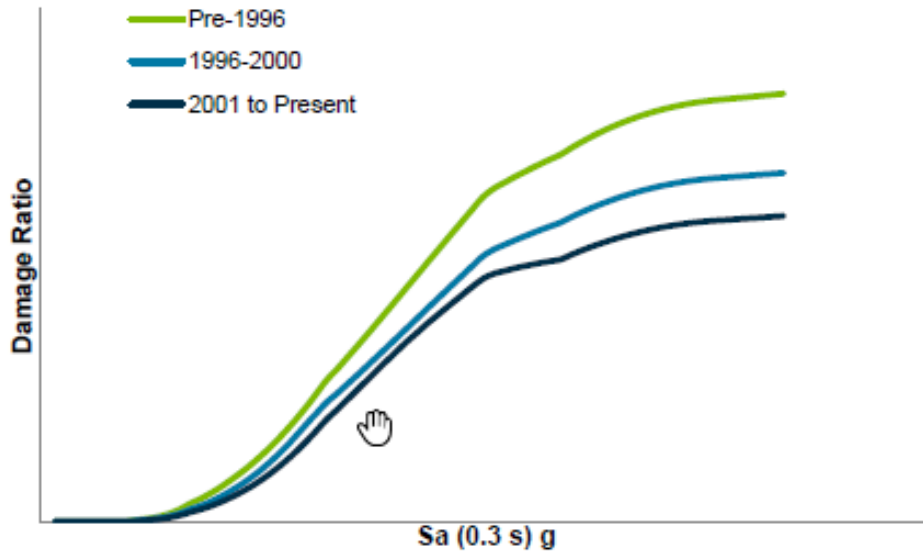


Figure 44. Damage functions for low-rise wood frame residential buildings for different age bands in Hawaii County

The impact that year built has on vulnerability has been demonstrated during historical events. For example, during the October 2006 Kiholo Bay earthquake, the most damaged buildings in Hawaii County were single wall wood frame residences set on posts. In particular, those single wall wood frame residences built prior to 2001 were the most greatly impacted; the primary reason being that starting in 1999, Hawaii County began implementing significant code requirements that included increasing seismic design loads (by switching from UBC seismic zone 3 to 4). This was followed by numerous recommendations for strengthening this construction type in 2007. Thus, the model includes explicit support for the single wall wood construction type (AIR code 102) of various ages. [Figure 45](#) shows the damage functions for this construction type for the three modeled age bands and unknown age.

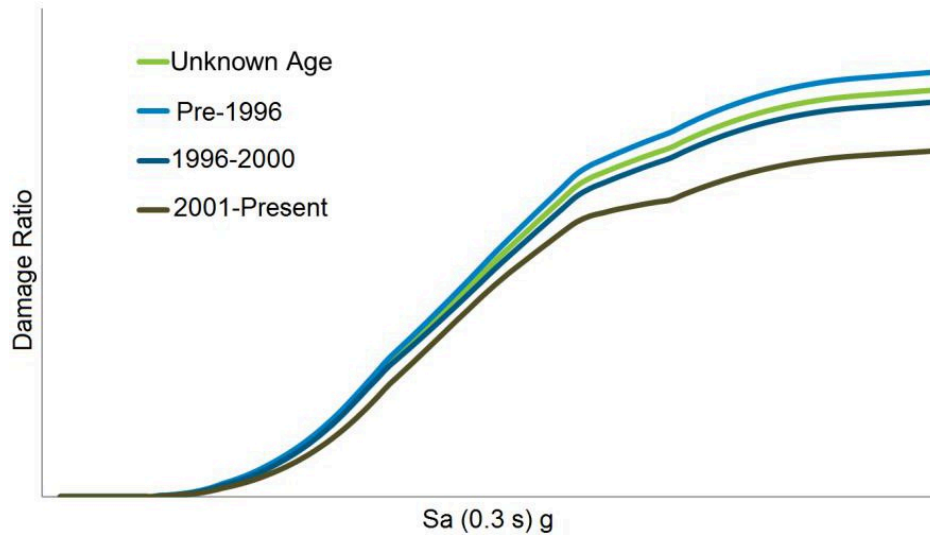


Figure 45. Damage functions for light wood frame, or single wall wood frame (AIR code 102), residential buildings for different age bands in Hawaii County

5.6 Assessment of business interruption losses for small-scale industrial facilities

Downtime, or the number of days before a business can return to full operation, is the primary parameter for estimating business interruption (BI) losses. The methodology used for estimating BI losses, as illustrated schematically in [Figure 46](#), utilizes an event tree approach, incorporating the latest research and findings from an extensive analysis of claims data. For each damage state, a probability is assigned to two possible outcomes: continued operations or cessation of operations at the location. If operations cannot continue at the location, a probability is assigned to whether the company will relocate. These probabilities vary by occupancy. For example, while relocation is feasible for an office, it is not for a hotel. Thus, the two will take different paths to recovery, and hence will have different downtimes in the event of business interruption.

Downtime is calculated for each stage of the damage assessment and recovery process. The first stage is the time before repairs can get underway (pre-repair). Damage must be assessed, repair costs negotiated with contractors, and the building permit obtained. The next stage is the repair time. Some businesses choose to relocate rather than wait for repairs, but relocation takes time as well. Once repairs are completed, revenues may not resume immediately at the pre-disaster level; it may take some time to regain market share, or to rebuild a labor force that may have been dislocated.

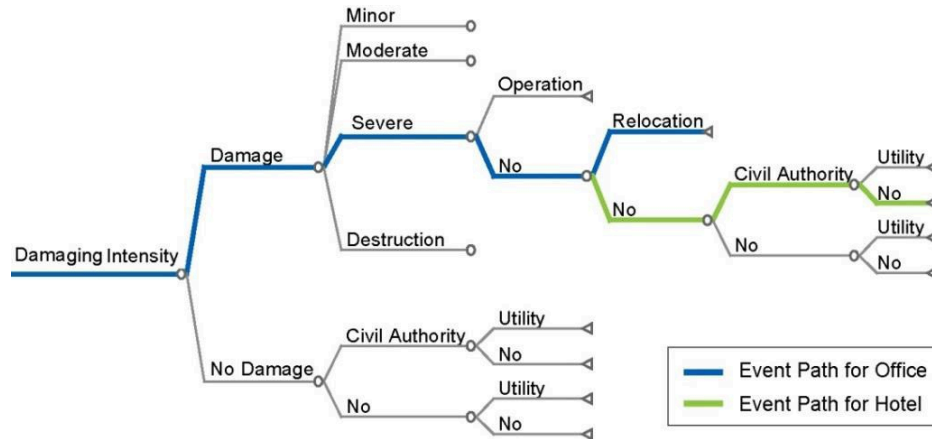


Figure 46. Hypothetical event tree of BI estimation for an office and a hotel

In the model, the estimated number of days needed to restore the business to full operation depends on a number of key factors, including the level of damage sustained, the size of the building (as approximated by building height) and its architectural complexity (as approximated by occupancy class).

For a given damage ratio, a 2,500 square meter hotel will take significantly longer to repair than a 450 square meter professional office. Since floor area is usually not directly available, it is estimated using building height. For a given floor area, buildings with significant architectural complexity will also take more time to repair. Warehouses can be quite large, but repairs are likely to take place quickly because of their architectural simplicity. Interior finishes must also be taken into account. Hotels are not only typically larger than offices, but can take more time to repair due to the higher quality of interior finishing.

Some types of businesses, such as hospitals, are more resilient than others and may be able to restart operations before repairs are complete, or they may have had disaster management plans in place that allow them to relocate some operations quickly. For other businesses, such as hotels, location is all-important and relocation is not an option. Since many parameters (such as building size, complexity, and business resiliency) critical to determining business interruption are generally not available for input into the model, occupancy class is used as a proxy to measure these parameters.

Occupancy is also used to estimate the probability that there may be business interruption at a dependent building within the damage footprint—such as the supplier of a necessary manufacturing input—that will exacerbate BI losses at the principal building. Estimation of the impact of the dependent building(s) damage on the principal building requires knowledge of the location and the degree of interdependence between dependent and principal buildings. Since this level of detailed information is generally not available, logical assumptions are made to estimate the impact of the dependent building(s) on the principal building's downtime. The methodology for estimating BI losses relies in part on loss experience data and in part on expert judgment in the face of limited available exposure information.

The functional relationship between building damage and loss of use is based upon published construction and restoration data along with expert engineering judgment. [Figure](#)

47 shows the relationship between repair time, or downtime, and the mean building damage, for a variety of occupancy classes.

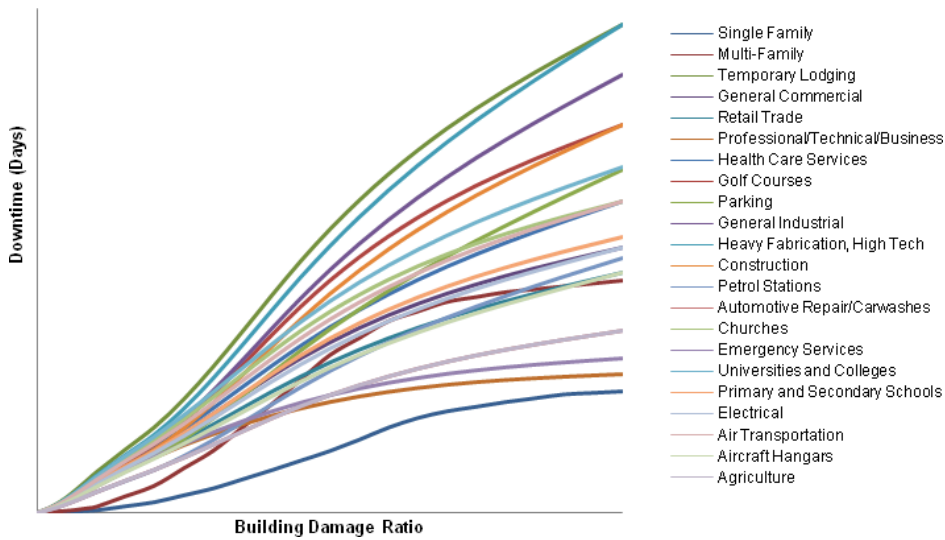


Figure 47. Business interruption damage functions for different occupancy classes

5.7 Large-scale industrial facility damage functions

To assess the damage and loss potential to a large-scale industrial facility as a whole, Verisk employed a component-based approach, which allows the damage functions to account for the many primary components intrinsic to this type of facility. These primary components are categorized into classes and subclasses based on their function as well as their vulnerability to ground shaking. Verisk developed separate damage functions for each of more than 400 such components. Verisk also obtained the valuation breakdown of a facility according to its components, and combined this information with the component damage functions to derive the damage function for an entire industrial facility. This approach provides loss estimates that are transparent and consistent across different facilities. Furthermore, the component-based approach is essential for a reliable assessment of business interruption (BI) losses, which depend heavily on the numerous interactions between the various components and lifelines within industrial sites.

Developing component-level damage functions

To predict the response of an industrial facility exposed to ground shaking, the Verisk model uses peak ground acceleration (PGA). Since the components are parts of a larger facility, a unique ground motion parameter has been used to estimate the response of all of the components. Using PGA as a ground motion parameter for assessing vulnerability of industrial components is advantageous for four reasons. First, the majority of components (e.g., machinery and equipment) in industrial plants are anchored and fairly rigid, and therefore PGA correlates well with their performance. Second, as discussed later in this

section, the damage functions for an entire industrial facility are obtained using a weighted average of component damage functions. This process can be streamlined without adding uncertainties in the process of aggregation of different components by using the same ground motion parameter for all components. Thirdly, some of the component damage functions developed by different researchers are generally PGA-based and therefore using PGA facilitates the consideration of damage functions already available. Finally, historical damage data for industrial plants is often available along with an estimate of the PGA at the site. Estimates of other ground motion parameters are generally not reported.

The main categories of components considered to develop the 400 series are listed in the following Table, but each has many sub-classes. All components chosen for analysis represent actual industrial facilities. They were selected from structural drawings, design specifications and other sources.

Table 9. Industrial facility components used in the Verisk Earthquake Model for Hawaii

Industrial Facility Components		
Air Handling Units	Distribution Panels	Open-Frame Structures
Baffles	Electric Power Backup	Paddles
Basins	Electric Transmission Towers	Pipe Racks
Battery Chargers	Elevated Pipes	Pipes and Pipelines
Battery Racks	Engine Generators	Potential Transformers
Boiler/Pressure Vessels	Equipment	Pressurized Reactors
Boilers	Fans	Process Towers
Buildings	Filter Gallery	Pumps
Chillers	Flares	Scrapers
Chlorination Equipment	Generators	Sediment Flocculation Equipment
Circuit Breakers	Highways/Runways/Railroads	Silos
Commercial Backup Power	Large Horizontal Vessels	Stacks/Chimneys
Compressors	Large Motor-Operated Valves	Switch Gears
Control Panels	Large Vertical Vessels with Formed Head	Tanks
Cooling Towers	Lightning Arrestors	Transformers
Coupling Capacitors	Loading Structures (Cranes/Cargo Handling/Conveyor Systems)	Tunnels
Current Transformers	Motor Control Centers	Wells
Dams	Large Motor-Operated Valves	Valves
Disconnect Switches	Motor-Driven Pumps	

The damage functions derived for each component vary depending on the county where the facility is located because the seismic hazard and, therefore, the design specifications are different in different Hawaiian counties. Thus, for each component and subcomponent, there are different damage functions for each of the five counties of the state: Hawaii, Maui, Kalawao, Honolulu, and Kauai. Verisk researchers leveraged data and information from the Verisk Earthquake Model for the United States to develop these damage functions, as there are similarities in seismicity, design load, and construction practices between the continental United States and Hawaii.

The following Figure illustrates damage functions for the most common components found in industrial facilities in Hawaii County. Similar sets of component functions were obtained for the other counties.

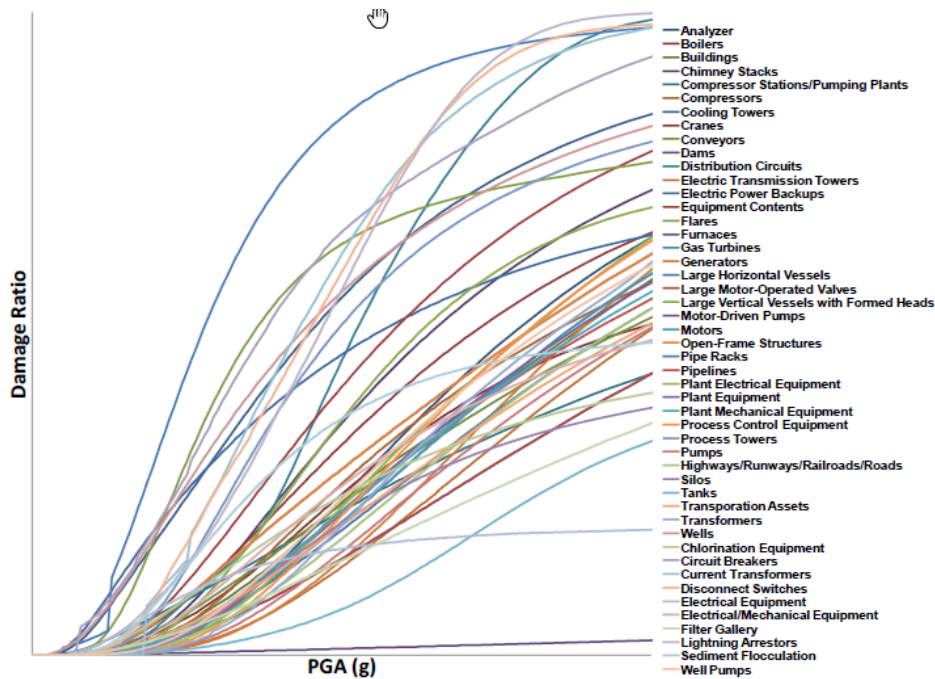


Figure 48. Damage functions for industrial facility components in Hawaii county

The following sections describe the various methods used to develop the component-level damage functions.

Damage functions for buildings

The damage functions for small industrial facilities were developed with the assumption that the facility comprises primarily buildings and some machinery. The damage functions for small facilities were therefore developed based on the building damage functions for different construction classes. These damage functions are identical to the building damage functions for large industrial facilities. However, since the cost of the components for the large industrial facilities is generally more than 80% of the cost of the facilities, there is significant difference between the damage functions for large and small facilities. To derive the building damage functions for each type of facility (e.g., heavy fabrication), Verisk

obtained a weighted average of all the damage functions for different types of low-rise buildings that are present in the industry exposure for that type of facility. The weights assigned to each damage function are simply the fraction of each building type in the mix. This process was completed for all of the counties to obtain a building damage function for each industrial type.

Figure 49 shows the damage functions for the different building construction classes that are often found within industrial facilities in Hawaii County. Since different types of industrial facilities (e.g., chemical plants versus manufacturing plants) have a different mix of building types, the overall damage functions for buildings vary depending on the type of industrial facility. Figure 50 shows the derived building damage functions for various industrial facility types in Hawaii County.

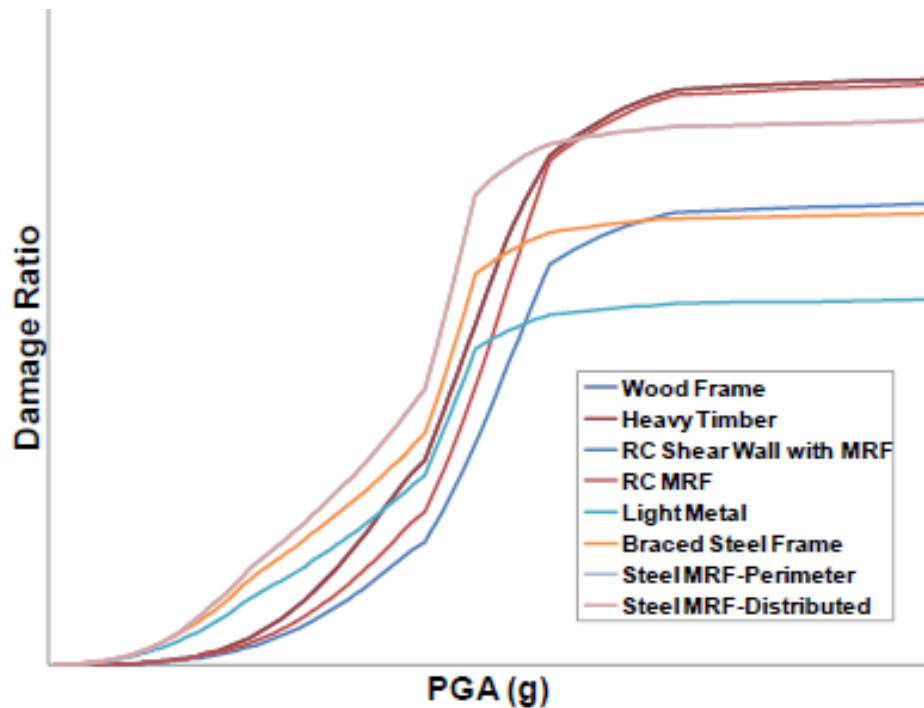


Figure 49. Building damage functions in Hawaii county

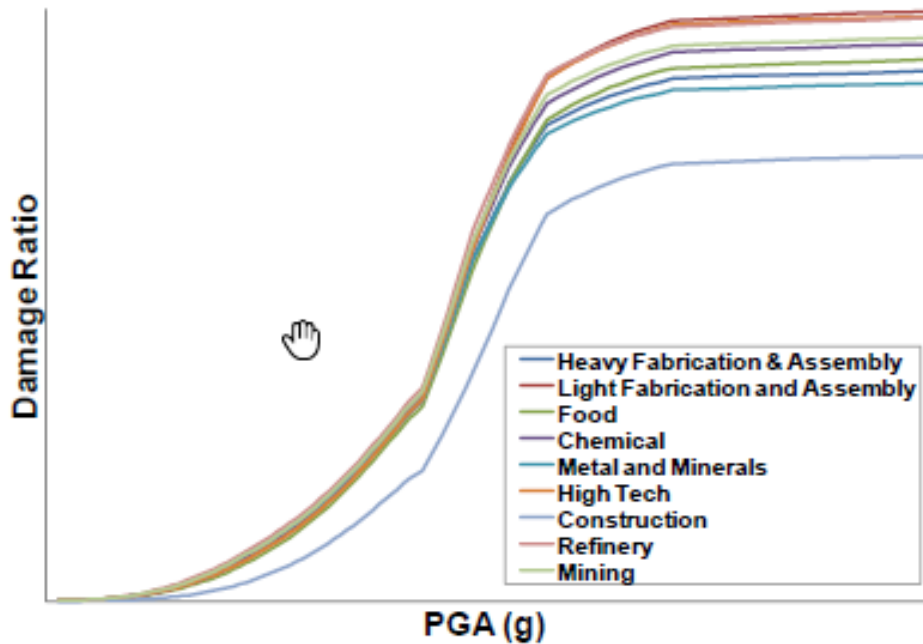


Figure 50. Building damage functions for various industrial facilities in Hawaii county

Damage functions for components derived from observational data

For tanks, dams, tunnels, and several other components, damage data are available from historical records and publications. For these components, damage functions have been derived using a combination of observational data from historical earthquakes and engineering studies.

The following figures show damage functions for tanks from published literature. [Figure 51](#) uses the generic tank type (e.g., the average functions of unanchored and anchored, fill-level, etc.). [Figure 52](#) shows on-grade tanks and tanks with specific anchorage type and fill-level. The final damage function is the average of these damage functions.

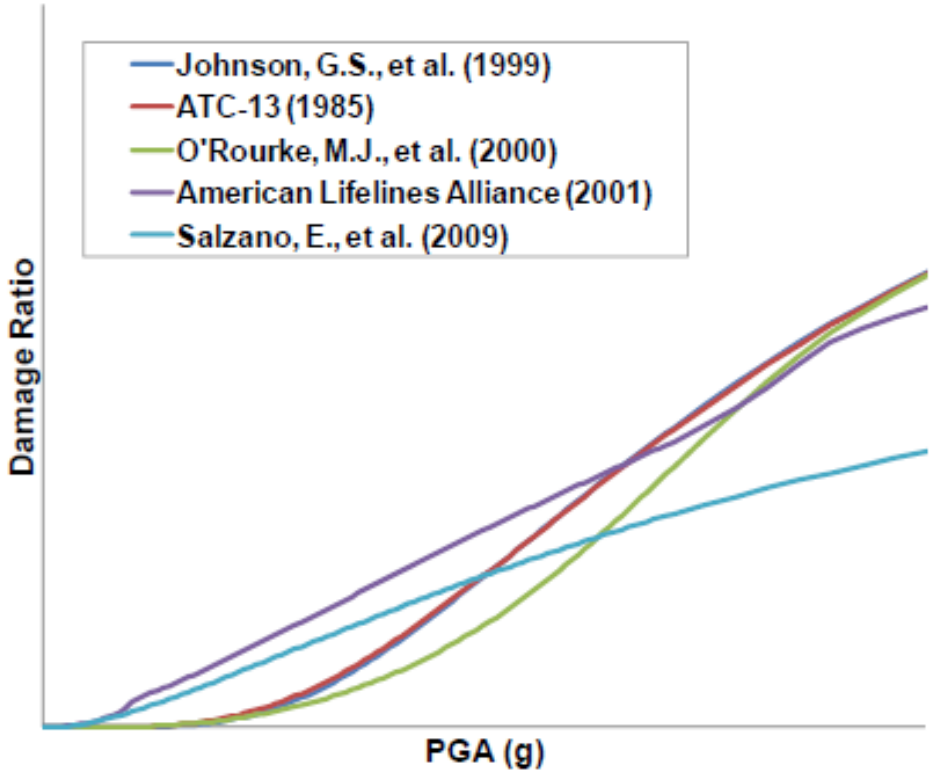


Figure 51. Damage functions for tanks based on technical literature and reviews, average damage from each source

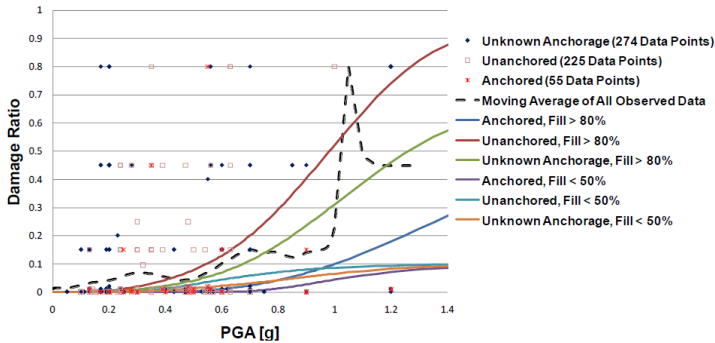


Figure 52. Damage functions for on-grade tanks based on observed damage data

The data in [Figure 52](#) is observational tank damage data collected from 19 historical earthquakes, listed in the following Table.

Table 10. Historical earthquakes used for tank damage data

Earthquake	Year		Earthquake	Year
Long Beach, CA	1933		Northridge, CA	1994
Kern County, CA	1952		Kobe, Japan	1995
Alaska	1964		Chichi (Jiji), Taiwan	1999
San Fernando, CA	1971		Izmit, Turkey	1999
Imperial Valley, CA	1979		Athens, Greece	1999
Coalinga, CA	1983		Nisqually, WA	2001
Morgan Hill, CA	1984		Southern Peru	2001
Loma Prieta, CA	1989		Bam, Iran	2003
Costa Rica	1992		San Simeon, CA	2003
Landers, CA	1992			

Component damage functions derived from nonlinear structural analysis

For many industrial components (e.g., chimneys, cooling towers, flare towers, open-frame structures, pipes, pipe racks, process towers, and silos), there is insufficient damage data or studies in the literature to derive damage functions accurately. In these cases, Verisk used engineering analyses—primarily nonlinear static pushover analyses (see [Development of building damage functions](#) for more detail). Most industrial components are simple structures and vibrate in essentially one mode, which makes static pushover analysis appropriate. All analyses were carried out in accordance with state-of-the-art, performance-based provisions, taking into account the complexity of each component and its characteristic response to shaking.

Structural models were subjected to a progressively increasing lateral force (corresponding to increasing levels of ground motion) to evaluate the trigger of key limit states, ranging from the onset of inelastic response to complete structural collapse. The response of each structure was quantified in terms of a functional relationship between the ground motion intensity (PGA) and the key limit states of the structure (e.g., first yield, buckling, ultimate strength of anchor bolts, instability, etc.). The damage ratio associated with each limit state was derived in accordance with ATC-13 guidelines.

The following Figure shows pushover analysis results for an open-frame plant structure being displaced in two orthogonal directions. As the figure indicates, under the action of transverse lateral loads, the first limit state is the buckling of a knee brace (shown by the red dot in the left figure in the top panel), and is associated with a sharp drop in the lateral strength. As the lateral load increases, an additional brace buckles resulting in another drop in the lateral strength.

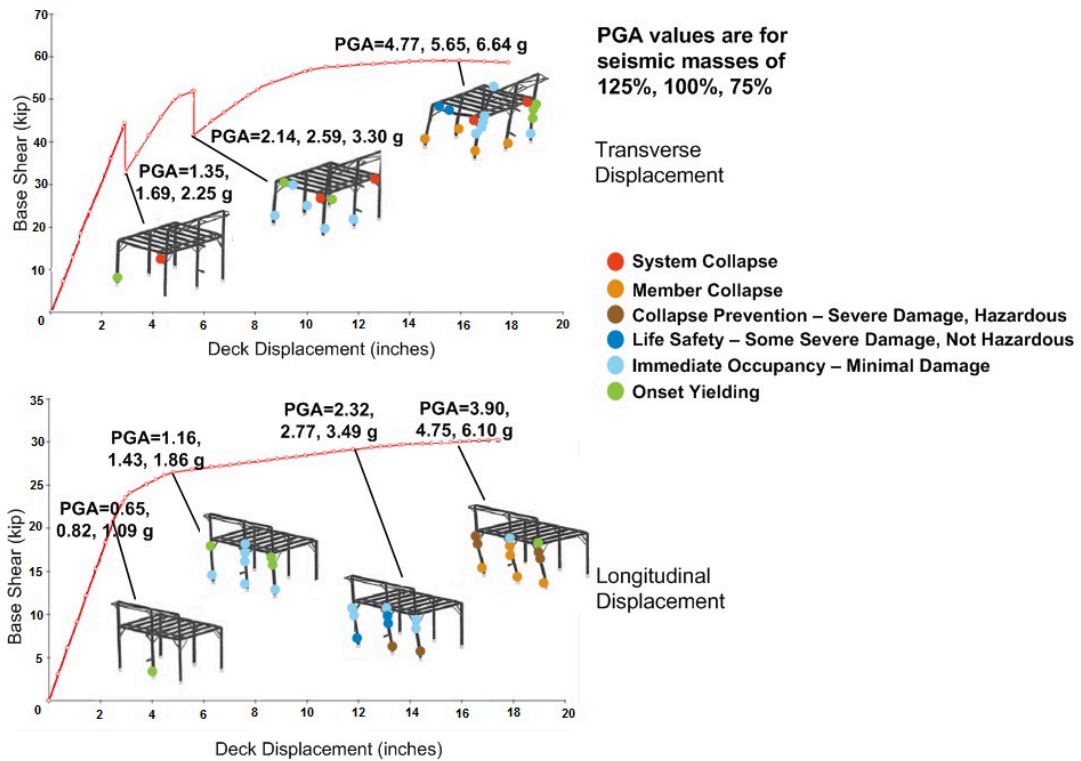


Figure 53. Pushover analysis results for an open-frame structure showing PGA values at several limit states

Additional stress in the legs and braces results in more deformation and eventual collapse. With increasing lateral loads in the longitudinal direction, the first plastic hinge forms at the base of a leg, followed by more plastic hinges at the leg bases and braces.

Each engineering analysis takes into account three different loading conditions: light, moderate, and heavy. This is done to take into account the variability in the live load, which affects the performance of structures in earthquakes. The transverse displacement has three limit states while the longitudinal displacement shows four limit states. These correspond to live loads (seismic loads) equal to 75%, 100%, and 125%, respectively, of the dead load of the structure itself. The dead load includes the self-weight of the structure and appurtenances, plus any equipment that it supports. The three PGA values close to each illustration represent the average ground motion level that brings that structure to the specified level of deformation, for each of the three loading conditions.

With a lighter load, a higher level of PGA is needed to bring the structure to the onset of a specific limit state. For example, at the first longitudinal displacement, a PGA value of 0.65 g is needed to bring this open frame structure with heavy load conditions (i.e., live loads equal to 125% of dead load) to the onset of minor damage. However with moderate loading on the same structure, a higher PGA (0.82 g) is needed, on average, to reach the same level of damage.

The following two figures show damage functions for open-frame structures with different load conditions derived from pushover analysis. [Figure 54](#) shows the damage functions for

an open-frame steel plant structure. [Figure 55](#) shows the damage functions for an open-frame steel dock, which has a narrow frame supporting pipes and equipment.

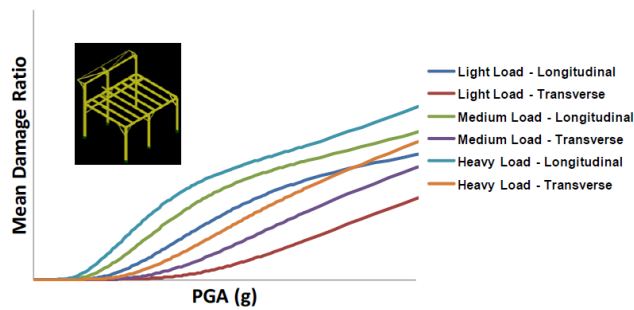


Figure 54. Damage functions for an open-frame steel plant structure

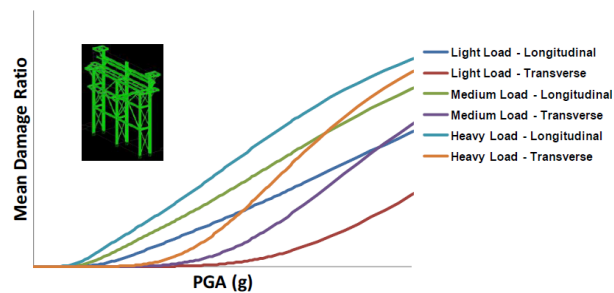


Figure 55. Damage functions for an open-frame steel dock structure

Developing damage functions for different counties of Hawaii and for unknown facility types

To develop damage functions for industrial facilities across Hawaii, Verisk engineers studied the differences in the design base shear of components in all four Hawaiian counties. The values of PGA that induce, on average, the onset of a limit state on the same type of structure (e.g., an open frame structure) in different regions were evaluated by considering the different design base shears.

The following Figures show the relativity of damage functions for each industrial facility type along with the damage function for an Unknown type of industrial facility, for each of the Hawaiian counties. In all counties, the Unknown facility type (represented by the thick red line) represents a weighted average of the damage functions for the different known industrial facility types.

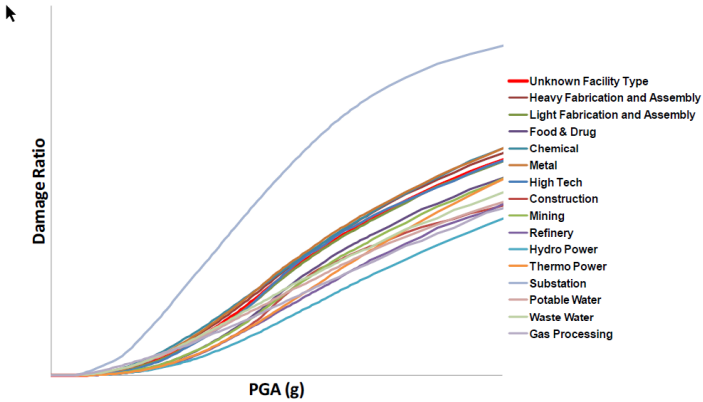


Figure 56. Damage functions for industrial facilities in Hawaii county

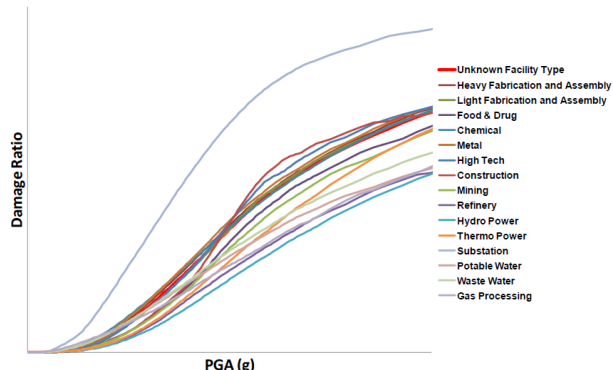


Figure 57. Damage functions for industrial facilities in Maui/Kalawao and Honolulu counties

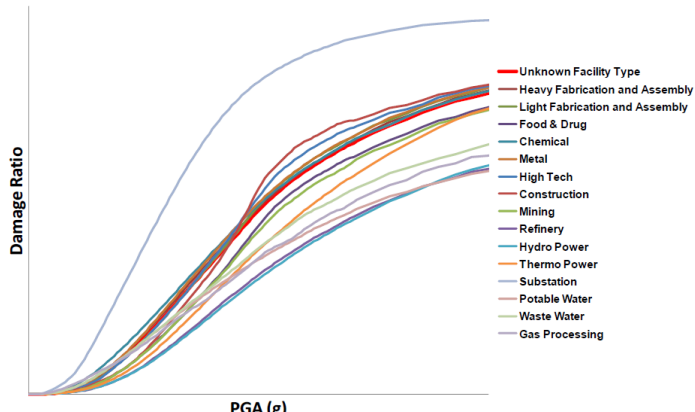


Figure 58. Damage functions for industrial facilities for Kauai county

Assessment of business interruption losses for industrial facilities

Assessing business interruption (BI) loss for industrial facilities is an extremely complex task, particularly in the case of highly integrated facilities with multiple process chains, bottlenecks, and redundancies. The major contribution to BI losses is the loss of revenues incurred when product chains are not functional (either partially or completely). Loss of functionality can occur as a result of physical damage to components and lifelines, such as electricity, water, steam systems, and others.

Verisk’s approach for the assessment of BI losses for these complex risks is the same as that used for other business lines. Because industrial facilities generally consist of a large number of components, Verisk again uses a component-based approach. To assess the possible downtime of an entire industrial facility, Verisk starts by determining time element damage functions for each component.

For each component, the time needed for repair or replacement, if necessary, is estimated. As in any other business interruption assessment, the time before repairs can get underway (pre-repair) is determined and added to the time needed for the actual repair. The information on the pre-repair and actual repair time for different components is based both on historical data and on the experience gained by Verisk’s engineers by consulting with the operators and managers of industrial facilities. In addition, the model takes into account components that are still operable or even undamaged, and therefore have no downtime at all. Once the time element functions are determined for all the components, the model aggregates the functions by determining a weighted average of the component functions—a process similar to that adopted for developing facility level property damage functions.

The following Figure illustrates downtime functions for industrial facility components of unknown subclass (e.g., type of anchorage, level of liquid fill, type of material, etc.) in Hawaii County.

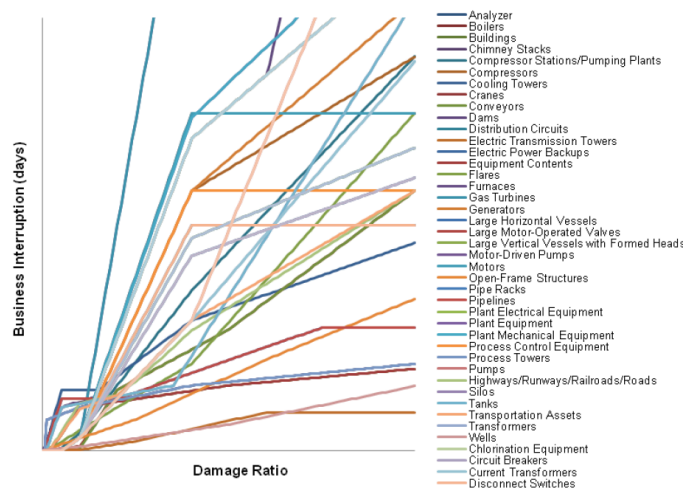


Figure 59. Time element functions for industrial facility components

As described above, the business interruption (BI) functions at the facility level are the weighted average downtime functions of the individual component and sub-component class. [Figure 60](#) shows the BI functions for facilities in Hawaii County. The BI function for the Unknown industrial facility type, represented by the thick red line, is an industry-exposure weighted average of those of all facilities.

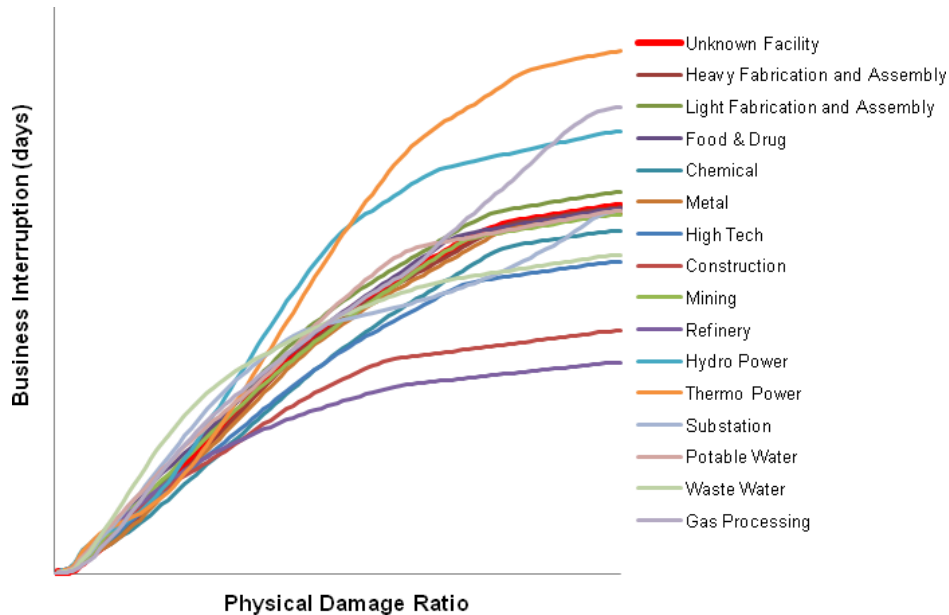


Figure 60. Time element functions for industrial facilities in Hawaii county

5.8 The distribution of damage: uncertainty in damage estimation

The model's damage functions provide estimates of the mean, or expected, damage ratio corresponding to median ground motion at each affected site. However, as is commonly seen in the course of damage surveys in the aftermath of earthquakes, similar structures at the same location experience different levels of damage. This variation in building damage can arise due to the inherent randomness in building response or to differences in building characteristics, construction materials or workmanship. Verisk has developed a distribution around the mean damage ratio to capture this uncertainty in damage, as illustrated in the sample damage function shown in the Figure below.

Observations have shown that, after an earthquake, similar buildings within close range of one another sustain a wide range of damage. Many will be severely damaged or completely destroyed while others in the same vicinity sustain only very light damage or none at all. These damage patterns are commonly represented by a beta distribution, which accounts for this variation in damage.

However, after an extensive study of claims data, Verisk engineers have found that a combination of two beta distributions (referred to here as a bi-beta distribution) provides a much better fit to the observed damage patterns in past earthquakes. Therefore, the Verisk model has adopted the bi-beta distribution, which shows a much higher level of accuracy when used for insured loss estimations.

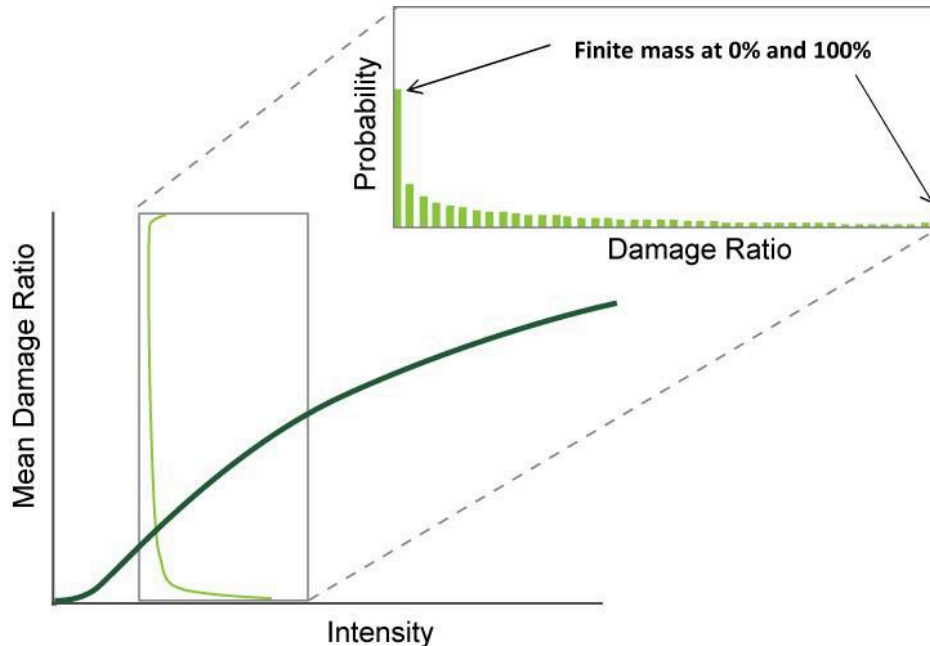


Figure 61. Sample damage function and distribution with non-zero probabilities of 0% and 100% loss

5.9 Builders risk

The builders risk line of business determines potential losses resulting from earthquake damage to buildings while they are still under construction. This line of business can be applied to all supported 100-series construction classes and 300-series occupancy classes, for all height and age bands. Note that contractor equipment is not modeled under builder's risk; it is modeled using existing construction and occupancy classes.

Builders risk is implemented in the Verisk Earthquake Model for Hawaii by applying time-dependent secondary modifiers to loss estimates for a building whose construction is complete. The model provides annualized average project loss estimates for the duration of the construction (defined as the duration of the policy), for each phase of construction, and for the worst case scenario (i.e., when an earthquake occurs at the end of construction, or when the replacement value approaches the replacement value of the completed building). The time-dependency of these modifiers is based on the variability of the building's vulnerability and replacement value from one construction phase to another.

To develop the builders risk damage functions, Verisk engineers conducted extensive structural analyses of buildings during the four phases of construction (see the Table below) using data from RS Means 2011 (Reed Business Information), United States Construction 2010 Census, and the National Building Construction Manual for 2009.

Table 11. Building phases during construction

Building Phases	
I Foundation and Substructure	III Walls and Roofing
II Superstructure	IV Finishing, Mechanical and Electrical Installation

Duration of building phases

The four construction phases in [Table 11](#) overlap one another, with the timeline of each dependent on the type of building. For commercial buildings, for example, phase IV will be much longer than it would be for residential ones. To determine the phase duration, Verisk engineers used engineering cost estimation data. [Figure 62](#) shows an example of the phase timeline for a mid-rise (4-7 stories) commercial building. The duration for each phase is presented as a percentage of the total time to complete a building

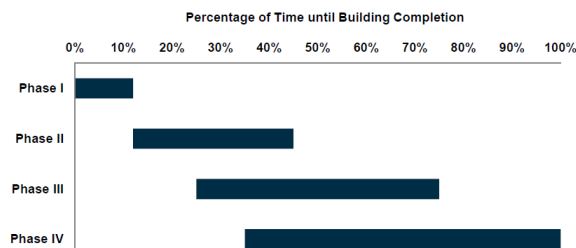


Figure 62. Duration of phases for a mid-rise commercial building

Verisk engineers also took into consideration the subcomponents at each phase. For example, to determine the vulnerability curves for phase III, the vulnerability of the roofing, windows, and exterior walls were all considered. The Figure below illustrates the duration of some of the subphases for a mid-rise commercial building. This Figure includes the duration and overlap of the main four phases, illustrating how the many subphases are included in more than one main phase.

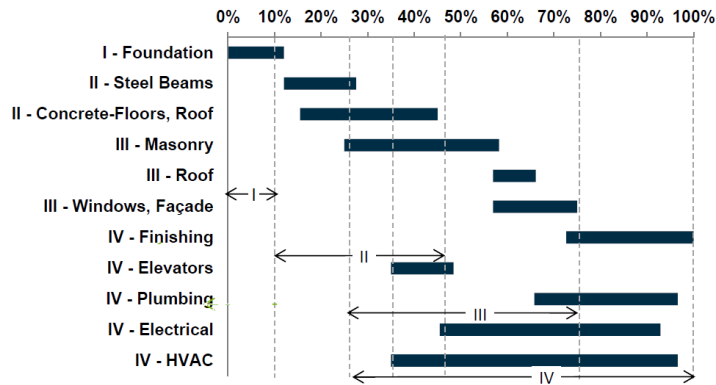


Figure 63. Duration of some sub-phases for a mid-rise commercial building

Variations in the replacement value during construction

The relationship between the building cost, or replacement value, and project duration is captured in a cost ramp-up curve, which shows the evolution of a total project cost over time. At each construction phase, the percentage of the ultimate replacement cost of the building depends largely on the building’s height and occupancy class.¹³ (Construction class does not have a significant effect on the variations in the percentage.)

The effects of height on building costs can be illustrated by examining the percentages of the total cost at each construction phase for buildings of the same occupancy type but different heights, as shown in [Table 12](#), which uses the example of apartment buildings. For each height band, the cost of each phase is presented as a percentage of the total cost; therefore, a change in the costs at particular phase causes the costs of other phases to be adjusted.

For low-rise buildings, the foundation and substructure account for a larger percentage of the entire building (and its cost) than they would for a mid-rise building. This is because the absolute cost of phase II in mid-rise buildings has a higher increase over phase I than it does for low-rise buildings, making the percentage of the phase I cost lower. The cost percentage for high-rise buildings is greater since these buildings require a more elaborate foundation than shorter buildings.

The cost percentages at phase II increase steadily with height, with a larger increase from phase I for taller buildings. This is to be expected since the columns and other elements of the superstructure are more elaborate for taller buildings than for lower ones. It is also the reason for the decrease in the percentage of cost with height at phases III and IV. Due to the large increase in the costs of phase II for mid-rise and high-rise buildings, the percentages of the total cost at phases III and IV are diminished.

¹³ Only a subset of the model occupancies is supported in builders’ risk. The main occupancies modeled with unique phase durations are residential and commercial buildings; they do not include industrial facilities.

Table 12. Percentage of the total cost at each construction phase for apartment buildings of different heights

Construction Phase	Low Rise (1-3 Stories)	Mid Rise (4-7 Stories)	High Rise (8+ Stories)
I Foundation and Substructure	6%	5%	7%
II Superstructure	9%	12%	13%
III Walls and Roofing	14%	12%	10%
IV Finishing, Mechanical and Electrical Installation	71%	71%	70%
All Phases	100%	100%	100%

The cost ramp-up curve in [Figure 64](#) shows the changes in the replacement value for commercial buildings of different heights. The sharp bend in the curves indicate the beginning of phase IV when the interior work occurs, mechanical and electrical systems are installed, and the finishing touches are applied. (This corresponds to the bend in the replacement value curve shown in [Figure 68](#).) The replacement value then levels off slightly once the finishing touches begin since the costliest parts of this phase are complete at that time.

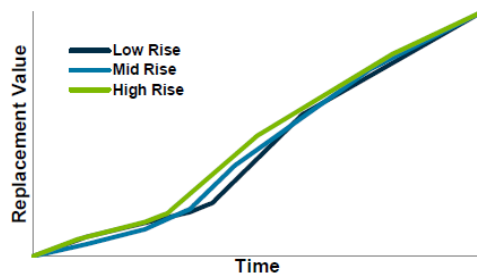


Figure 64. Changes in replacement value during construction of a commercial building, for different heights

[Figure 65](#) compares the cost ramp-up curves for low-rise buildings of different occupancy classes. After phase IV, the curve ramps up more sharply for apartment buildings. Apartment buildings have a larger amount of interior work and finishing, which have to be done in each unit. In addition, the materials used for residential kitchens and bathrooms are generally of a higher quality than in commercial and industrial buildings. While commercial and industrial

buildings have more wall partitions, facilities, and fixtures, the materials are not as costly as those in apartment buildings.

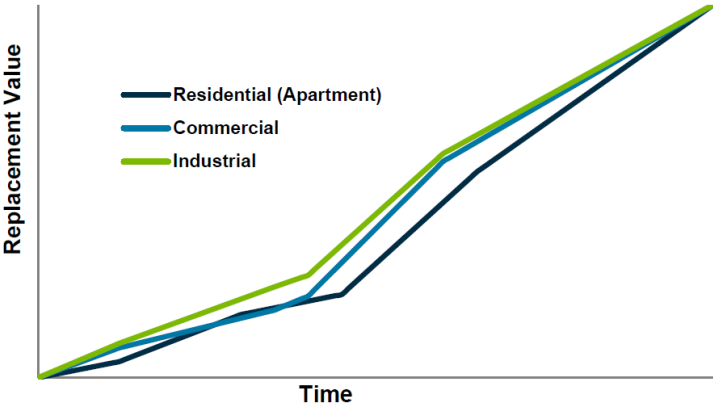


Figure 65. Changes in replacement value during construction of low-rise buildings with different occupancy classes

The various occupancy types within each class can have a significant effect on the variations in replacement value during construction, as shown in [Figure 66](#). For example, phase IV of a hospital can take up a larger percentage of the total cost than of other buildings, due to the extensive electrical and mechanical fittings that are required for a hospital. For other large structures, such as a wholesale trade centers, costs are more concentrated in phases II and III due to the extensive walls, roofing, and other elements of the superstructure. Phase IV is less important in these cases since the interior walls and fixtures are not as costly as in other buildings.

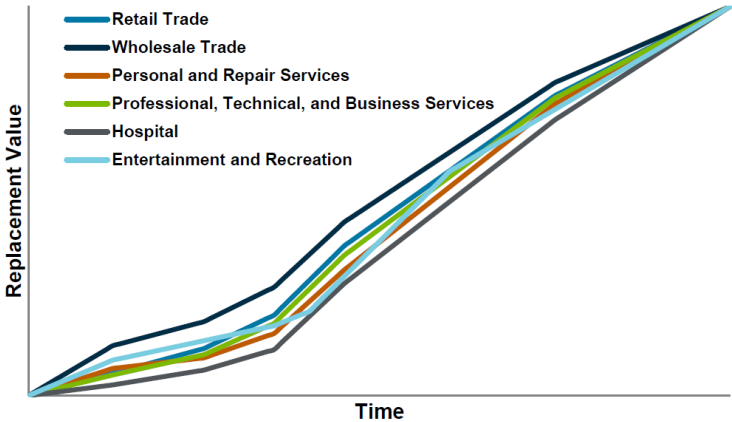


Figure 66. Changes in replacement value during construction of mid-rise commercial buildings with different occupancy types

Variations in vulnerability during construction

As construction progresses, the changes in vulnerability must be considered along with the replacement value. The seismic effects on the building are different during each building phase.

I. Foundation and Substructure. The vulnerability is lowest at this phase.

II. Superstructure (Frame and Decks). The vulnerability is highest at this phase. Specifically, it increases rapidly during this phase, eventually exceeding the vulnerability of the completed building; its shorter natural period results in a higher seismic demand. The lateral load-resisting systems also may not be complete at this phase (e.g., connections may be loose and bracing may be incomplete). As this phase progresses the vulnerability eventually decreases until it is close to that of the completed building.

III. Exterior Walls, Doors, Windows, Roofing. At this phase the vulnerability is close to that of the completed buildings.

IV. Finishing, Mechanical and Electrical Installation. The seismic response remains unaffected during this stage; vulnerability is that of the completed building.

These changes in seismic vulnerability are illustrated in [Figure 67](#), which clearly shows the low vulnerability for phase I as well as the similarity in vulnerability changes for the other phases.

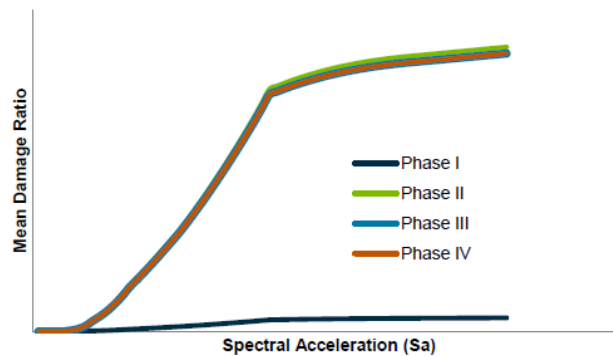


Figure 67. Changes in seismic vulnerability at each construction phase

[Figure 68](#) shows how the replacement value and vulnerability vary during construction, with the vulnerability at any given time corresponding to a specific replacement value at that time.

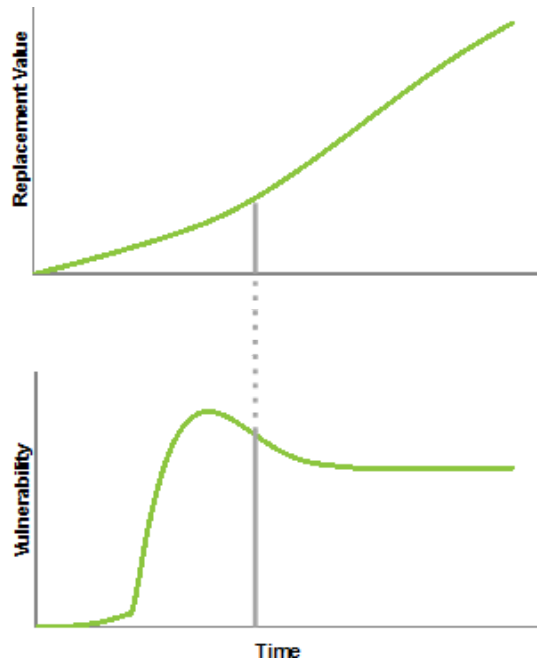


Figure 68. Variations of replacement cost and vulnerability of buildings under construction

5.10 Contents damage

In the Verisk Earthquake Model for Hawaii, contents damage is a function of spectral acceleration and also of the occupancy class. Note that each occupancy class is associated with a set of typical contents and their vulnerability to shake damage. Contents damage is generally higher in commercial occupancies than residential ones, and higher in industrial facilities than in commercial facilities.

At low levels of shaking, the primary determinant of contents damage is floor acceleration, which imposes inertial lateral forces. At higher levels of shaking, contents damage depends on both inertial forces and building damage. For example, contents may be damaged due to the collapse of both structural and nonstructural components, including ceilings, beams, and columns. Content damage generally increases at higher levels of shaking. Unreinforced masonry structures have the highest content damage of the construction classes.

5.11 Automobile damage

Automobile damage during an earthquake occurs primarily as a result of debris falling from damaged buildings; therefore, damage to automobiles is modeled as a function of building damage. The damage function in the Verisk model is calibrated against the observed damage from the 1994 Northridge earthquake.

5.12 Workers compensation losses due to earthquakes

The Verisk Earthquake Model for Hawaii offers an auxiliary damage estimation component that generates losses due to injuries and deaths that occur under workers compensation insurance policies. When ground shaking during an earthquake damages a workplace, employees who are in or near the building at the time can sustain a wide variety of injuries, with severity ranging from minor to fatal. Depending on the time of day the earthquake occurs, the number of people at work at the time, and other factors, a significant percentage of the total insured losses can be due to workers compensation.

The Verisk model offers a complex analysis that incorporates the most likely types of injuries that are incurred in buildings of different construction types, with different levels of damage, along with a large number of other factors that affect workers compensation losses. These include the number of injuries and deaths as a function of the injury rates, the nature of the damage sustained by the buildings where the workers are located, and the number of workers who are at risk at the time of the earthquake. The model does not account for any loss of income due to these injuries.

Types of building damage that cause injury

The primary cause of injury during earthquakes is due to debris falling inside damaged buildings and, in the most severe cases, the collapse of occupied buildings. Therefore, the nature and severity of injuries from earthquakes are modeled as a function of building damage. For each construction type and occupancy class, the Verisk model divides the full distribution of building damage into four distinct damage states: minor, moderate, extensive, and complete.

Note that “complete” damage means that a building is not recoverable; it does not necessarily mean that a building has collapsed. However, the state of collapse of a building has significant consequences in a workers compensation loss estimation, since building collapse typically increases the number of fatalities and severe injuries. In the Verisk model, the probability of collapse is used to create two categories within the complete damage state: “complete damage without collapse” and “complete damage with collapse.”

Building construction, and its effect on a building’s ability to withstand ground shaking, has been shown to affect injury and fatality rates significantly. For example, the 1995 Great Hanshin earthquake in Kobe, Japan, which occurred at 5:46 a.m., caused more than 5,000 deaths. In contrast, the 1994 Northridge earthquake, which occurred at 4:30 a.m., resulted in fewer than 60 deaths. The earthquakes were of similar magnitude and both occurred during early morning hours when most people were not yet at work. The difference in fatality counts can be largely explained by differences in building construction. As construction practices vary widely by location, it is inadvisable to use international damage and casualty experience when estimating workers compensation losses in the United States.

However, within the United States, the structural requirements for buildings and the degree to which they are enforced vary greatly with location. In earthquake-prone areas, structural requirements are generally more stringent than in areas where there has been little historical

earthquake activity. The Verisk model takes these requirements into consideration, since they have a significant effect on a building's ability to withstand ground shaking.

Probability of collapse

The probability of collapse for any given building is determined primarily by its construction class. Masonry buildings, for example, are more likely to collapse than concrete buildings. Steel buildings may experience significant deformation under severe ground shaking, but collapse is less likely.

The collapse probabilities used in the Verisk model are adopted from the HAZUS MR4 Technical Manual (FEMA 2009), with adjustments made based on engineering judgment and damage reports from building collapses due to earthquakes in the United States. The Table below shows examples of the collapse probability used in the Verisk model.

Table 13. Collapse probabilities used in the Verisk Earthquake Model for Hawaii

Construction Type	Probability of Collapse (%) Given Complete Damage State
Wood Frame, Low-Rise	2
Masonry, Low-Rise	12
Masonry, Mid-Rise	9
Reinforced Concrete, Low-Rise	10
Reinforced Concrete, Mid-Rise	8
Reinforced Concrete, High-Rise	4
Steel, Low-Rise	8
Steel, Mid-Rise	5
Steel, High-Rise	3

Injuries due to earthquakes

Historical evidence shows that most of the injuries resulting from small to moderate earthquakes are lacerations, sprains, and contusions caused by non-structural building components falling on people. Life-threatening or fatal injuries are typically caused by the structural damage that occurs with larger magnitude events.

The Table below shows the percentage of nonfatal injury types for five historical earthquakes of moderate magnitude in California. The data used to construct this table comes from various sources, including studies by Aroni and Durkin (1985). Because these statistics come from multiple studies, the "Other" category contains injuries such as fractures, pain/soreness, respiratory or inhalation injuries, eye injuries, and unspecified injuries, which may not be represented the same way in each study.

Table 14. Distribution of nonfatal injuries for five California earthquakes

Earthquake		Lacerations	Sprains	Contusions	Cardio-vascular	Neuro-logical/ Psych-ological	Other
Santa Barbara (1978)	M5.7	33%	19%	23%	2%	2%	21%
Imperial County (1979)	M6.4	25%	14%	18%	0%	13%	30%
Coalinga (1983)	M6.7	32%	14%	23%	1%	5%	25%
Loma Prieta (1989)	M6.9	7%	39%	22%	N/A	0%	32%
Northridge (1994)	M6.7	31%	13%	6%	11%	4%	35%

The Verisk model also estimates the probabilities, or rates, of injury severity for each of the damage states of each construction class. There are four injury severity levels used in the Verisk model, as shown in the Table below.

Table 15. Injury severity levels used for workers compensation (FEMA 2009)

Severity Level	Description
Minor	Basic medical aid that can be administered by paraprofessionals is sufficient. Examples are sprains, severe cuts requiring stitches, minor burns (first or second degree on a small part of the body), and bumps on the head without loss of consciousness.
Moderate	A greater degree of medical care is necessary. The use of medical technology such as x-rays or surgery is needed, but the injury is not life-threatening. Examples include second or third degree burns over large parts of the body, bumps on the head that cause loss of consciousness, fractured bones, dehydration, or exposure.
Life-Threatening	Injuries pose an immediate life-threatening condition if they are not treated expeditiously. Examples include: uncontrolled bleeding, internal injuries such as punctured organs, spinal injuries, and crush syndrome.
Fatal	Person is instantaneously killed or mortally injured.

Calculating the number of casualties

To estimate the number of casualties that correspond to different combinations of damage states and injury severity levels, the Verisk model uses an event-tree framework, such as the one shown in [Figure 69](#). By following the event tree, the number of casualties for each of the four injury severity levels is estimated separately for each building damage state. The casualty numbers are then combined according to their associated probabilities to produce the total injury estimation for a building.

This calculation is completed for the damage states for each construction type. Casualty rates depend to a large degree on construction type. For example, the casualty rate for a wooden house differs significantly from that of a high-rise concrete building.

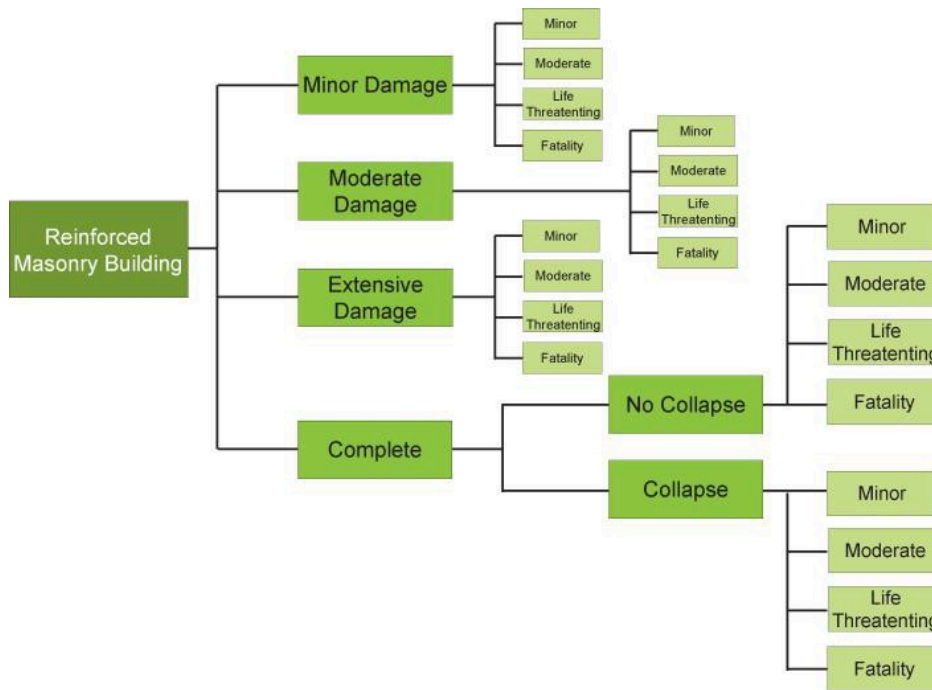


Figure 69. Injury severity level by building damage state for a reinforced masonry building

Calculating the number of casualties due to an earthquake is a complex process because each building damage state must be correlated with the likelihood of injury and the severity level. Injury rates are separately derived for each injury level and are conditional on the building’s damage state. They are derived using casualty data from historical earthquakes in the United States (FEMA 2009 and Peek-Asa et al. 2000).

Estimating workers compensation losses

For each injury severity category an estimate of the number of workers that are injured is calculated using a probabilistic process that accounts for inherent uncertainties. First, the injury rate distribution is applied to the number of employees present in the building. The cost of the injuries, which also varies by their severity, is then applied and summed probabilistically to achieve an estimate of total workers compensation losses for that building (see Figure below).

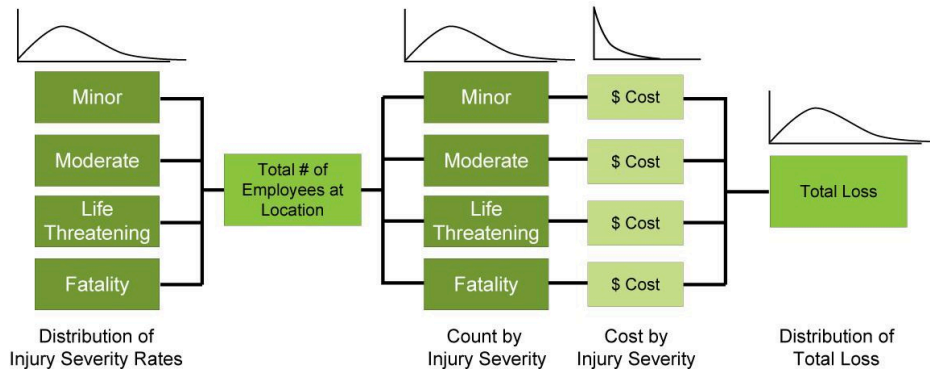


Figure 70. Calculation of Workers Compensation Loss for an Individual Building

The total number of workers at each location is derived using a comprehensive business demographics database of U.S. businesses and employee counts from a premier market research company. In the Verisk model, the estimate of the percentage of workers who are injured depends on the day of the week and the time of day that the earthquake took place.

The model utilizes a six-day work week (since many businesses operate on Saturday or Sunday). Daytime is defined as the hours from 9 a.m. to 5 p.m., while night is defined as 7 p.m. to 7 a.m. Separating these time periods are two commuting periods: one from 7 a.m. to 9 a.m. and another from 5 p.m. to 7 p.m. Therefore, for the days Monday-Saturday, the model assumes an 8-hour working period, 4 hours of commute time, and a 12-hour night. (Sunday falls into the same category as night.) This means that there is less than a 30% probability that an earthquake, which can occur at any time of day or night with equal probability, will occur during the hours when the majority of employees are at work. The difference in the number of workers during each of the three time periods has a direct consequence on the estimated number of casualties.

Developing default injury costs and benefit levels

Estimates of workers compensation losses are calculated based on the number of employees who have sustained injuries at each severity level and on the cost of the injury, which depends on its severity as well as the location of the workplace. In cases where claims costs are not provided by the client, the model uses objective average costs, specific for each state.

The mental stress that usually accompanies catastrophic events is also taken into consideration. An adjustment is made to the average cost of nonfatal injuries to incorporate an increased level of mental stress. The amount of the adjustment is based on the “mental stress” historically associated with an injury using observational data.

5.13 Validating the model's damage estimation module

The model's damage functions report the mean damage ratio for each level of intensity, where the mean damage ratio is the ratio of the repair cost of the building or contents to its replacement value. Thus, validating the damage estimation component of the model is inextricably intertwined with validating modeled losses. A discussion of modeled loss validation can be found in Verisk Industry Exposure Database. Validating event losses, which accounts for ground motion, vulnerability, and industry inventory data, ensures a model's overall performance.

For regions where detailed data on damage and loss is scarce, as is the case in Hawaii, Verisk engineers leverage the extensively validated damage functions from other, more mature insurance markets, such as the continental United States, and then modify them to reflect local conditions, including the age of the building stock, local design and, seismic codes, local construction practices and socioeconomic circumstances.

A sample of validation exhibits relating to the model's damage functions and worker compensation losses are provided below.

Validating the model's damage estimation module against data from the 2006 Kiholo Bay earthquake

The strongest earthquake to occur in recent history in Hawaii was the M6.7 event, which struck off the northwest coast of Hawaii Island on October 15, 2006. This earthquake was studied in great detail, as Verisk researchers used the data to validate the model's damage estimation module.

This earthquake caused damage to over 1800 residential buildings with the worst damage occurring along the northern and western portions of Hawaii Island. In the month following the event, Hawaii county engineers followed the ATC-20 post-earthquake building safety evaluation procedure to inspect approximately 1700 homes. As a result, 67 homes were "red tagged" as severely damaged and deemed unsafe for entry. 227 homes were "yellow tagged" as partially damaged and deemed safe only for restricted use. The remaining homes were green-tagged and considered safe for lawful occupancy.

The majority of the single-family homes that were red tagged consisted of single-wall wood frames set on post and pier foundation systems resting on small unanchored concrete foundation blocks locally known as "tofu blocks". These homes are particularly susceptible to earthquake damage, as the posts are resting and are not connected to the foundation. Thus, the building may fall off the foundation if the relative movement between the posts and the supporting foundation exceeds the size of the "tofu block" or successive shaking leads to "walking" of the posts. (Chock et. al. 2006). The distribution of all of the damaged buildings evaluated by the Hawaii county engineers is shown in the following Figure.

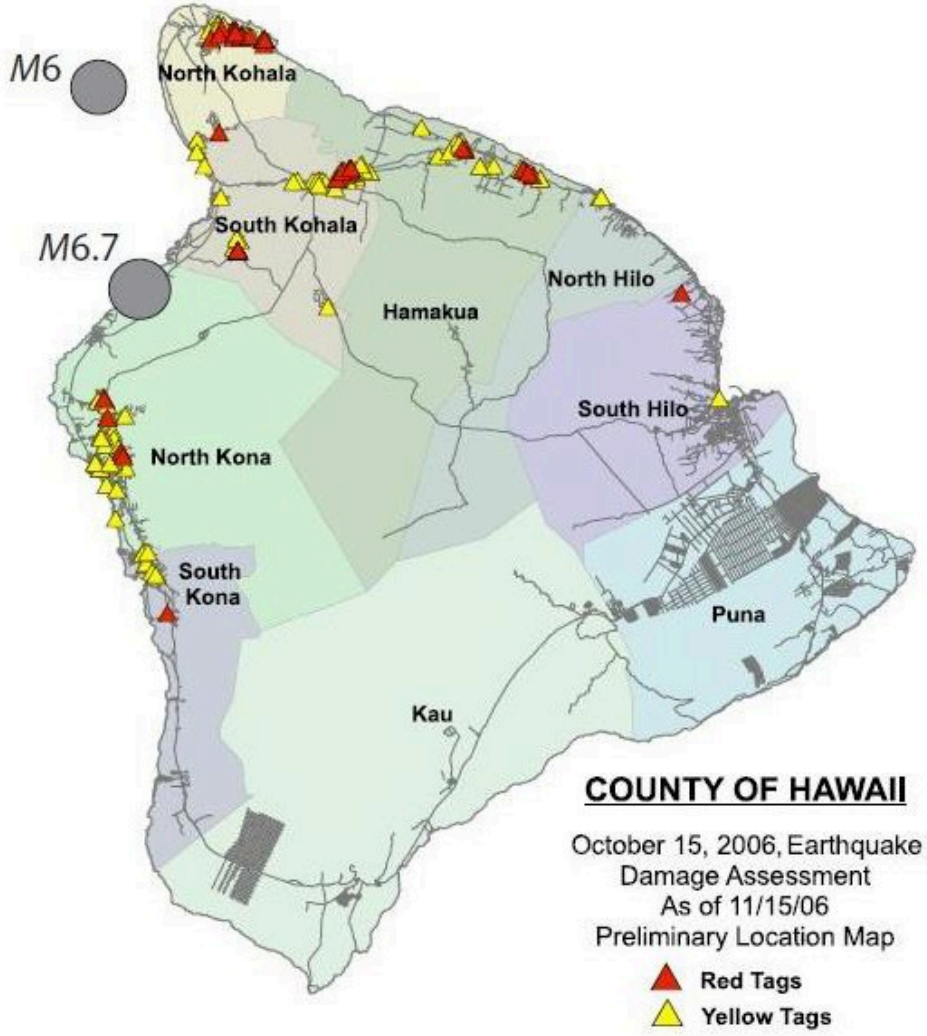


Figure 71. Damage distribution in Hawaii County, according to data obtain from Hawaii County (Takahashi et al. 2011)

Figure 72 shows the modeled damage footprint as a result of the 2006 Kiholo Bay earthquake. This footprint was constructed using exposure in the IED from which damage ratios were computed. Note that the modeled mean damage ratio in this region is about 3.5%, with a maximum value of 70% as indicated by the figure.

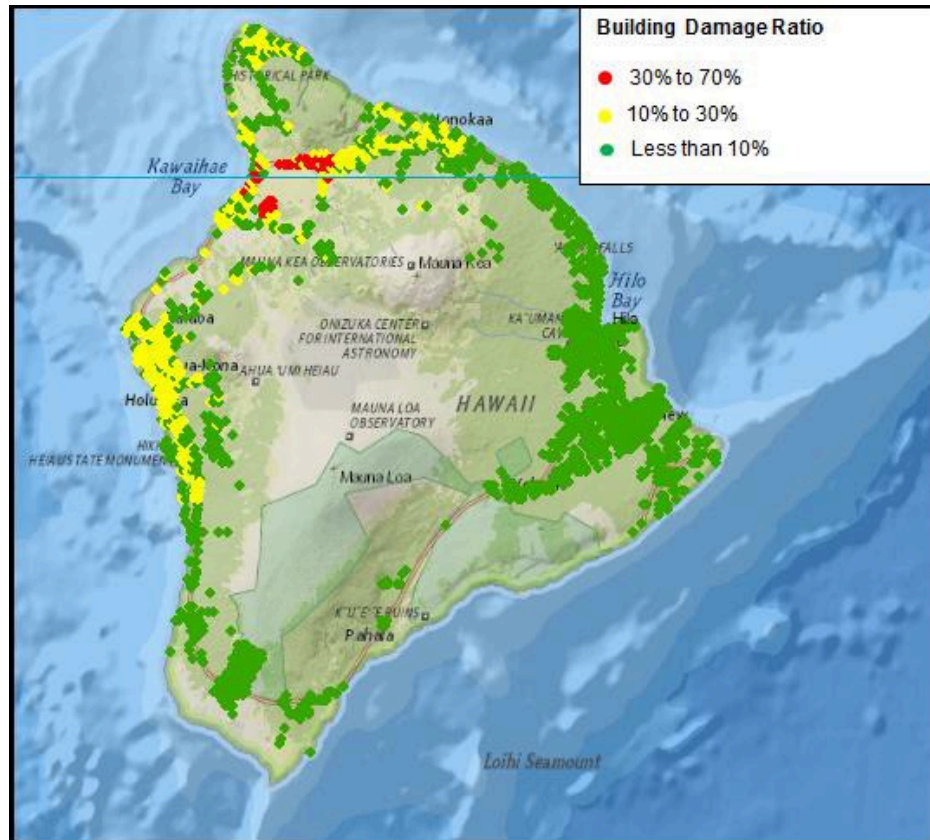


Figure 72. Modeled damage ratio footprint for the 2006 Kiholo Bay earthquake

The modeled damage footprint is reasonably close to the distribution of damaged buildings evaluated by the Hawaii county inspectors. Note that Hawaii county inspectors evaluated homes impacted by both the main M6.7 event and the M6.0 aftershock. The combination of both events caused severe damage to many homes near North Kohala along the northern tip of Hawaii. This damage is not reflected in the modeled damage footprint because this footprint was constructed for the M6.7 event only.

Additional validation was undertaken through analysis of findings from post-disaster surveys conducted in the aftermath of earthquakes in the continental United States. Due to similarities in design load, construction practices, and code requirements between the continental United States and Hawaii, such validation is applicable to the Verisk Earthquake Model for Hawaii. Thus, the relative vulnerabilities of different construction/occupancy/height combinations in the Verisk damage functions are borne out by observations.

Validating damage functions for large-scale industrial facilities

To validate the damage functions (at both the component and facility level), observational damage data to industrial facilities was collected from damage reconnaissance reports after historical earthquakes.

The following Table lists 40 historical earthquakes from which damage data was collected for validating the damage functions for industrial facilities.

Table 16. Historical earthquakes used for facility and component damage function validation

Earthquake	Year	Earthquake	Year
Gediz, Turkey	1970	Dinar, Turkey	1995
San Fernando, California	1971	(Hyogo-Ken Nanbu) Kobe, Japan	1995
Imperial Valley, California	1979	Lijiang, Yunnan Province, China	1996
Borah Peak, Idaho	1983	Adana-Cayhan, Turkey	1998
Coalinga, California	1983	El Quindio, Colombia	1999
Morgan Hill, California	1984	Chichi (Jiji), Taiwan	1999
Chile	1985	Kocaeli, Turkey	1999
Michoacan, Mexico	1985	Duzce, Turkey	1999
San Salvador, El Salvador	1986	Nisqually, Washington	2001
Palm Springs, California	1987	Bhuj, India	2001
Whittier Narrows, California	1987	Southern Peru	2001
Tejon Ranch, California	1988	Molise, Italy	2002
Armenia	1988	Denali, Alaska	2002
Loma Prieta, CA	1989	Boumerdes, Algeria	2003
Philippines	1990	San Simeon, CA	2003
Costa Rica	1991	Bam, Iran	2003
Erzincan, Turkey	1992	Tecoman, Mexico	2003
Hokkaido-Nansei-Oki, Japan	1993	Nigata Ken Chuetsu, Japan	2004
Guam	1993	Sumatra, Indonesia	2004
Northridge, CA	1994	Hawaii	2006

Some types of industrial facilities and components, whose damage functions have been validated using damage data from historical earthquakes, are listed below.

Table 17. Some facilities and components validated with damage data from historical earthquakes

Facility	Earthquake	Year
Chemical Plants	Borah Peak, ID	1983
	Coalinga, CA	1983
	Morgan Hill, CA	1984
	Chile	1985
	Hokkaido Nansei-Oki, Japan	1993
	Izmit, Turkey	1999
	Athens, Greece	1999
	Bam, Iran	2003
Thermo-Power Plants	San Fernando, CA	1971
	Imperial Valley, CA	1979
	Chile	1985
	Loma Prieta, CA	1989
	Northridge, CA	1994
	Kobe, Japan	1995
	Chichi (Jiji), Taiwan	1999
	Izmit, Turkey	1999
	Athens, Greece	1999
	Southern Peru	2001
	San Simeon, CA	2003
	Sumatra, Indonesia	2005
	Hawaii	2006
Metal Processing Plants	Chile	1985
	Kobe, Japan	1995
	Izmit, Turkey	1999
	San Simeon, CA	2003
Potable Water Systems	Imperial Valley, CA	1979
	Coalinga, CA	1983
	Northridge, CA	1994
	Kobe, Japan	1995
	Central Colombia	1999
	Chichi (Jiji), Taiwan	1999

Facility	Earthquake	Year
	Nisqually, WA	2001
	Southern Peru	2001
	Bam, Iran	2003
	San Simeon, CA	2003
Pipes	Imperial Valley, CA	1979
	Coalinga, CA	1983
	Morgan Hill, CA	1984
	Chile	1985
	Loma Prieta	1989
Poles	San Fernando, CA	1971
	Imperial Valley, CA	1979
	Whittier Narrows, CA	1987
	Northridge, CA	1994
	Kobe, Japan	1995
	Chichi (Jiji), Taiwan	1999
Pipe Racks	Loma Prieta, CA	1989

The following three Figures show facility-level damage functions plotted against observational data from some historical earthquakes.

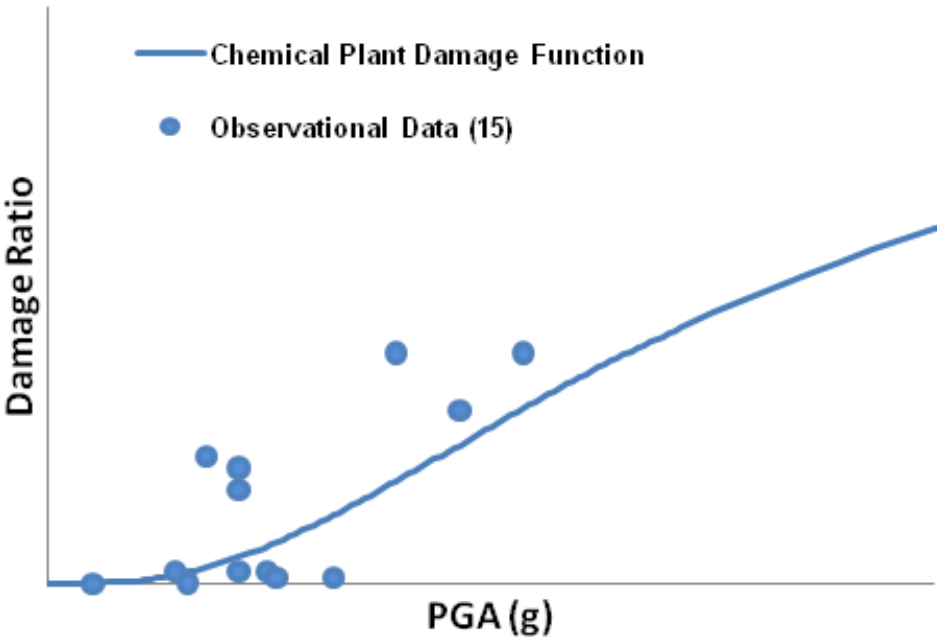


Figure 73. Damage functions and observed damage data for chemical processing plants in a high seismicity area

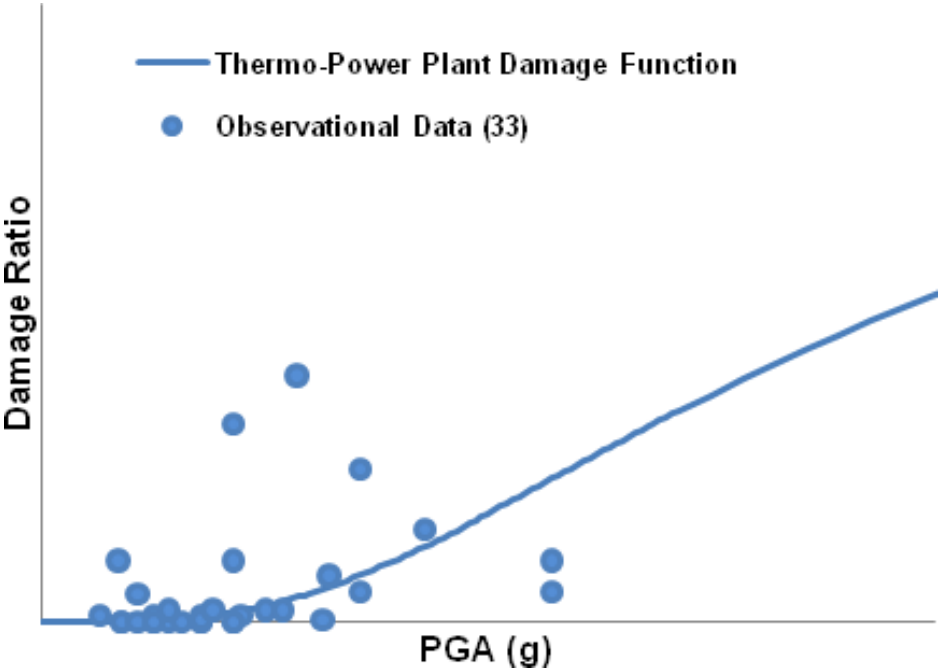


Figure 74. Damage functions and observed damage data for a thermo-power plant in a high seismicity area

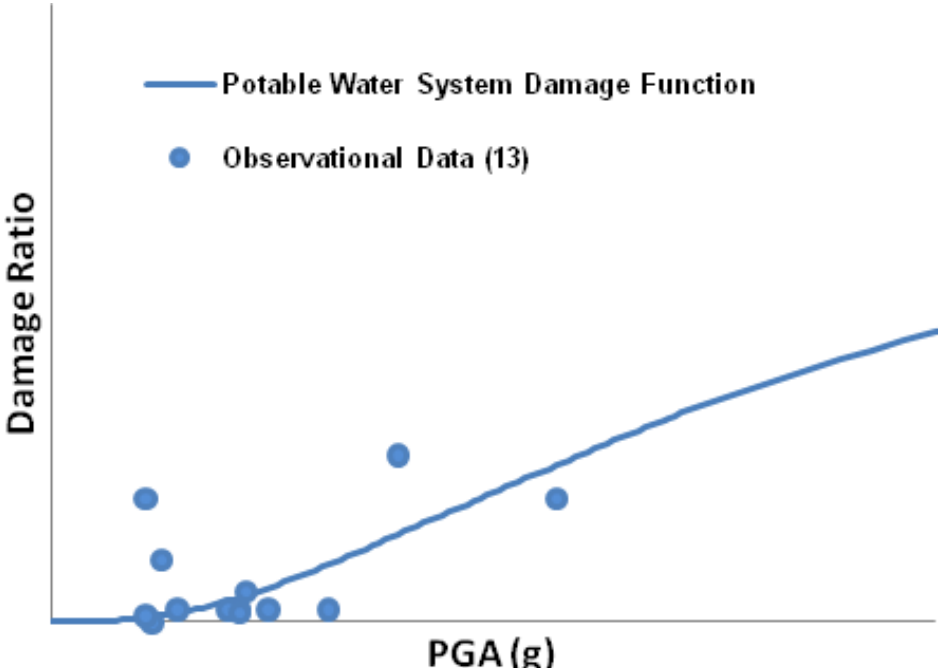


Figure 75. Damage functions and observed damage data for potable water systems in a high seismicity area

Validating modeled workers compensation losses

The workers compensation component of the Verisk Earthquake Model for the Hawaii relies on published studies of casualty rates as well as data from actual earthquakes that occurred in the continental United States. For validation, however, the availability of appropriate data is limited. Some of the challenges are discussed in this section, along with a comparison between modeled and historical injury counts for some recent earthquakes. Note that a meaningful comparison of losses is made more challenging because of the significant changes in benefit levels that have occurred over time. Note that the modeled results reflect industry exposures as of 2008, both in terms of population and exposed properties.

There is only limited information on workers compensation insurance claims in the United States available to the public. In addition, there is a certain amount of uncertainty regarding the change over time in number of workers and their workplaces. Therefore, a reliable validation uses a comparison between the modeled and historical injury counts based on the total population, rather than on the injury counts of workers.

The Table below shows the total number of casualties based on observational data after some recent historical earthquakes in California. These observations are compared to the number of casualties that are estimated by the Verisk model were these earthquakes to recur today. Given an average population growth of approximately 1.6% annually in California between 1980 and 2008 (U.S. Census Bureau), the number of casualties reported at the time of these events are adjusted based on a formulation (Vranes et al., 2009). These adjusted values provide estimates of the number of casualties that would occur had these events taken place with today's population. With population growth taken into account, the modeled results are within a reasonable range for these earthquakes.

Table 18. Comparison of observed and modeled casualties for selected historical earthquakes in California

Year	Location	Observed Casualties*		Modeled Casualties	
		Nonfatal	Fatal	Nonfatal	Fatal
1987	Whittier	1,913	11	3,015	25
1989	Loma Prieta	5,161	87	8,297	95
1992	Landers	457	1	449	1
1994	Northridge	36,035	76	39,761	81

*Values have been adjusted to account for population growth in California.

The uncertainty surrounding the number of injuries and fatalities observed during older earthquake events is considerably greater than for more recent events. This is due to less reliable data for older earthquake, and the fact that the impact of population growth on the number of casualties that would occur if those earthquakes took place today is difficult to predict. Moreover, the improvement in building design as well as increased public awareness of earthquake hazards over the past several decades play an important role in reducing the number of casualties. The combined impact of these factors on the injury counts is not quantifiable, especially in cases where the earthquakes occurred several decades ago.

However, information from all of the past earthquakes can be used to verify the overall model performance. Fatality data from 29 historical earthquakes in the U.S. that occurred between 1886 and 2003 was collected (NOAA, 1972; Cutter et al., 2005; Ramirez et al., 2005; and Vranes et al., 2009) and compared with the model estimates.

The following Figure shows a scatter plot of observed and modeled fatalities. The horizontal line associated with each event indicates a range of the observed fatalities, suggesting uncertainties in the observed numbers. While the model underestimates the fatalities for some of the events and overestimates for others, the plots are tightly scattered around the 45° line, which indicates that the model estimates in general are reasonable and that the model does not have a bias.

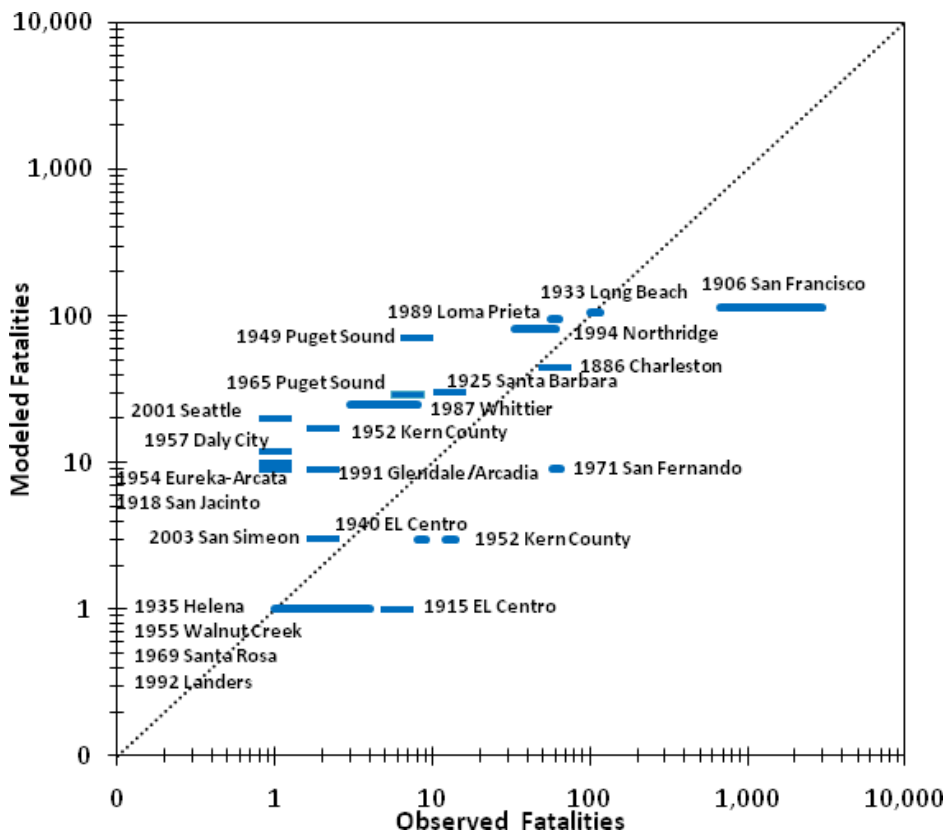


Figure 76. Modeled vs. observed fatalities from 29 historical earthquakes in the U.S.

The loss estimates produced by the Verisk workers compensation module are well within the range of reasonability when compared to the available historical data. Although there have been no significant casualties from earthquakes since the 1906 event in San Francisco, there is no doubt that earthquakes pose a significant hazard. It is therefore important to use a realistic modeling approach for workers compensation to determine injuries due to ground shaking from earthquakes.

6 Insured Loss Calculation

The Verisk Earthquake Model for Hawaii uses a comprehensive cost model to estimate the repair cost of each damaged component in order to translate ground-up damage into monetary losses. Insured losses are calculated by applying policy conditions to the total damage estimates resulting from the damage estimate module. A wide variety of policy conditions are supported in this model, including franchise deductibles, coverage limits, loss triggers and risk-specific reinsurance terms.

6.1 Aggregating losses probabilistically

Post-disaster surveys and actual claims data reveal an inherent variability in the damage that results from a given level of ground motion. Loss estimates generated by the Verisk Earthquake Model for Hawaii capture this variability by accounting for both primary and secondary uncertainty.

Primary uncertainty is associated with the randomness in the location and size of future events, which is captured in the stochastic catalog event-generation process. Secondary uncertainty describes the uncertainty in building damage *and* in the local intensity estimation. The former arises due to inherent randomness in the response of buildings of similar construction to a given level of shaking originating from variability in building characteristics, material properties, and workmanship. The uncertainty in the local intensity of the hazard can be attributed to the phenomena of inter- and intra-event variability. The secondary uncertainty is modeled through a probabilistic distribution around the calculated mean damage ratio.

Damage is calculated using damage functions that provide, for a given local intensity, a mean damage ratio (MDR) and a probability distribution around the mean that captures the secondary uncertainty in damage. For the Verisk Earthquake Model for Hawaii, a bi-beta distribution combined with empirically derived probabilities of 0% and 100% damage levels are used to model the uncertainty around the mean damage.

The damage functions are used to produce, for each event, a distribution of ground-up loss by location and coverage. Limits, deductibles, and reinsurance are applied in the financial module to the ground-up loss distribution to produce gross and net loss estimates. Note that insured losses can accumulate even if the mean damage ratio is below the deductible, because some structures are damaged above the mean damage ratio and the deductible. The distributions are applicable to the analysis of a single exposure and usually have a high degree of uncertainty. The individual distributions are combined to obtain the portfolio distribution, where the uncertainty is lower.

In the financial module, there clearly is a need for aggregating losses probabilistically, at various levels. Computational techniques have thus been developed for statistically aggregating nonparametric distributions.¹⁴ Even though the ground-up, coverage-level

¹⁴ Nonparametric statistical methods do not rely on the estimation of parameters, such as the mean or the standard deviation, to describe the distribution of the variable of interest. They also do not rely on assumptions that the data are drawn from a

damage distributions typically utilize parametric distributions, after the application of location and policy terms, the distributions cannot be represented in a parametric way. Further aggregations of such loss distributions are achieved using numerical algorithms.

Convolution is the statistically correct way of deriving the probability distribution of the sum of multiple loss distributions. The probability density function of the convolution of two random variables F and G with density functions $f(x)$ and $g(x)$, respectively, is represented by the equation:

$$(f * g)(x) = \int_{-\infty}^{\infty} f(x-t)g(t)dt$$

where t is a dummy variable.

The Verisk models employ an efficient and accurate numerical algorithm for “convolving” any number of nonparametric loss distributions. Extreme care has to be taken when combining distributions with differing loss sizes. The technique used allows the correct representation of the shape of the loss distributions throughout the financial loss estimation process. Preserving the right shape is particularly important when insurance terms apply to the tails of the distributions.

Verisk’s financial module allows for the application of a wide variety of location, policy, and reinsurance conditions. Location terms may be specified to include limits and deductibles by site or coverage. Supported policy terms include blanket and excess layers, minimum and maximum deductibles, and sublimits.

6.2 Demand surge

Market forces generally ensure that the availability of materials and labor in any particular geographical area is sufficient to accommodate a normal level of demand without affecting price. However, demand can increase sharply and unexpectedly after a catastrophe such as a significant hurricane or earthquake. The resulting widespread property damage can cause a sharp increase in the need for building materials and labor, which in turn can cause prices to inflate temporarily. Demand for related services and resources such as transportation, equipment, and storage might also escalate in the affected area.

Scarce resources can also result in an increase in the time required to repair and rebuild damaged property, which may cause greater business interruption losses and additional living expenses. Infrastructure damage, delayed building-permit processes, and a shortage of available building inspectors also increase time-element loss. These factors can lead to insured losses exceeding expectations for a particular event and portfolio, a phenomenon known as demand surge. The greater and more widespread the damage from an event, the greater the resulting demand surge and insured losses will be.

Verisk engineers and statisticians have developed a demand surge function that relates the amount of demand surge to the amount of modeled industry insurable losses from a

given probability distribution. Parametric methods assume that the variable fits a probability distribution in order to make predictions regarding how that variable may behave in repeated samples.

particular event. This function was developed based on historical data, statistical analysis, economic time-series reviews, and analysis of construction-material and labor-cost data.

The demand surge function currently implemented in the Verisk software systems is the result of over 15 years of research and refinement. Verisk will continue to make improvements as new data becomes available. For details on the methodology used to develop the Verisk demand surge function and its validation, please see the client-confidential technical document *Verisk Demand Surge Function*, which is available on the Verisk website. Clients may choose to apply the default U.S. demand surge function or a user-defined demand surge function at their discretion.

6.3 Validating modeled losses

Although Hawaii experiences frequent earthquakes, few of these events are close enough and strong enough to cause significant damage to buildings in populated areas. Therefore, validating modeled losses is difficult due to the limited number of significant historical events and damage observations.

On October 15, 2006, a magnitude 6.7 earthquake struck off the northwest coast of Hawaii, causing damage to over 1,800 structures on the island. Reported (Munich Re) insured losses from this event were 50 million (2006 USD). The Verisk Earthquake Model for Hawaii was used to estimate losses from this earthquake based on source parameters obtained from USGS (see Table, below) and calculated using the formulas of Wells and Coppersmith (1994), with assumed uncertainties. The modeled insured losses are compared to reported losses in [Figure 77](#).

Table 19. Source parameters for the October 15, 2006 Hawaii earthquake

Source Parameters	
Moment Magnitude*	6.7
Depth*	29.0 km
Epicenter Longitude*	- 156.027
Epicenter Latitude*	19.82
Rupture Mechanism*	Reverse
Rupture Area*	315 km ²
Rupture Width+	13.7 km
Rupture Length+	23.0 km
*USGS	
+Wells and Coppersmith (1994)	

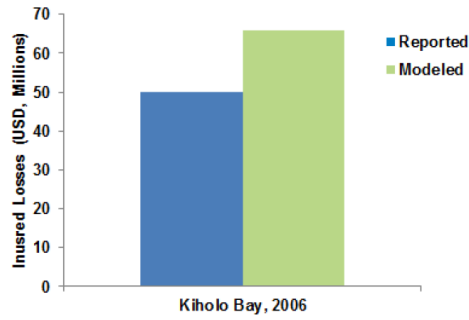


Figure 77. Comparison of modeled (Green) and Munich Re reported (Blue) losses for the October 15, 2006 Hawaii earthquake (2006 USD millions)

Selected References

Listed below are selected references used in the development of the Verisk Earthquake Model for Hawaii.

Abrahamson, N., and W. Silva 2008, "Summary of the Abrahamson and Silva NGA Ground-Motion Relations," *Earthquake Spectra*, 24, 67-97.

Aki, K. 1965, "Maximum Likelihood Estimate of b in the Formula $\log N=a-bM$ and Its Confidence Limits," *Bulletin of the Earthquake Research Institute*, 43, 237-239.

American Lifelines Alliance 2001, "Seismic Fragility Formulations for Water Systems, Part 1: Guideline," a report written under contract by the American Lifelines Alliance, a partnership between the Federal Emergency Management Agency and the American Society of Civil Engineers.

Applied Technology Council 2005, "FEMA 440: Improvement of Nonlinear Static Seismic Analysis Procedures," Redwood City, California: Applied Technology Council.

Aroni, S., and M. Durkin 1985, "Injuries and Occupant Behavior in Earthquakes," *Proceedings of the Joint U.S.-Romanian Seminar on Earthquakes and Energy*, Bucharest, Romania, September 2- 9, 1985.

ATC-13 "Earthquake Damage Evaluation Data for California," 1985.

Atkinson, G. M., and D. M. Boore 2003, "Empirical Ground Motion Relations for Subduction-Zone Earthquakes and their Application to Cascadia and Other Regions," *Bulletin of Seismological Society of America*, 93, 1703–1729.

Atkinson, G. M. 2010, "Ground motion prediction equations for Hawaii from a referenced empirical approach," *Bulletin of the Seismological Society of America*, 100, 751-761.

Boore, D. M., and G. M. Atkinson 2008, "Ground-Motion Prediction Equations for the Average Horizontal Component of PGA, PGV, and 5%-damped PSA at Spectral Periods Between 0.01 s and 10.0 s," *Earthquake Spectra*, 24, 99–138.

Campbell, K. W., and Y. Bozorgnia 2008, "NGA Ground Motion Model for the Geometric Mean Horizontal Component of PGA, PGV, PGD and 5% Damped Linear Elastic Response Spectra for Periods Ranging from 0.01 to 10s," *Earthquake Spectra*, 24, 139–171.

Chiou, B. S. J., and R. R. Youngs 2008, "Chiou-Youngs NGA Ground Motion Relations for the Geometric Mean Horizontal Component of Peak and Spectral Ground Motion Parameters," *Earthquake Spectra*, 24, 173–215.

Chock, G., T. Kindred, I. Robertson, G. Iinuma, P. Nicholson, E. Lau, H. Brandes, A. Sarwar, E. Medley, J. Dal Pino, P. Okubo, W. Holmes, B. Hirshorn, J. Sumada, Structural Engineers Association of Hawaii, and Hawaii State Earthquake Advisory Committee 2006, "Compilation of Observations of the October 15, 2006 Kiholo Bay (Mw 6.7) and Mahukona (Mw 6.0) Earthquakes, Hawai'i," *Earthquake Engineering Research Institute*

- EERI / Structural Engineers Association of Hawaii SEA0H / University of Hawaii (UH) report, December 31, 2006.
- County of Maui Department of Public Works and Environmental Management, "Adoption of Chapter 15-110 Rules Pertaining to Indigenous Hawaiian Architecture Structures."
- Cox, D. C. 1986, "Frequency Distributions of Earthquake Intensities on Oahu, Hawaii," report from the Environmental Center, University of Hawaii.
- Gupta, A., and B. M. McDonald 2008, "Performance of Building Structures during the October 15, 2006, Hawaii Earthquake," Proceedings of the 14th World Conference on Earthquake Engineering, Beijing, China, October 12-17, 2008.
- Johnson, G. S., R. E. Sheppard, M. D. Quilici, S. J. Eder, and C. Scawthorn 1999, "Seismic Reliability
Assessment of Critical Facilities: A Handbook, Supporting Documentation and Model Code Provisions," Technical Report, MCEER-99-0008, Multi-disciplinary Center for Earthquake Engineering Research, SUNY-Buffalo, Buffalo, New York.
- King, R. O. 2006, "Tsunamis and Earthquakes: Is Federal Disaster Insurance in Our Future?" CRS Report for Congress, Congressional Research Service, The Library of Congress, November 7, 2006.
- Klein, F. W., A. D. Frankel, C. S. Mueller, R. L. Wesson and P. G. Okubo 2001, "Seismic Hazard in Hawaii: High Rate of Large Earthquakes and Probabilistic Ground Motion Maps," Bulletin of the Seismological Society of America, 91, 479.
- Klein, F., A. Frankel, C. Mueller, R. Wesson, and P. Okubo 1998, "Documentation for Draft Seismic- Hazard Maps for the State of Hawaii," Report from the United States Geological Survey, March 9, 1998.
- Munich Re 2011, "Significant earthquakes in the United States 1980-2011," NatCatSERVICE, Geo Risks Research.
- Munson, C. G., and C. H. Thurber 1997, "Analysis of the Attenuation of Strong Ground Motion on the Island of Hawaii," Bulletin of the Seismological Society of America, 87, 945.
- O'Rourke, M. J., and S. Pak 2000, "Seismic Fragility Curves for On-Grade Steel Tanks," Earthquake Spectra, 16, 801-815.
- Peek-Asa, C., M. R. Ramirez, K. Shoaf, H. Seligson, and J.F. Kraus 2000, "GIS Mapping of Earthquake-Related Deaths and Hospital Admissions from the 1994 Northridge, California, Earthquake," Annals of Epidemiology, 10, 5-13.
- Power, M., Chiou, B., Abrahamson, N., Bozorgnia, Y., Shantz, T., & Roblee, C. 2008, "An overview of the NGA project," Earthquake Spectra, 24, 3.

- Sadigh, K., C. Y. Chang, J. A. Egan, F. Makdisi, and R. R. Youngs 1997, "Attenuation Relationships for Shallow Crustal Earthquakes Based on California Strong Motion Data," *Seismological Research Letters*, 68, 180.
- Salzano E., A. G. Agreda, A. Di Carluccio, and G. Fabbrocino 2009, "Risk Assessment and Early Warning Systems for Industrial Facilities in Seismic Zones," *Reliability Engineering & System Safety*, 94, 1577–1584.
- State of Hawaii, Department of Accounting and General Services, Uniform Statewide Building Code Task Force 2005, "Uniform Statewide Building Code Task Force Report and Recommendations to the Hawaii Legislature," Report and Recommendations to the Hawaii Legislature, December 9, 2005. State of Hawaii the Senate Twenty-Fourth Legislature 2007, "S.R. No. 67 Senate Resolution." Available at: http://www.capitol.hawaii.gov/session2007/bills/SR67_.htm.
- State of Hawaii, Department of Accounting and General Services 2010, "Annual Report on the Building Code Council Submitted to the Twenty-Sixth State Legislature in Response to Act 82, SLH 2007," Annual Report, December 2010. Available at: http://hawaii.gov/dags/rpts/bldg_code_council_09-10.pdf.
- Takahashi T.J., Ideda, N.A., Okubo P.G., Sako, M K., Dow, D.C., Priester, A.M., Steiner, N.A. 2011, "Selected Images of the Effects of the October 15, 2006 Kīholo Bay-Māhukona, Hawaii, Earthquakes and Recovery Efforts", 2011.
- Walling, M., W. Silva, and N. Abrahamson 2008, "Nonlinear Site Amplification Factors for Constraining the NGA Models," *Earthquake Spectra*, 24, 243–255.
- Weichert, D. H. 1980, "Estimation of Earthquake Recurrence Parameters for Unequal Observation Periods of Different Magnitudes," *Bulletin of the Seismological Society of America*, 70, 1337-1356.
- Wells, D. L., and K. J. Coppersmith 1994, "New Empirical Relationships among Magnitude, Rupture Length, Rupture Width, Rupture Area, and Surface Displacement," *Bulletin of the Seismological Society of America*, 84, 974-1002.
- Wong, I. G., K. H. Stokoe II, R. B. Cox, J. Yuan, K. L. Knudsen, F. Terra, P. Okubo, and Y. Lin 2011, "Shear-Wave Velocity Characterization of the USGS Hawaiian Strong-Motion Network on the Island of Hawaii and Development of an NEHRP Site-Class Map," *Bulletin of Seismological Society of America*, 101, 5, 2252-2269.
- Wyss, M., and R. Y. Konanagi 1992, "Seismic Gaps in Hawaii," *Bulletin of the Seismological Society of America*, 82, 1373-1387.
- Youngs, R. R., S. J. Chiou, W. J. Silva, and J. R. Humphrey 1997, "Strong Ground Motion Attenuation Relationships for Subduction Zone Earthquakes," *Seismological Research Letters*, 68, 58–73.

About Verisk

Verisk Analytics (Verisk) provides risk modeling solutions that make individuals, businesses, and society more resilient to extreme events. In 1987, a Verisk subsidiary founded the catastrophe modeling industry and today models the risk from natural catastrophes, terrorism, pandemics, casualty catastrophes, and cyber incidents. Insurance, reinsurance, financial, corporate, and government clients rely on Verisk's advanced science, software, and consulting services for catastrophe risk management, insurance-linked securities, longevity modeling, site-specific engineering analyses, and agricultural risk management. Verisk (Nasdaq:VRSK) is headquartered in Jersey City, New Jersey with many offices throughout the United States and around the world. For information on our office locations, visit <https://www.verisk.com/about/locations/>.

Contact Information

Verisk Analytics
Lafayette City Center, 2nd Floor
Two Avenue de Lafayette
Boston, MA 02111
USA

Tel: (617) 267-6645
Fax: (617) 267-8284

Verisk welcomes feedback on its documentation. If you need assistance in using the software or understanding the information in this document, please email us at DocumentationFeedback@verisk.com.

